Improved tracer techniques for georeservoir applications

–

Artificial tracer examination identifying experimentally relevant properties and potential metrics for the joint application of hydrolysis tracer and heat injection experiments

Dissertation

zur Erlangung des mathematisch-naturwissenschaftlichen Doktorgrades
"Doctor rerum naturalium"
der Georg-August-Universität Göttingen
im Promotionsprogramm Geowissenschaften
der Georg-August University School of Science (GAUSS)

vorgelegt von

Friedrich Maier

aus Böblingen

Göttingen 2014

Betreuungsausschuss

PD Dr. Tobias Licha, GZG – Abteilung Angewandte Geologie, Universität Göttingen

Prof. Dr. Martin Sauter, GZG – Abteilung Angewandte Geologie, Universität Göttingen

Mitglieder der Prüfungskommission

Referent:
PD Dr. Tobias Licha, GZG – Abteilung Angewandte Geologie, Universität Göttingen

Korreferent:
Prof. Dr. Martin Sauter, GZG – Abteilung Angewandte Geologie, Universität Göttingen

weitere Mitglieder der Prüfungskommission:
Prof. Dr. Wilhelm Heinrich, Sektion 3.3: Chemie und Physik der Geomaterialien, Deutsches GeoForschungszentrum GFZ

Prof. Dr. Günter Zimmermann, Sektion 4.1: Reservoirtechnologien, Deutsches GeoForschungszentrum GFZ

Dr. Iulia Ghergut, GZG – Abteilung Angewandte Geologie, Universität Göttingen

Dr. Rüdiger Schulz, Sektion 4 "Geothermik und Informationssysteme", Leibniz-Institut für Angewandte Geophsik LIAG

Tag der mündlichen Prüfung: 24.10.2014

Short Summary

For an efficient and sustainable use of georeservoirs, optimal reservoir management procedures are required. Such procedures often rely on tracer tests. Due to in-situ interactions between the tracer and the reservoir, recorded tracer signals contain an integral signal of the reservoir properties. For this reason, tracer test application offers a powerful technique for the characterization and observation of georeservoirs. This is especially true when reactive tracers are used, because the dynamic approach involved is unlike the established routines that are used with conservative tracers. Yet, the analysis and interpretation of reactive tracer signals is often biased, misguided or downright impossible due to the application of inappropriate physicochemical models, or false assumptions regarding tracer-behavior in the reservoir. The use of a selective and specific reaction pattern allows the diagnostic capacity of reactive tracers to be expanded to include accurate estimates for such significant reservoir metrics as (for example), heat exchange surfaces and prevailing temperatures.

In this thesis, hydrolyzing tracers, which are characterized by their reaction with water, were examined. As thermo-sensitive tracers, they provide information regarding in-situ temperatures and cooling fractions, as expressed by means of the observed concentrations in the recorded response curves, for which, the well-known Arrhenius parameters for the employed pseudo first-order reaction are necessary prerequisites. Theoretical and experimental investigations with regard to this group of tracer-compounds are elaborated here, in order to mitigate interpretation uncertainties with their application in the field.

Controlled laboratory experiments are conducted, in order to investigate the sensitivity and practical limitations of thermo-sensitive tracers. The designed experimental setup consists of two consecutively connected columns: both of which are sand-packed and heated to a specified temperature using a rapid-flow water bath, enabling the assessment of various thermal setups. Different experimental schemes are applied to mimic such various field scenarios as: Flow-through, Moving Thermal Front and Push-pull. The tracers are either injected continuously, or pulsed. Furthermore, the employed compounds have fluorescent properties which allow online measurement. Not only do the results of the lab experiments confirm the inherent expectations of the underlying theory, but when the pH dependency of the hydrolysis reaction is considered in the analysis, reservoir temperatures can be estimated with a precision and accuracy of up to

1 K. Such estimates are not influenced by variability in residence time or measured concentration. Furthermore, it is also possible to derive an estimate for the fraction of cooling when different temperatures are applied to the columns. Finally, under controlled and well-defined laboratory conditions, the effective application of thermo-sensitive tracers is, reliably achieved for the first time since their introduction.

An additional application of hydrolysis tracers is also proposed. How effectively CO_2 is trapped in water, by solubility trapping for carbon capture and storage applications, is determined by the interface area between CO_2 and the formation brine in deep reservoirs. With the employment of target-designed kinetic interface sensitive tracers (KIS-tracers), the respective dissolution properties of the tracer and the reaction product, in both the organic phase and in water can be combined with the hydrolysis reaction at the interface to potentially estimate the interface area. In addition to the basic concept of, and requirements for KIS-tracers, an initial laboratory experiment is presented which demonstrates the successful molecular target design and provides an experimental basis for the development of a macroscopic numerical model. Then, the related numerical simulations are implemented to examine the interplay of KIS-tracers with a dynamic interface area in various hypothetical scenarios.

Due to the temperature dependent reaction-speed of hydrolysis tracers, thermal transients are typically observed. Hence, the last part of this thesis endeavors to further exploit the available information from such recorded temperature signals. For an idealized single-fracture system, a set of analytical solutions is discussed; spatial and temporal profiles are derived for thermal single well injection/withdrawal experiments. With the application of a mathematically efficient inversion method known as "Iterated Laplace Transform", computationally efficient real-space solutions can be obtained. With the introduction of three dimensionless numbers, the 'return profiles' can be analyzed for fracture-width or heat-transport rate, variable pumping/injection rates and nearby spatial observations. Finally, an application of the aforementioned inversion method is used to derive a set of kernel functions for nonlinear optimization algorithms.

The presented work narrows the existing gap of tracer choice and field application: helping to mitigate future planning and analysis uncertainties, while demonstrating a sensitivity to resolve temperatures, cooling fractions, liquid/liquid interface, fracture-width and heat transport rate. The capability to estimate an expanded set of reservoir metrics, as made possible by the presented tracer concept/methods, promises to enhance

reservoir management procedures. The experimental results, in combination with the new analytical models, afford a more comprehensive insight into the collective role of the parameters controlling hydrolysis reaction and heat transport in georeservoirs.

Kurzfassung

Für eine effiziente und nachhaltige Nutzung von Georeservoiren sind bestmögliche Reservoirmanagementverfahren erforderlich. Oft setzen diese Verfahren auf Tracer-Tests. Dabei enthalten die aufgezeichneten Tracersignale integrale Informationen der Reservoireigenschaften. Tracer-Tests bieten somit eine leistungsfähige Technik zur Charakterisierung und Überwachung der bewirtschafteten Georeservoire. Im Gegensatz zu Tracer-Tests mit konservativen Tracern, welche bereits etablierte Testroutinen zur Verfügung stellen, ist die Verwendung von reaktiven Tracern ein neuer Ansatz. Aufgrund unpassender physikalisch-chemischer Modelle und/oder falschen Annahmen ist die Analyse und Interpretation von reaktiven Tracersignalen jedoch oft verzerrt, fehlinterpretiert oder sogar unmöglich. Reaktive Tracer sind dennoch unersetzbar, da sie durch die gezielte Ausnutzung selektiver und spezifischer Reaktionen mögliche Metriken von Reservoirtestverfahren auf einzigartige Weise erweitern. So liefern reaktive Tracer für ein integriertes Reservoirmanagement geforderten Aussagen über Reservoirmetriken wie z.B. Wärmeaustauschflächen oder in-situ Temperaturen.

Um Unsicherheiten bei der Auswertung von Tracerexperimenten zu reduzieren, werden theoretische und experimentelle Untersuchungen zu hydrolysierenden Tracern vorgestellt. Diese Tracer sind durch ihre Reaktion mit Wasser charakterisiert. Einerseits können sie als thermo-sensitive Tracer Informationen über Temperaturen und abgekühlte Anteile eines beprobten Reservoirs liefern. Für die Interpretation von thermo-sensitiven Tracerexperimenten sind die Kenntnis der zugrunde liegenden Reaktionsmechanismen sowie bekannte Arrhenius-Parameter Voraussetzung, um die verwendete Reaktion pseudo erster Ordnung nutzen zu können. Darüber hinaus ermöglichen die verwendeten Verbindungen durch ihre Fluoreszenzeigenschaften eine Online-Messung. Um die Empfindlichkeit und praktischen Grenzen thermo-sensitiver Tracer zu untersuchen, wurden kontrollierte Laborexperimente in einem eigens dafür entwickelten Versuchsaufbau durchgeführt. Dieser besteht aus zwei seriell geschalteten Säulen, die beide mit Sand gefüllt sind und jeweils auf eine eigene Temperatur eingestellt werden können. Somit ist es möglich, verschiedene thermische Einstellungen zu betrachten. Die untersuchten experimentellen Szenarien imitieren größtenteils Feldanwendungen: Durchflussexperimente sowie auch Experimente mit einer Umkehr der Fließrichtung. Darüber hinaus wurde untersucht, ob thermo-sensitive Tracer auch sensitiv gegenüber der Position der Temperaturfront sind. Dabei wurden die Tracer kontinuierlich oder gepulst injiziert. Die Ergebnisse bestätigen die zugrunde liegende

Theorie experimentell. Wenn die pH-Abhängigkeit der Hydrolyse bei der Analyse berücksichtigt wird, kann eine Temperaturschätzung mit einer Genauigkeit und Präzision von bis zu 1 K erreicht werden. Die Schätzungen sind von Verweilzeit und gemessenen Konzentrationen unabhängig. Weiterhin lässt sich eine Schätzung über den ausgekühlten Anteil des Systems erhalten. Durch die steuerbaren und definierten Laborbedingungen ist es erstmals möglich, die geforderte Anwendbarkeit von thermo-sensitiven Tracern belastbar nachzuweisen.

Des Weiteren wird eine zweite Anwendung hydrolysierender Tracer vorgeschlagen. Beim Lösen von CO_2 für „Carbon Capture and Storage"-Anwendungen hängt die Effizienz maßgeblich von der Grenzfläche zwischen CO_2 und der Sole in tiefen Reservoiren ab. Somit ist diese Metrik wichtig, um die Effizienz der CO_2 Auflösung in Wasser zu bewerten. Die gezielt entwickelten Kinetic-Interface-Senitive-Tracer (KIS-Tracer) nutzen, zusätzlich zur Hydrolyse an der Grenzfläche, die unterschiedlichen Lösungseigenschaften von Tracer und Reaktionsprodukt im entsprechenden Fluid. Somit lassen sich potentiell Aussagen über die Dynamik der Grenzfläche machen. Neben dem grundlegenden Konzept sowie den theoretischen Tracer-Anforderungen wird eine erste Anwendung im Laborexperiment vorgestellt. Diese zeigt das erfolgreiche, zielorientierte Moleküldesign und bietet eine experimentelle Basis für ein makroskopisches numerisches Modell, mit welchem numerische Simulationen verschiedener Testszenarien durchgeführt werden, um das Zusammenspiel von KIS-Tracer und dynamischer Grenzfläche zu untersuchen.

Aufgrund der Temperaturabhängigkeit der Reaktionsgeschwindigkeit hydrolysierender Tracer werden in der Regel auch thermische Signale aufgezeichnet. Der letzte Teil prüft die Möglichkeit, Informationen aus den aufgezeichneten Temperaturen zu extrahieren. Für ein idealisiertes Einzelkluftsystem wird eine Reihe von analytischen Lösungen diskutiert. Aus thermischen Injektion-/Entzugsversuchen können damit räumliche und zeitliche Profile abgeleitet werden. Mit der Verwendung von mathematisch effizienten Inversionsverfahren wie der iterativen Laplace-Transformation lassen sich rechentechnisch effiziente Realraum-Lösungen ableiten. Durch die Einführung von drei dimensionslosen Kennzahlen können die berechneten Temperaturprofile auf Bruchbreite oder Wärmetransportrate, wechselnde Injektions-/ Pumpraten und/oder auf in der Nähe beobachtbare räumliche Informationen analysiert werden. Schließlich werden analytische Lösungen als Kernel-Funktionen für nichtlineare Optimierungsalgorithmen vorgestellt.

Zusammenfassend bearbeitet die vorliegende Arbeit den Übergang zwischen Tracerauswahl und Traceranwendung. Die Ergebnisse helfen Planungs- und Analyseunsicherheiten zu reduzieren. Dies wird bezüglich der Empfindlichkeit gegenüber Temperaturen, Kühlungsanteilen, flüssig/flüssig-Grenzfläche, Kluftbreite und Wärmetransportrate gezeigt. Somit bieten die vorgestellten Tracerkonzepte neue Metriken zur Verbesserung von Reservoirmanagementverfahren. Die experimentellen Ergebnisse und die neuen analytischen Modelle ermöglichen einen tiefen Einblick in die kollektive Rolle der Parameter, welche die Hydrolyse und den Wärmetransport in Georeservoiren kontrollieren.

Danksagung

x

Table of Contents

List of Figures

xvii

List of Tables

1 Introduction

1.1 Motivation and background

With the world's increasing energy demand and required supply security, efficient and sustainable production technologies are critical for a secure future. Within this context, limited geo-resources (e.g. water, fossil energy, rare earth elements, etc.) and ongoing climate change are both substantial challenges (Wefer, 2010). To face this issue, the transition towards renewable forms of energy is currently a vital task of mankind. Likewise, for the associated fields of greenhouse gas emissions reduction and energy storage, which moved recently into the focus of an intensified research, all disciplines of science must contribute to achieve a fast and significant advancement. In this light, the geosciences must contribute, inter alia, to the emerging technologies of deep geothermal energy (GE), sensible energy storage (SES) and carbon capture and storage (CCS). These technologies have in common that the utilized geological horizons are solely accessed by wells.

With an estimated global technical potential of >1000 EJ yr^{-1}, GE represents the second largest of all renewable energy sources (IPCC, 2011). Despite the increasing global willingness to use this energy source for base load supply and for direct use, it is still at an early stage (Bertani, 2012). To date, GE provides roughly 0.1% of the total primary energy supply (IPCC, 2011). For a future increase, the critical factor is "*the technological ability to use GE, not its quantity*" (WEA, 2000). So far, the biggest obstacle to investment in GE production is the discovery risk. For hydrothermal systems, a critical unknown is whether or not there is a sufficient amount of thermal water available, while for petrothermal systems, a key factor is whether or not it is possible to enhance a potential reservoir with chemical and physical methods, in order to achieve the needed, thermally stable, production rates.

In contrast, the discovery risk for both CCS and SES is relatively minor. The major risk then for each of these two technologies arises from the reliability of the respective reservoirs, since potential advective/diffusive leakages serve to limit the deposit and (long term) storage. CCS typically utilizes saline aquifers, (depleted) oil/gas fields, or caverns which have already been explored, while SES relies on shallower geological formations. Discussed also is the option of combining distinct applications, such as GE with CCS/SES, or conventional oil and gas applications with CCS, in order to both offset costs and augment efficiency through the added synergy effects (e.g. Freifeld et

al., 2013; Nielsen et al., 2013). Considering that most of the investment for GE, CCS and SES enterprises is required for well-drilling, a prior combined geological/geophysical exploration and risk assessment is essential. Ideally, this is based on an extensive survey, using e.g. seismic surveys, geothermometry, electromagnetic, or gravitational methods (Barbier, 2002).

Once the initial obstacles have been surmounted and the wells have been successfully installed, the main goal is to raise efficiency to the maximum, in order to realize profits. Hence, a sustainable reservoir management procedure must be installed (Ungemach et al., 2005). In this work, 'Reservoir Management' is defined, following the Society of Petroleum Engineers, as a dynamic process whose goal is to mitigate reservoir performance uncertainties by incorporating synergy effects from multiple systematic applied technologies (PetroWiki, 2014). To account for the unlimited variety of reservoir compositions, a tailor-made reservoir management procedure which considers geometry, reservoir/fluid properties and depletion-state must be established. Economic and legal aspects must also be considered. Usually a proper reservoir management procedure is based on geological and numerical reservoir models. Such models include data from the above-mentioned explorations, as well as results from well testing. Various methods can provide point information within the local vicinity of the well, e.g. well logs and core samples, while such techniques as fluid chemistry analysis, pumping tests and tracer tests utilize the integrated reservoir signals to derive target metrics, e.g. temperatures, water origin, rock composition, permeability, storage coefficients, flow paths and residence times. Tracer testing is particularly noteworthy in that, based on its specific experimental design, a tracer test can potentially yield a wide range of possible metrics. For example, residence time and heat exchange surface density (both of which are necessary for the prediction/estimation of thermal breakthrough) are each solely measureable with tracer tests. Also, repeated tracer tests can be applied to resolve long and short-term reservoir changes.

1.1.1 Theoretical basis for tracer experiments

To restrict the various respective definitions from engineering, medical and natural sciences for tracer, indicator or marker methods, this work is strictly limited to georeservoir tracers. Here, a georeservoir tracer is defined as matter, or energy, with a temporally and spatially known input function of a measurable quantity (e.g., the temperature of the injected fluid, or the concentration of a specific chemical compound) intentionally introduced into a reservoir.

Table 1.1:   Parameters of Equation (1.1) for the tracers used in this thesis with φ the porosity, ρ the density, c_p the heat capacity, k the heat conductivity and D the dispersion coefficient. The subscripts s, f refers to the solid or fluid phases, respectively.

u	A	B	C
Temperature (T)	$(1-\varphi)(\rho c_p)_s + \varphi(\rho c_p)_f$	$(1-\varphi)k_s + \varphi k_f$	$(\rho c_p)_f$
Concentration (c)	1	D	1

In this thesis, the theoretical basis for the applied tracer interpretation models is given by the theory of transport in porous media, as expressed by means of a partial differential equation (PDE):

$$A\frac{\partial u}{\partial t} = \nabla \cdot (B\nabla u) - C\vec{v} \cdot \nabla u + S \qquad (1.1)$$

where the coefficients A, B and C depend on the considered tracer and are found in Table 1.1, u is the scalar field of the considered tracer variable, $\vec{v}$ is the water velocity and S is a source/sink term.

From Equation (1.1) which describes the temporal evolution of u, the contributing processes leading to spatial and temporal changes can be identified. The first term on the right hand side (RHS) describes spatial movement due to existing tracer gradients (diffusion and dispersion), the second term RHS considers the spatial movement due to the moving carrier fluid (advection or convection) and the third term RHS summarizes all remaining alteration processes which can be expressed in a source/sink formulation (e.g. chemical fate, sorption, matrix diffusion, etc.). In this context, a conservative tracer is defined as a tracer whose transport can be sufficiently described by the first and the second term RHS, while a reactive tracer is defined by means of an additional specified interaction pattern (third term RHS).

For the analysis of the tracer signals the known input function provides is advantageous. Together with reasonable initial conditions it can be exploited/introduced as a (time dependent) boundary condition to specify Equation (1.1). Thus, a unique solution exists and the observed, time-evolved response functions, containing system-specific, integral information of the tested georeservoir, can be applied to enhance what would otherwise be (merely) a qualitative interpretation with quantitative information (e.g. Małoszewski and Zuber, 1982). For special cases, the descriptive PDEs can be solved analytically and a corresponding closed-form response function can be derived. Unfortunately for most systems this is impossible; thus, numerical simulators provide a general method for

solving Equation (1.1). A successfully recorded tracer response curve enables the direct extraction of some quantitative information e.g. breakthrough or residence time and hence maximum fluid velocity, concentration maximum (average velocity), and tracer recovery as a function of time (Axelsson et al. 2005). Nevertheless, most of the information is derived/interpreted from the specific evolution of the input function itself over time. For example, the tailing of the response reflects matrix diffusion and/or flow heterogeneities, while the width of the pulse corresponds with the dispersion coefficient. Such metrics can only be quantitatively estimated via analytical or numerical solutions of Equation (1.1) for sufficient geometry assumptions. As a result, a reliable quantitative analysis of a tracer experiment is, in general, challenging; new concepts and their limitations will be discussed in this work.

1.1.2   Tracer methods for reservoir testing, characterizing and monitoring

The first tracer test for geological application, using chaff, was reported almost 2000 years ago in Trachonitis (today southern Syria; Davis et al., 1980). The modern scientific history of tracers is nearly 150 years old. One of the first successfully reported tracer tests was conducted in 1877 in which dye was used to reveal a hydraulic connection (Knop, 1878). In general, tracer tests can be categorized into two major types. The first involves Inter- or Multi-well scenarios, where the tracer is injected at a given point (e.g. injection well) and measured elsewhere (e.g. observation or pumping well). In recent decades, several successful Inter-well Tests have been reported: e.g., Dash et al. (1983), Adams and Davis (1991), Rose et al. (2001) and Sunjan et al. (2006). However, it is also possible to measure again at the injection point, as reported by Haggerty et al. (2000), Altman et al. (2002), Behrens et al. (2009) and Maier et al. (2011). These tests, known as Single-Well Injection-Withdrawal (SWIW), Push-pull or Huff-puff, complement Inter-well Tests with additional information. While the primary advantage of Inter-well Tests is that they are able to investigate flow-path properties over long distances, encompassing large reservoir volumes, SWIW enable flow reversibility observations which are advantageous for the evaluation of time-dependent processes (e.g. Nordqvist and Gustafsson, 2002; Ghergut et al., 2012). For the planning and implementation of a successful tracer experiment, four essential questions must be addressed:

(1) What is the target/goal of the experiment?

Usually this question is straight-forward. Nevertheless, due to the large costs involved, it is essential to evaluate the desired metrics and therefore the experimental boundary conditions and limitations carefully. Various metrics can be evaluated from tracer experiments. A great overview of possible tracers for different applications and target metrics can be found in e.g. Davis et al. (1980), Chrysikopoulos (1993), Nottebohm (2011), Schaffer (2013) or Serres-Piole et al. (2012). The definition of the experimental target leads to the next question.

(2) Which tracer is optimal?

In review (Davis et al., 1980; Chrysikopoulos, 1993) and guideline (Serres-Piole et al., 2012) publications, the authors emphasized that the proper choice of an appropriate tracer is a fundamental key parameter to avoid failure. Generally, a sound understanding of the hydromechanical reservoir properties or additional information regarding rock and fluid properties is required to estimate the target metrics successfully. Also the expected flow patterns (e.g. divergent/convergent versus dipole) and representative volumes must be considered. Furthermore, during the planning process it is important to consider interaction of the tracer with temperature, pressure, pH, rock properties, ionic strength, salinity, biological activity, etc. (Bjornstad et al., 1994). While conservative tracers should show only negligible interaction, reactive tracers apply the interaction in a targeted manner. Whenever tracer tests are intended to be employed in a quantitative analysis, a specified description of the expected interaction is considered essential (Axelsson et al, 2005). Such a description is addressed in this thesis for both Hydrolysis Tracers and for Heat Injection. Once the target metric has been defined and the proper tracer has been chosen, the design of an injection scheme is the following step.

(3) How should the input function be designed?

The design of an appropriate tracer input function is always challenging. If not altogether unknown, the flow pattern in heterogeneous georeservoirs very often holds a high degree of uncertainty. Nevertheless, several degrees of freedom can be identified to adjust the experimental design (Nordqvist and Gustafsson 2002; Axelsson et al., 2005):

- Flow rates
- Tracer injection duration
- Chaser fluid duration
- Waiting phase duration
- Tracer injection concentration
- Detection limit

- Return rate anticipated
- Total experimental time
- Used wells
- Distances involved
- Tracer background
- Reservoir conditions (pH, Temperature, etc.)

The determination of the tracer injection concentration is hereby the critical crux of the input function design, being that it is itself dependent on all adjustment factors as well as on the future in-situ development of the injected tracer pulse. A rough estimate of the optimal injection concentration can be obtained from mass-balance calculations, or better from numerical models.

(4) How to obtain the response function with regard to sampling points and sampling frequency?

In their review of nearly 50 years of tracer history in oilfield characterization, Du and Guan (2005) identified poor sampling strategies as the most common reason for failure, which has often been due to such technical restrictions as: lack of manpower, lack in the quantity of sampled wells, or faulty measurement techniques (Axelsson et al., 2005). The potential experimental duration of a tracer test can conceivably span a very wide range: from a matter of mere seconds to a scale of years. The actual sampling rate is typically case specific, but as a general rule it is recommended to sample with a decreasing frequency (Axelsson et al., 2005). The reason for this is that rapid tracer returns with steep gradients should be expected at the beginning of a tracer test. Such features become less distinct over time, due to ongoing dispersion/diffusion processes, thus, a reduced sampling rate is deemed sufficient during later stages of the test. The optimal experimental duration is hardly predictable, particularly since late-stage data also contains valuable information, which is driven mainly by sorption and diffusion processes (Haggerty et al., 2000, 2001).

1.1.3 Hydrolysis tracers as a reservoir management tool

In such reservoir applications as GE and SES, fluids having a distinct temperature from that of the ambient reservoir are injected. Therefore, reservoir management procedures must deal with a spatial and temporal temperature distribution within the employed domain. GE also contains the potential risk of an early thermal breakthrough (e.g. Malate and O'Sullivan, 1991; Stefansson, 1997). Such a feature serves to limit the practical duration of use, or life-span for a given reservoir, limiting its economic potential. To improve reservoir management procedures, chemical tracer testing has been identified as perhaps the most important tool for measurement of possible cooling at the production well (e.g. Axelsson, 2003). Due to the faster advective transport of dissolved chemical tracers, in comparison with temperature signals, their use affords a better means of evaluating thermal drawdown (Chrysikopoulos, 1993). To date, the best method available for estimating the position of the thermal-front is through the application of a retardation relation, resulting from the linear relationship between the thermal-front and the concentration-front of conservative tracers (e.g. Bodvarson, 1972). This indirect method is, however, restricted to linear-flow environments and is yet to be successfully applied in a single field experiment. Thus, a reliable method to estimate the thermal state of a georeservoir remains to be developed. To overcome this limitation, thermo-sensitive tracers which feature a specific hydrolysis reaction were first proposed in the 1980s (Robinson et al., 1984; Tester et al., 1986). Nowadays, there are three applications of hydrolysis tracers: Partitioning Tracers for the estimation of residual saturations (e.g. Tomich et al., 1973; Meyers et al., 2012), Thermo-sensitive Tracers for thermal-state investigations (examined in this thesis) and Kinetic Interface Sensitive Tracer (KIS-Tracer) for CCS application (proposed and examined in this thesis). The expression: thermo-sensitive tracer refers in this work exclusively to tracers that are based on the hydrolysis reaction. Hydrolysis is the cleavage of a chemical compound (X–Y) by reaction with water (H–OH):

$$X-Y \;+\; H-OH \;\xrightarrow{\;\;k\;\;}\; X-H \;+\; Y-OH \tag{1.2}$$
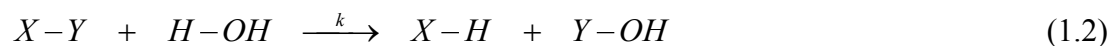
The rate of this reaction (k), as expressed by The Arrhenius Law, is controlled mainly by ambient temperature. Thus, DuTeaux and Callahan (1996) conclude that adequate Arrhenius parameters (activation energy and frequency factor) must be identified prior to the successful application of a tracer in the field. The term 'adequate' is understood here as being obtained when the reciprocal of the reaction rate at the highest formation

temperature falls within the same order of magnitude as that of the tracer test duration (Chrysikopoulos, 1993).

Relatively few field experiments have been performed using thermo-sensitive tracers. The first experiments, which used two ester compounds (ethyl acetate and isopentyl acetate), were performed in Fenton Hill (e.g. Tester et al., 1986). In the subsequent analysis, an assumption for pH value was used to derive a temperature estimation from the ethyl acetate concentration data. Batchelor (1986) and Kwakwa (1988) implemented ethyl acetate as a tracer (HDR doublet, Camborne School of Mines, England), but were unable to identify a reservoir temperature. The failure of the initial experiments was attributed to false or missing pH values and poorly determined pH dependencies. Further problems occur when the highly volatile tracers are measured at reservoir temperatures greater than 80 °C (the boiling point of Ethanol is 78.3 °C and for Ethyl acetate is 77.1 °C). Substances which show attenuation under isothermal conditions are closely related to thermo-sensitive hydrolysis tracers (Adams and Davis, 1991; Adams et al., 1992; Rose et al., 2001, 2003; Rose and Clausen, 2014). Adams & Davis (1991) performed a dual tracer experiment using fluorescein and aromatic acids (Dixie Valley, Nevada), using an analysis based on differing degradation rates to successfully solve for the effective temperatures, as confirmed by a priori known temperatures. Due to a lack of general geochemical behavior characterization and reaction mechanism description, a transfer of this experiment has not been possible (Fenton Hill, New Mexico; Du Teaux & Callahan, 1996). In general, further sensitivities (e.g., pH and pOH), could cause potential difficulties in controlling the reaction kinetics of thermo-sensitive tracers (Robinson and Birdsell, 1987; Batchelor, 1986, Nottebohm et al. 2012).

In order to overcome setbacks leading to the employment of thermo-sensitive tracers as a useful tool for reservoir management, a comprehensive evaluation of their physicochemical properties must be elaborated. For this purpose, the theoretical background of thermo-sensitive tracers for reservoir characterization, as established by Tester (1985), Robinson (1985), and Tester et al. (1986, 1987), as well as recently proposed tracer compounds (Nottebohm et al., 2012) provide a stable basis to build upon. From the pioneering research of Robinson (1985), four generalized and essential research fields for successful field implementation of thermo-sensitive tracers can be deduced.

1.) An evaluation of Push-pull and Inter-well Tests must be performed, with regard to appropriate kinetic parameters which are dependent on residence-time, pumping-rate, reservoir volume/geometry and expected temperatures. Robinson (1985) concluded that for Inter-well Tests, a change in pumping-rate results in a relatively insignificant difference in residence-time; however, this is not true for SWIW tests, which are less restrictive. SWIW tests can then be designed more freely; thus, a tracer with appropriate kinetics can be found more easily. Based on the deduced theory for thermo-sensitive tracers and due to the absence of experimental data, a vast set of preliminary studies using numerical methods were recently performed by various scientists (e.g. Behrens et al., 2009; Plummer et al., 2010, 2012; Williams et al., 2010, 2013; Reimus et al., 2011; Ghergut et al,. 2013a). Behrens et al. (2009) stated that the sensitivity of thermo-sensitive tracers might not be sufficient to detect changes in the position of the thermal front. Plummer et al. (2010) found that the sensitivity of such tracers can be significantly increased through specific adjustment of the Arrhenius Parameters. For two benchmark reservoir models, both of which are dominated by parallel fractures and dipole flow conditions, an optimal range of kinetic parameters for quantitative analysis can be identified (Plummer et al., 2012; Willams, 2013). Ghergut et al. (2013a) presented a review of thermo-sensitive tracer tests that were used for the estimation of thermal life-span for four distinct types of geothermal systems: featuring a range from porous to fractured media flow conditions. Thermo-sensitive tracers were found to be useful in all scenarios for a general thermal characterization, but deemed less capable in systems with a complex residence time distribution (Ghergut et al., 2013a).

2.) Laboratory flow experiments have been proposed and conducted, in order to test the utility of thermo-sensitive tracers. With the use of an open-pipe laminar-heat exchanger, thermo-sensitive tracers were identified as a tool with a high potential to estimate internal temperatures (Robinson, 1985). However, due to a combined forced/free convection flow-field in the non-isothermal experimental setups, only a qualitative analysis was possible (Robinson, 1985). The stated experimental limitations can be overcome through the use of an alternative experimental laboratory design, as presented in this work. The results from the proposed column experiments are directly transferable to systems which feature a linear correlation between thermal and tracer velocity (Bodvarson, 1972; Shook, 2001). Such general limitations as tracer/matrix interactions and the relative sensitivity of various thermo-sensitive tracers can be evaluated with these analogue experiments (e.g. Robinson, 1985; Leecester et al., 2012). With the

successful transfer from static-batch to dynamic-flow experiments, the underlying theory can be validated and extended to consider further dependencies.

3.) The identification and synthesis of possible tracer compounds should be forced. The obtained (time-dependent) dependencies on, e.g., dissolved ions, CO_2 and OH^- concentration complicate the analysis (Robinson, 1985). It would be desirable to minimize the effects of secondary processes, but until such minimization has been achieved, the stability of thermo-sensitive tracers must be carefully evaluated in such a way that further alteration processes can later be considered. Adams et al. (1992) and Nottebohm et al. (2012) found that the main parameter determining tracer stability is the Acid Dissociation Constant. This is expressed by the identified linear free-energy relationships (Shorter, 1985) between the relative acid-strength and reaction-speed of the corresponding derivates (e.g. ester, amides, etc.). Thus, the use of a classification system according to different functional groups serves as a rule of thumb to forecast thermal stability. Taking further advantage of the influence of steric hindrance, as well as mesomeric and inductive effects for compounds with the same basic structure, allows/enables the adjustment of Arrhenius parameters for target-designed tracers (Adams et al., 1992; Nottebohm et al., 2012). On this basis, the studies regarding the stability of tracers (e.g. Robinson, 1985; Nottebohm et al., 2010, 2012; Idzik et al., 2014) can be used as a starting point.

4.) Finally, the mentioned advances should result in adjusted analysis methods. Such methods should be based on comprehensive models, which account for an advanced understanding with regard to potential processes (e.g. sorption) and sensitivities (e.g. pH). The use of such comprehensive models not only augments the design and planning of successful tracer experiments, but enables their quantitative interpretation. For piston-flow dominated reservoirs, Chemburkar (1991) presented an assumption-free method to resolve temperature profiles; the only restriction is that two thermo-sensitive tracers are needed. For more complex systems, elaborate inversion techniques must be found, based on the residence time distribution function (Robinson, 1985; Ghergut et al., 2013a). One other important finding is that a minimum of three consecutive tests must be performed, in order to estimate the thermal breakthrough time (Willams, 2013).

In summary, a successful thermo-sensitive tracer experiment, or more generally, a successful hydrolysis tracer experiment, rests on four pillars: **numerical modeling** (planning, sensitivity analysis, etc.), **tracer synthesis and characterization** (Arrhenius

parameters, dependencies, etc.), **dynamic analogue experiments** (tracer/fluid and tracer/matrix interaction) and **elaborate analysis methods** (numerical models, analytical solutions, etc.). The need for systematic research as a pre-requisite for the successful application of thermo-sensitive tracers in field experiments is also emphasized by Plummer et al. (2011), who stated that, "*the basic theory behind the concept of thermal tracers [sic] has been understood for some time, but an effective application of the method has yet to be demonstrated.*"

1.1.4 (Semi-)Analytical solutions to evaluate tracer tests

As demonstrated in the previous chapter, a quantitative analysis of tracer test data relies on sophisticated analysis methods. Geological reservoirs are often heterogeneous, but those in which the representative volume is dominated by relatively few central features (e.g. fractures, faults, homogeneous porous media, etc.) can be sufficiently described using idealized models. In such cases, an analysis based on analytical solutions is desirable.

For several hydrogeological systems (e.g. rivers, karst systems, aquifers, fractures, etc.), transport is based on the mathematical formulation given above (cf. Equation (1.1); e.g. van Genuchten et al., 2013; Axelsson et al., 2005). The problems are usually expressed with coupled one-dimensional PDEs, one for the flow domain and one describing the adjacent matrix. Because they are restricted to hypothetical assumptions for reservoir geometry and boundary conditions, analytical solutions are less flexible than the analysis afforded by comprehensive numerical models. Nevertheless, in each of these scenarios, heterogeneous conditions are simplified by confined linear, or radial-flow assumptions, since the use of analytical solutions allows the following advantages for GE, SES and CCS applications: benchmarking of numerical simulations (e.g. Jung and Pruess, 2012; Maier et al. 2012; van Genuchten et al. 2013), implementation in nonlinear regression procedures for data inversion with best estimate and reliability of the estimated value (e.g. Dogru et.al. 1977), sensitivity analysis of the dependent variable due to perturbations in the value of the fitting parameter (e.g. McElwee & Yukler, 1978, McElwee, 1987), quantification of the uncertainty, supporting the optimal design of field experiment (e.g. Beck & Arnold 1977). To date, various heat and solute transport scenarios have been addressed:

- Linear heat transport: e.g. in Cartesian coordinates: Lauwerier (1955), Bodvarson (1972), Gringarten and Sauty (1975), Ziagos and Blackwell (1986); in radial coordinates Bödvarsson and Tsang (1982)

- Linear solute transport: in Cartesian coordinates: e.g. Barker (1982), Sudicky and Frind (1982), Kocabas and Islam (2000a); in radial coordinates: e.g. Falade and Brigham (1989), Kocabas and Islam (2000b), Veling (2001)

Based on the initial findings for linear transport, various scientists also developed analytical solutions for experiments featuring flow reversal:

- SWIW solute transport: Falade et al. (1987), Kocabas and Horne (1987), Haggerty et al. (1998).

- SWIW heat transport: Kocabas and Horne (1990), Kocabas (1995), Kocabas (2005), Jung and Pruess (2012).

Kocabas and Kucuck (2011) found that the same solutions can be used for radial and Cartesian coordinate systems when measurements are taken at the well (injection point) for a SWIW experiment. The solutions for solute transport employ various specific source-terms, which consider the influence of sorption or reaction processes. An established method to derive analytical solutions from the descriptive PDE is to solve the equation in the Laplace domain, which affords the transformation of derivatives into algebraic expressions. The transformation of the solutions from the Laplace domain into real-space are usually challenging, for which, various methods have been applied such as: numerical inversion techniques (the un-inverted solutions in the Laplace domain are defined as semi-analytical solutions), the application of approximate solutions through the use of series expansion techniques, or the application of such various transformation techniques as Fourier, Fourier Sine, Laplace, Iterated Laplace, etc. (real-space solutions are defined as exact solutions). When heat is used as a tracer only SWIW experiments are feasible, due to the slow advancement of the thermal signal along the flow direction. However, the diffusive transport into the adjacent matrix is several orders of magnitude faster than that of solute tracers. SWIW can improve reservoir management procedures with information regarding reservoir geometry (radial or linear flow field e.g. Kocabas and Horne, 1990; fracture aperture e.g. Kocabas, 2005) or heat transport rate (Kocabas, 2005). Ghergut et al. (2011) discuss the role of fracture aperture as an equivalent measure for the heat exchange area density, which is considered to be the controlling

factor for the thermal life-span of the reservoir. However, the sensitivity of thermal SWIW to this metric has been questioned (e.g. Ghergut et al. 2011, Jung and Pruess; 2012, Ghergut et al. 2013b). Kocabas and Horne (1990) derived a solution which describes a SWIW with equal pumping-rates for injection and backflow. For unequal injection and backflow-rates a semi-analytical solution was later presented (Kocabas, 1995). Jung and Pruess (2012) derived a closed-form real-space solution, including quiescence phases; however, the applied transformation techniques lead to multidimensional improper integrals, which require impractical solving durations of up to several weeks (Jung and Pruess, 2012).

1.2 Scope, objectives and further outline

Although the ability to estimate such reservoir metrics as thermal state, fracture apertures, heat transport rates and CO2/H2O interface areas is vital for the improvement of reservoir management strategies for GE, SES, and CCS applications; no reliable method exists for the estimation of these metrics. This thesis explores the potential of utilizing tracer experiments for such estimations: with the implementation of hydrolysis tracers (thermal state, including in-situ temperatures and cooling fractions) and heat (fracture apertures and heat transport rates). Furthermore, a new concept is proposed: the use of hydrolysis tracers for the determination of the CO2/H2O interface area in a given reservoir. To use synergy effect Kocabas (2005) suggests the joint application of heat and chemical tracers, in order to increase tracer test capability. With the use of hydrolysis tracers, it is recommended to log also the temperature of the in/effluent. Heat and hydrolysis tracer experiments are complementary.

In general, tracers have already been established as a standard tool for reservoir management (e.g. Serres-Piole et al., 2012). However, due to poor sampling techniques and insufficient knowledge regarding tracer behavior, the majority of the performed tracer experiments have only been analyzed qualitatively, rather than quantitatively (e.g. Axelsson, 2003; Shook et al., 2009). Schaffer (2013) stated that the knowledge of tracer behavior is an indispensable prerequisite for a successful interpretation. Therefore, an investigation of the tracer's properties is required prior to its injection in a reservoir. (Björnstad et al., 2001). This work aims to narrow the gap between tracer design and tracer field application with extensive laboratory experiments and analytical investigations (for hydrolysis tracers and the use of heat), in order to provide a reliable basis for the planning and evaluation of future field experiments. With regard to the use of thermo-sensitive tracers, the transferability of results, from static batch to dynamic

flow experiments is initially assessed. The theory is validated and inherent limitations are identified with laboratory experiments, designed to mimic various field scenarios. In order to further extend the potential metrics of hydrolysis tracers, a new class of liquid/liquid interface sensitive tracers, which utilize a controllable hydrolysis reaction, is proposed. The last part of this study explores the utilization of temperature observations from a tracer experiment. A set of closed form analytical solutions, which consider an idealized fractured system, are also presented. A more detailed outline is presented below.

Chapter 2 deals with the application of thermo-sensitive tracers. The transferability of results from static isothermal batch experiments to dynamic isothermal systems is shown. For this purpose, such parameters as pH value, used buffer and the set temperature are maintained. The only change is the additional flow field. An innovative column experiment is designed for the performance of the tests. Additionally, the effects of different materials and chemicals on the thermo-sensitive tracers' underlying hydrolysis reaction are assessed.

In **Chapter 3**, the potential behavior of a thermo-sensitive tracer in isothermal flow fields is explored. Firstly, the influence of pH on the validity of thermo-sensitive tracers is examined. Moreover, it is shown that evaluation is possible over the entire range of observed tracer concentrations. The experiments use three different temperatures, comparable with those commonly used for injection. It is further demonstrated that the experimental duration has no influence on the validity of the experiments: neither with pulse, nor with constant input of tracer solution. The observed uncertainties of the temperature estimation indicate only small fluctuations of around 2 K. This work enables the experimental confirmation of the underlying theory, which is based on the combination of the transport in porous media with that of the hydrolysis reaction.

Chapter 4 discusses the extension of the experimental laboratory system through the application of a thermal gradient, which enables the investigation of non-isothermal scenarios. In the resulting two temperature system, three different scenarios are tested. From the results of inter-well, SWIW and variable thermal front experiments, the potential to detect temperature and cooling fractions with thermo-sensitive tracers can be derived. In addition to the advantages and disadvantages of different temperature evaluations from the recorded tracer breakthrough curves, the sensitivity to the thermal front position can be proven over the entire cooling range. Furthermore, the dependence

of the results on "shut-in" phases of the pumping system is examined. The ability to detect the metrics of cooling fraction and thermal state, as expressed by a system describing temperature, are experimentally confirmed.

In **Chapter 5**, the hydrolysis reaction is utilized to synthesize a further class of tracers (KIS-tracer). Presented here is the functional concept and development of KIS-tracers, as well as their potential suitability for the determination of CO_2/H_2O interface area is presented. The interfaces formed by the injection of supercritical CO_2 into saline aquifers are an important metric for the quantification of the effectiveness of dissolution. The relative distinction between the dissolution behavior of the tracer molecule and that of the reaction product forms the basis of the presented conceptual model. In addition, a laboratory experiment is presented and evaluated with a numerically-based, macroscopic model. Based on the calibrated model, several expansion scenarios are discussed.

The temperature signal, which is commonly recorded during (hydrolysis) tracer experiments, may offer further insights. **Chapter 6** discusses the possibility of using heat injection. The scientific discourse presents computationally highly-efficient, analytical solutions of a thermal SWIW experiment. The set of four real-space analytical solutions presented here are based on a revised solution, extending its application to variable pumping/injection flow-rates as well as spatial information. Such solutions are derived for an idealized single-fracture system. The derived solutions in Laplace domain are inverted through the employment of an iterative Laplace transformation and are used as a kernel for non-linear optimization algorithms. Because of the chosen approach, very efficient analytical solutions are found, which reduce by orders of magnitude the amount of computing time required for evaluation, when compared with other existing solutions. Discussed are both the solutions and their computational efficiency. The potential use of a thermal-injection backflow test to estimate fracture-width and heat transport-rate is also examined. Since the solutions utilize the temperature signal as a tracer, they provide valuable additional information to thermo-sensitive tracer experiments, without the involvement of extensive technical effort.

Chapter 7 presents a further analytical solution for a thermal SWIW taking an additional "shut-in" phase into account. As already shown by the experiments with thermo-sensitive tracers, such an extension serves to bolster the potential expressiveness

of tracer experiments. To derive the analytical solution, the describing PDEs are transformed triple Laplace and the obtained solutions are transformed back by means of the already established method of iterative Laplace The sensitivity of such a test as well as its utility as a reservoir management method are discussed.

Chapter 8 summarizes the conclusions with respect to the focus of the thesis and gives an outlook for future research activities.

Appendix A presents additional information regarding Chapter 3.

Appendix B presents additional information regarding Chapter 7.

Appendix C presents a complete list of journal articles, conference contributions, and miscellaneous publications related to the present work from the author.

Since this thesis is a cumulative dissertation including published journal articles, cited literature is listed separately at the end of each chapter.

1.3 References

Adams, M.C., Davis, J., 1991. Kinetics of fluorescein decay and its application as a geothermal tracer. Geothermics, 20(1), 53-66.

Adams, M.C., Moore, J.N., Fabry, L.G., Ahn, J.H., 1992. Thermal stabilities of aromatic acids as geothermal tracers. Geothermics, 21(3), 323-339.

Altman, S.J., Meigs, L.C., Jones, T.L., McKenna, S.A., 2002. Controls of mass recovery rates in single-well injection-withdrawal tracer tests with a single-porosity, heterogeneous conceptualization. Water resources research, 38(7), 30-1.

Axelsson, G., 2003. Essence of geothermal resource management. Lectures on the Sustainable Use and Operating Policy for Geothermal Reservoirs, 2003-1.

Axelsson, G., Björnsson, G., Montalvo, F., 2005. Quantitative Interpretation of Tracer Test Data. In: Proceedings World Geothermal Congress 2005, 24-29

Barbier, E., 2002. Geothermal energy technology and current status: an overview. Renewable and Sustainable Energy Reviews, 6(1), 3-65.

Barker, J.A., 1982. Laplace transform solutions for solute transport in fissured aquifers. Advances in Water Resources, 5(2), 98-104.

Batchelor, A.S., 1986. Reservoir behaviour in a stimulated hot dry rock system. In: Proceedings of the 11th Workshop on Geothermal Reservoir Engineering, Stanford University, Stanford, California, January 21-23, SCP-TR-93

Beck, J.V., Arnold, K.J., 1977. Parameter Estimation in Engineering and sciences. New York. John Wiley and Sons.

Behrens, H., Ghergut, I., Sauter, M., Licha, T., 2009. Tracer properties and spiking results (from geothermal reservoirs. In: Proceedings of the 34th Workshop on Geothermal Reservoir Engineering Stanford University, Stanford, California, February 9-11, SGP-TR-187

Bertani, R., 2012. Geothermal power generation in the world 2005–2010 update report. Geothermics, 41, 1-29.

Bjornstad, T., 1994. Recent and current oil fields tracer development for interwell application. Second Tracer Workshop. University of Texas at Austin, Austin, TX, 101–113.

Bjørnstad, T., Dugstad, Ø., Galdiga, C., Sagen, J., 2001. Interwell tracer technology in oil reservoirs: State-of-the-art. In: Proc. of the" First International Congress on Tracers and Tracing Methods, 29-31.

Bodvarsson, G., 1972. Thermal problems in the siting of reinjection wells. Geothermics, 1(2), 63-66.

Bodvarsson, G.S., Tsang, C.F., 1982. Injection and thermal breakthrough in fractured geothermal reservoirs. Journal of Geophysical Research: Solid Earth (1978–2012), 87(B2), 1031-1048.

Borden, R.C., Kao, C., 1989. Water flushing of trapped residual hydrocarbon: Mathematical model development and laboratory validation. In Proceedings of the Petroleum Hydrocarbons and Organic Chemicals in Ground Water: Prevention, Detection and Restoration, 175-189.

Chemburkar, R.M., Brown, L.F., Travis, B.J., Robinson, B.A., 1991. Numerical determination of temperature profiles in flowing systems from conversions of chemically reacting tracers. Chemical engineering science, 46(5), 1349-1360.

Chrysikopoulos, C. V. (1993). Artificial tracers for geothermal reservoir studies. Environmental Geology, 22(1), 60-70.

Dash, Z.V., Murphy, H.D., Aamodt, R.L., Aguilar, R.G., Brown, D.W., Counce, D.A., Fisher, H.N., Grigsby, C.O., Keppler, H., Laughlin, A.W., Potter, R.M., Tester, J.W., Trujillo Jr., P.E., Zyvoloski, G., 1983. Hot dry rock geothermal reservoir testing: 1978 to 1980. Journal of Volcanology and Geothermal Research, 15(1), 59-99.

Davis, S.N., Thompson, G.M., Bentley, H.W., Stiles, G., 1980. Ground-Water Tracers—A Short Review. Ground Water, 18(1), 14-23.

Dogru, A.H., Dixon, T.N. Edgar, T.F. 1977. Confidence Limits on the Parameters and Predictions of Slightly Compressible Single-Phase Reservoirs. Society of Petroleum Engineers Journal, 17(01), 42-56.

Du Teaux, R., Callahan, T.J., 1996. Comparing reactive and non reactive tracers to measure changes in liquid dominated, fractured geothermal reservoirs (No. CONF-960913--). Geothermal Resources Council, Davis, CA (United States).

Du, Y., Guan, L., 2005. Interwell tracer tests: lessons learnted from past field studies. In SPE Asia Pacific Oil and Gas Conference and Exhibition. Society of Petroleum Engineers.

Falade, G.K., Antunez, E., Brigham, W.E., 1987. Mathematical analysis of single-well tracer tests. Technical Report, Supri Tr-57, Stanford University Petroleum Research Institute, Stanford, CA.

Falade, G.K., Brigham, W.E., 1989. Analysis of radial transport of reactive tracer in porous media. SPE reservoir engineering, 4(01), 85-90.

Freifeld, B., Zakim, S., Pan, L., Cutright, B., Sheu, M., Doughty, C., Held, T., 2013. Geothermal Energy Production Coupled with CCS: a Field Demonstration at the SECARB Cranfield Site, Cranfield, Mississippi, USA. Energy Procedia, 37, 6595-6603.

Genuchten, M.T., Leij, F.J., Skaggs, T.H., Toride, N., Bradford, S.A., Pontedeiro, E.M., 2013. Exact analytical solutions for contaminant transport in rivers 1. The equilibrium advection-dispersion equation. Journal of Hydrology and Hydromechanics, 61(2), 146-160.

Ghergut, I., Behrens, H., Licha, T., Maier, F., Nottebohm, M., Schaffer, M., Ptak, T., Sauter, M., 2012. Single-well and inter-well dual-tracer test design for quantifying phase volumes and interface areas. In: Proceedings of the 37th Workshop on Geothermal Reservoir Engineering, Stanford University, Stanford, California, January 30 - February 1, 2012, SGP-TR-194

Ghergut, I., Behrens, H., Licha, T., Sauter, M., 2013a. Tracer-based prediction of thermal lifetime: scope, limitations, and the role of thermosensitive tracers. In: Proceedings of the 38th Workshop on Geothermal Reservoir Engineering. Stanford University, Stanford, California, February 11-13, 2013, SGP-TR-198

Ghergut, I., Behrens, H., Maier, F., Karmakar, S., Sauter, M., 2011. A note about "heat exchange areas" as a target parameter for SWIW tracer tests. In: Proceedings of the 36th Workshop on Geothermal Reservoir Engineering, Stanford University, Stanford, California. January 31 - February 2, 2011, SGP-TR-191

Ghergut, I., Behrens, H., Sauter, M., 2013b. Single-well tracer push-pull test sensitivity to fracture aperture and spacing. In: Proceedings of the 38th Workshop on Geothermal Reservoir Engineering. Stanford University, Stanford, California, February 11-13, 2013, SGP-TR-198

Gringarten, A.C., Sauty, J.P., 1975. A theoretical study of heat extraction from aquifers with uniform regional flow. Journal of Geophysical Research, 80(35), 4956-4962.

Haggerty, R., Fleming, S.W., Meigs, L.C., McKenna, S.A., 2001. Tracer tests in a fractured dolomite: 2. Analysis of mass transfer in single-well injection-withdrawal tests. Water Resources Research, 37(5), 1129-1142.

Haggerty, R., McKenna, S.A., Meigs, L.C., 2000. On the late-time behavior of tracer test breakthrough curves. Water Resources Research, 36(12), 3467-3479.

Haggerty, R., Schroth, M.H., Istok, J.D., 1998. Simplified Method of "Push-Pull" Test Data Analysis for Determining In Situ Reaction Rate Coefficients. Groundwater, 36(2), 314-324.

Idzik, K.R., Nödler, K., Licha, T., 2014. Efficient synthesis of readily water soluble amides containing sulfonic groups. Synthetic Communications 44(1): 133–140.

IPCC, 2011: Summary for Policymakers. In: IPCC Special Report on Renewable Energy Sources and Climate Change Mitigation [O. Edenhofer, R. Pichs-Madruga, Y. Sokona, K. Seyboth, P. Matschoss, S. Kadner, T. Zwickel, P. Eickemeier, G. Hansen, S. Schlömer, C. von Stechow (eds)], Cambridge University Press, Cambridge, United Kingdom and New York, NY, USA.

Jung, Y., Pruess, K., 2012. A closed-form analytical solution for thermal single-well injection-withdrawal tests. Water Resources Research, 48(3).

Knop, A., 1878. Ober die hydrographischen Beziehungen zwischen der Donau und der Aachquelle im badischen Oberlande: N. Jb. Mineral (1878), pp 350-363

Kocabas, I., 1995. Using interwell test data to determine the interaction between geological structure and reinjection processes in geothermal reservoirs, Proceedings, International Earth Sciences Colloquim on the Aegean Region, Izmir-Gulluk, Turkey, 739-751.

Kocabas, I., 2005. Geothermal reservoir characterization via thermal injection backflow and interwell tracer testing. Geothermics, 34(1), 27-46.

Kocabas, I., 2010. Designing Thermal and Tracer Injection Backflow Tests. In: Proceedings World Geothermal Congress 2010, Bali, Indonesia, 25-29 April 2010, 25-29.

Kocabas, I., Horne, R.N., 1987. Analysis of injection-backflow tracer tests in fractured geothermal reservoirs. In: Proceedings of the 12th Workshop on Geothermal Reservoir Engineering, Stanford University, Stanford, California, January 20-22, 1987, SGP-TR-109

Kocabas, I., Horne, R.N., 1990. A new method of forecasting the thermal breakthrough time during reinjection in geothermal reservoirs. In Proceedings, of the 15th Workshop on Geothermal Reservoir Engineering, Stanford University, Stanford, California, January 23-25, 1990, SGP-TR-130.

Kocabas, I., Islam, M.R., 2000a. Concentration and temperature transients in heterogeneous porous media: Part I: Linear transport. Journal of Petroleum Science and Engineering, 26(1), 211-220.

Kocabas, I., Islam, M.R., 2000b. Concentration and temperature transients in heterogeneous porous media: Part II: Radial transport. Journal of Petroleum Science and Engineering, 26(1), 221-233.

Kocabas, I., Kucuk, I., 2011. Modeling Sensible Energy Storage in Aquifers. The 2011 International Conference on Water, Energy and the Environment to in Nov. 14-17, 201 AUS, Sharjah, UAE

Kwakwa, K.A., 1988. Tracer measurements during long-term circulation of the Rosemanowes HDR geothermal system. Proceedings of the Thirteenth Workshop on Geothermal Reservoir Engineering, Stanford University, Stanford, CA, USA, January 19–21, 1988, SGP-TR-113.

Lauwerier, H.A., 1955. The transport of heat in an oil layer caused by the injection of hot fluid. Applied Scientific Research, Section A, 5(2-3), 145-150.

Leecaster, K., Ayling, B., Moffitt, G., Rose, P., 2012. Use of safranin T as a reactive tracer for geothermal reservoir characterization. In: Proceedings of the 37th Workshop on Geothermal Reservoir Engineering, Stanford University, Stanford, California, January 30 - February 1, 2012, SGP-TR-194.

Maier, F., Hebig, K., Jin, Y., Holzbecher, E., 2011. Ability of Single-Well Injection-Withdrawal Experiments to Estimate Ground Water Velocity. In: Proceedings of 2011 COMSOL Conference Stuttgart.

Maier, F., Oberdorfer, P., Kocabas, I., Ghergut, I., Sauter, M., 2012. Using Temperature Signals to Estimate Geometry Parameters in Fractured Geothermal Reservoirs. In: Proceedings of the 2012 Comsol Conference Milan.

Malate, R.C.M., O'Sullivan, M.J., 1991. Modelling of chemical and thermal changes in well PN-26 Palinpinon geothermal field, Philippines. Geothermics, 20(5), 291-318.

Małoszewski, P., Zuber, A., 1982. Determining the turnover time of groundwater systems with the aid of environmental tracers: 1. Models and their applicability. Journal of hydrology, 57(3), 207-231.

McElwee, C.D. Yukler, M.A., 1978. Sensitivity of groundwater models with respect to variations in transmissivity and storage. Water Resources Research vol:13 no:3:451-459.

McElwee, C.D., 1987. Sensitivity analysis of groundwater models. In J. Bear & M. Y. Corapcioglu (eds), Advances in Transport Phenomena in Porous Media 750-817. Dordrecht. Martinus Nijhoff Publishers

Myers, M., Stalker, L., Ross, A., Dyt, C., Ho, K.B., 2012. Method for the determination of residual carbon dioxide saturation using reactive ester tracers. Applied Geochemistry, 27(10), 2148-2156.

Nielsen, C.M., Frykman, P., Dalhoff, F., 2013. Synergy Benefits in Combining CCS and Geothermal Energy Production. Energy Procedia, 37, 2622-2628.

Nordqvist, R., Gustafsson, E., 2002. Single-well injection-withdrawal tests (SWIW). Literature review and scoping calculations for homogeneous crystalline bedrock conditions. Swedish Nuclear Fuel and Waste Management Co., Stockholm (Sweden).

Nordqvist, R., Gustafsson, E., 2004. Single-well injection-withdrawal tests (SWIW). Investigation of evaluation aspects under heterogeneous crystalline bedrock conditions. Swedish Nuclear Fuel and Waste Management Co., Stockholm (Sweden).

Nottebohm, M., 2011. Stability and Reactivity of Organic Molecules in Geothermal Reservoirs. Ediss.uni-Goettingen.de. http://ediss.uni-goettingen.de/bitstream/handle/11858/00-1735-0000-0006-B307-2/nottebohm.pdf?sequence=1. (last accessed: 26.08.2014)

Nottebohm, M., Licha, T., Ghergut, I., Nödler, K., Sauter, M., 2010. Development of Thermosensitive Tracers for Push-Pull Experiments in Geothermal Reservoir Characterization. In: Proceedings World Geothermal Congress 2010 Bali, Indonesia, 25-29 April 2010

Nottebohm, M., Licha, T., Sauter, M., 2012. Tracer design for tracking thermal fronts in geothermal reservoirs. Geothermics, 43, 37-44.

PetroWiki, 2014. Reservoir Management. http://petrowiki.org/Reservoir_management (last accessed 02 July 2014)

Plummer M.A., Palmer C.D., Hull L.C., Mattson E.D., 2010. Sensitivity of a reactive-tracer based estimate of thermal breakthrough in an EGS to properties of the reservoir and tracer. In: Proceedings of the 35th Workshop on Geothermal Reservoir Engineering, Stanford University, Stanford, CA, SGP-TR-188.

Plummer M.A., Palmer C.D., Mattson E.D., Hull L.C., 2011. A reactive tracer analysis method for monitoring thermal drawdown in geothermal reservoirs. In: Proceedings of the 36th Workshop on Geothermal Reservoir Engineering, Stanford University, Stanford, CA, SGP-TR-191.

Plummer, M.A., Palmer, C.D., Hull, L.C., Mattson, E.D., 2012. Sensitivity of a reactive tracer based estimate of thermal breakthrough in an EGS to the properties of the reservoir and tracer. Proceedings of the 37th Workshop on Geothermal Reservoir Engineering, Stanford University, Stanford, CA, USA, February 1 – 3, 2012, SGP-TR-194.

Reimus, P.W., Watson, T., Vermeul, V., Newell, D., Williams, M., 2011. Laboratory testing and modeling to evaluate perfluorocarbon compounds as tracers in geothermal systems. In: Proceedings of the 36th Workshop on Geothermal Reservoir Engineering. Stanford University, Stanford, California, January 31 - February 2, 2011, SGP-TR-191

Robinson, B.A., 1985. Non-reactive and chemically reactive tracers: Theory and applications. PhD dissertation, Massachusetts Institute of Technology, Cambridge, MA

Robinson, B.A., Birdsell, S.A., 1987. Tracking thermal fronts with temperaturesensitive, chemically reactive tracers. Proceedings, 5th Geothermal Program Review, Washington, DC, 14-15 April

Robinson, B.A., Tester, J.W., Brown, L.F., 1984. Using chemically reactive tracers to determine temperature characteristics of geothermal reservoirs. Geothermal Resources Council Ann. Meeting, Reno, Nev., 26-29 Aug. 1984, 1, 26–29.

Rose, P., Clausen S., 2014. The use of Amino G as a thermally reactive tracer for geothermal applications In: Proceedings of the 39th Workshop on Geothermal Reservoir Engineering. Stanford University, Stanford, California, February 24 - February 26, 2014, SGP-TR-202

Rose, P.E., Benoit, W.R., Kilbourn, P.M., 2001. The application of the polyaromatic sulfonates as tracers in geothermal reservoirs. Geothermics, 30(6), 617-640.

Rose, P.E., Mella, M, Kasteler, C.,. 2003. A new tracer for use in liquid-dominated, high-temperature geothermal reservoirs. Geothermal Research Council Transactions, 27.

Sanjuan, B., Pinault, J.L., Rose, P., Gérard, A., Brach, M., Braibant, G., Crouzet, C., Foucher, J.C., Gautier, A., Touzelet, S., 2006. Tracer testing of the geothermal heat exchanger at Soultz-sous-Forêts (France) between 2000 and 2005. Geothermics, 35(5), 622-653.

Schaffer, M,. 2013. On the Possibility of Using Organic Molecules in the Characterization of Subsurface Processes. http://ediss.uni-goettingen.de/bitstream/handle/11858/00-1735-0000-001A-6C64-A/Dissertation_Schaffer_final.pdf?sequence=3. (last accessed: 26.08.2014)

Serres-Piole, C., Preud'homme, H., Moradi-Tehrani, N., Allanic, C., Jullia, H., Lobinski, R., 2012. Water tracers in oilfield applications: Guidelines. Journal of Petroleum Science and Engineering, 98, 22-39.

Shook, G.M., 2001. Predicting thermal breakthrough in heterogeneous media from tracer tests. Geothermics, 30(6), 573-589.

Shook, G.M., Pope, G.A., Asakawa, K., 2009. Determining reservoir properties and flood performance from tracer test analysis. In SPE Annual Technical Conference and Exhibition. Society of Petroleum Engineers.

Shorter, J., 1985. Die Hammett-Gleichung–und was daraus in fünfzig Jahren wurde. Chemie in unserer Zeit, 19(6), 197-208.

Stefansson, V. Ð., 1997. Geothermal reinjection experience. Geothermics, 26(1), 99-139.

Sudicky, E.A., Frind, E.O., 1982. Contaminant transport in fractured porous media: Analytical solutions for a system of parallel fractures. Water Resources Research, 18(6), 1634-1642.

Tester J.W., 1985. Inert and reacting tracers for reservoir sizing. Proc. Geothermal Program Review IV, CONF-8509142, US Department of Energy, Washington, D.C.

Tester J.W., Robinson B.A., Ferguson J.H., 1986. Inert and reacting tracers for reservoir sizing in fractured, hot dry rock systems. In: Proceedings of the. 11th Workshop on Geothermal Reservoir Engineering, Stanford University, Stanford, CA. SGP-TR-93, 149-159

Tester J.W., Robinson B.A., Ferguson J.H., 1987. The theory and selection of chemically reactive tracers for reservoir thermal capacity production. In: Proceedings of the 12th Workshop on Geothermal Reservoir Engineering, Stanford University, Stanford, CA. SGP- TR-109, 219-227

Tomich J.F., Dalton R.L. Jr., Deans H.A., Shallenberger L.K., 1973. Single-Well Tracer Method to Measure Residual Oil Saturation. Journal of Petroleum Technology / Transactions, 255, 211-218.

Ungemach, P., Antics, M., Papachristou, M., 2005. Sustainable geothermal reservoir management. In: Proceedings World Geothermal Congress 2005, Paper 0517

Veling, E., 2001. Analytical solution and numerical evaluation of the radial symmetric convection-diffusion equation with arbitrary initial and boundary data. IAHS PUBLICATION, 271-276.

WEA, 2000. World energy assessment: energy and the challenge of sustainability. Prepared by UNDP, UN-DESA and the World Energy Council United Nations Development Programme, New York. 508pp.

Wefer, G., 2010. Dynamische Erde-Zukunftsaufgaben der Geowissenschaften: Strategieschrift. MARUM.

Williams, M.D., Reimus, P.W., Vermeul, V.R., Rose, P.E., Dean, C.A., Watson, T.B., Newell, D., Leecaster, K., Brauser, E., 2013. Development of Models to Simulate Tracer Tests for Characterization of Enhanced Geothermal Systems. , PNNL-22486.

Williams, M.D., Vermeul, V.R., Reimus, P.W., Newell, D., Watson, T.B., 2010. Development of Models to Simulate Tracer Behavior in Enhanced Geothermal Systems, PNNL-19523 ; OSTI ID: 992377.

Ziagos, J.P., Blackwell, D.D., 1986. A model for the transient temperature effects of horizontal fluid flow in geothermal systems. Journal of Volcanology and Geothermal Research, 27(3), 371-397.

2 Controlled column experiments to determine the theory and sensitivity of thermo-sensitive tracers

Friedrich Maier*, Adriatik Olloni, Tobias Licha

Geoscience Centre, Dept. Applied Geology, University of Göttingen, Goldschmidtstr. 3, 37077 Göttingen, Germany

* Corresponding author

Abstract

The reinjection of abstracted thermal water is a common procedure in geothermal reservoir management. It provides several advantages e.g. disposal of geothermal wastewater, the maintenance of the reservoir strain and the reduction of the subsidence due to compaction. On the other hand, due to this practice the reservoir cools down since the extracted energy may exceed the natural heat flow. This limits the life time of a geothermal system. For an optimal reservoir management during geothermal power plant operation it is essential to locate and describe the thermal front in the subsurface. Currently, there is no method available for measuring this thermal drawdown. One promising tool to overcome this shortage is the application of thermo-sensitive tracers. Unfortunately, earlier reported field experiments failed due to inappropriate tracer compounds. Recently, new compounds were synthesized in our group with fluorescent properties allowing in-situ measurement of tracer breakthrough curves. These tracers have well known kinetic parameters, which is a prerequisite in tracking thermal fronts. According to the obtained pre-exponential factor A and the activation energy E_a of the Arrhenius law these thermo-sensitive tracers may already be used in short-term experiments (e.g. PushPull) or low temperature reservoirs (T < 100 °C). This circumstance gave us the opportunity to conduct controlled laboratory experiments with focus on tracer breakthrough curve correlation to reservoir temperature. The experimental setup consists of two consecutively connected columns, where each is heated to a certain temperature using a rapid flow water bath. Preliminary results, with sieved sand as a packing material, show a precise estimate of the applied temperature from the recorded tracer breakthrough curve. It is the first time that reliable experiments were performed to evaluate the underlying theory.

Nomenclature

α dispersivity

A pre-exponential factor

c concentration

D_0 molecular diffusion coefficient

D_l longitudinal dispersion coefficient

E_a activation energy

I ionic strength

k 1st order reaction rate

l spatial coordinate

L column length

Q pumping rate

R ideal gas constant

t time

T temperature

v interstitial velocity

2.1 Introduction

In the currently ongoing energy transition discussion, geothermal energy is considered to be one of the major potential sources for the worlds energy supply (IPCC, 2011). To enlarge the efficiency of the hereby used geothermal power plants, these facilities require a proper geothermal reservoir management. Common practice is the reinjection of abstracted thermal water, which provides a safe disposal of the geothermal wastewater, the maintenance of the reservoir strain and the reduction of the subsidence due to compaction. Unfortunately, this practice leads to a thermal drawdown in the exploited geothermal reservoir since the extracted energy exceeds the natural heat flow (O'Sullivan et al., 2010). To improve the reservoir management procedures and raise the efficiency of geothermal power generation knowledge on the thermal front's position would be extremely valuable. In the broad range of available monitoring and characterisation tools e.g. geophysical, borehole and tracer methods, none of them is currently able to measure and/or quantify the thermal drawdown directly. The best available tool today is the analysis of tracer breakthrough curves using chemically inert tracers and the thermal retardation relation to estimate the position of the thermal front (Pruess and Doughty, 2010; Shook, 2001). To overcome this shortage one promising tool are thermo-sensitive tracers. This class of tracers were proposed for the first time in the mid-eighties (Robinson et al., 1984; Tester et al., 1986). Unfortunately, earlier reported laboratory and field experiments failed due to inappropriate compounds and measurement methods (Tester et al., 1987; Kwakwa, 1988). Recently, new compounds were synthesised and tested (Nottebohm et al., 2012). Their thermal dependency is described by a pseudo first order hydrolysis reaction (Nottebohm et al., 2010). The biggest advantage of these new tracers is that they show fluorescent properties hence, it is possible to perform online measurements under in-situ conditions. In analysis of their breakthrough curve (BTC) a well studied kinetic behaviour is a prerequisite for tracking thermal fronts. Our experimental setup allows a reliable contribution in the currently ongoing discussion about the applicability and sensitivity of thermo-sensitive tracers (Behrens et al., 2009; Plummer et al., 2012). To answer the raised questions based on theoretical and numerical work this study presents results from laboratory experiments, which allow the application of thermo-sensitive tracers in flowing systems with an applied temperature field.

2.2 Experimental Design

The scope of this laboratory work is to experimentally investigate the capability of thermo-sensitive tracers. These tracers extend the possibilities of tracer tests, as they provide estimates of spatial and temporal information on the reservoir temperature evolution. Hence the experimental setup should provide possibilities to examine temporal and spatial changes of temperature. Hereby, the reduction to a limited number of processes controlling the system and well defined and adjustable boundary conditions are essential in order to obtain reliable results (Schaffer et al., 2013). Every additional process, e.g. catalysis from column filling or column material, sorption or flow field heterogeneities influences the shape of the BTC and hence, will complicate the analysis. Vice versa, every deviation from the expected BTC tells the experimenter that additional processes are present (Schaffer et al., 2013) and must be considered or suppressed by setup changes. The understanding gained from these laboratory experiments is vital for interpreting later field experiments with thermo-sensitive tracers.

2.2.1 Experimental Setup

Due to the above mentioned spatial and temporal requirements the experimental setup should be capable of providing a non-isothermal flow field. Therefore the selected experimental setup is governed by the advection-dispersion-reaction-equation,

$$\frac{\partial c}{\partial t} = D_l \frac{\partial c}{\partial l^2} - v \frac{\partial c}{\partial l} - kc \qquad (2.1)$$

where the flow field is determined by Darcy's law and the thermal dependency is given by the first order reaction rate k expressed by Arrhenius law

$$k = Ae^{-\frac{E_a}{RT}}. \qquad (2.2)$$

Note that for inert tracers $k = 0$, where all other processes are still valid. The presented results were conducted under steady state flow and isothermal conditions. That operation mode of the system, as a plug-flow-reactor, allows us initially to compare results directly with isothermal batch experiments (Nottebohm et al., 2012). This is done to gauge the system prior to more complex operations modes, e.g. applied temperature field, unsteady flow, change of flow direction and others.
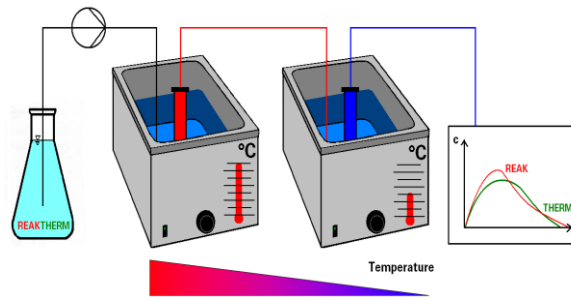
Figure 2.1: *Upper: Initial sketch of the experimental setup. From left to right the tracer solute flows from the reservoir via the pump through two differentially heated columns. At the outlet the BTC is recorded.*

Lower: Final column experimental design. From left to right the fluorescence detector connected to the PC, the pumping module, the vertically standing column setup and two temperature water reservoirs (one for each column)

The experimental system consists of three separated flow systems. On the one hand, the tracer system in which tracer solute is pumped from the tracer reservoir through two columns, mounted in separate chambers to the fluorescence detector. On the other hand, the two temperature-controlled water reservoirs which are connected to the column chambers via thermally insulated pipes. Note that each thermostat corresponds to one chamber and therefore one column only (Figure 2.1).

The core of the system comprises of two stainless steel columns 0.5 m each with $\varnothing = 3$ cm. They are coupled together in series via interconnecting pipes and are positioned vertically. The use of stainless steel ensures that the applied temperatures of the surrounding water bath is conducted into the porous media packed columns and maintain a fixed thermal boundary condition. The columns where filled with sieved sand of grain sizes between 125–250 µm. The uniform size of the sieved sand provides

a homogeneous porous media packing, which maintains its hydraulic properties over a number of experiments. It further reduces the influence of dispersion towards an ideal plug flow regime. Natural materials (e.g. reservoir sediments and sand) showed no influence on the reaction speed of hydrolysis (Nottebohm et al., 2012).

The packing was done after the slurry method which provides best results for natural materials. The packed columns are mounted coaxially in the thermally insulated column chambers (Figure 2.2). Finally the experimental core is connected to external devices (Figure 2.1):

- Two thermostats which allow differential heating/cooling of the two columns

- The pump with adjustable flow rate and back pressure control

- Fluorescence spectrophotometer together with a tempered flow-through cell allowing simultaneous online measurements of multi-compound tracer solutions.

The operating procedure of the experimental setup starts with heating the inner columns bearing the porous media packing. After regulating the temperature of the water in the temperature reservoirs, the fluid will start circulating around the stainless steel columns and transmit the heat. Then the flow through cell inside the fluorescence detector is also pre-heated to the same temperature as the outlet from the upper column, in order to maintain isothermal conditions and accurate reading (Figure 2.3). Experiments are started once the system is in thermal equilibrium. The presented results were conducted under steady state flow and isothermal conditions. The tracers to be considered are uranine as an inert reference tracer (similar to an internal standard) and phenyl acetate as thermo-sensitive tracer (Nottebohm et al., 2012). Due to the experimental design it takes almost one week to exchange the columns. Hence one aim is to maintain stable conditions, so that several thermo-sensitive tracer experiments can be conducted with one set of mounted columns.

Figure 2.2: *Installation of isothermal insulation; In gray is the column chamber surrounded by insulation (green) and coating (orange).*
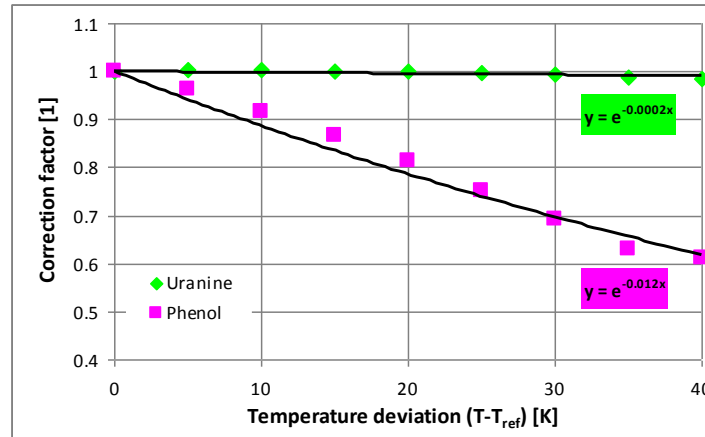
Figure 2.3: *Temperature dependency of the uranine and phenol fluorescence signals. The correction factor applies for deviations of the sample temperature from the reference temperature.*

2.3 Results

2.3.1 Hydraulic characterisation

Prior to the thermal experiments the packed columns where hydraulically characterised. This is done by classic step input tests using only uranine. Beside the estimation of the hydraulically relevant parameters (Table 2.1) e.g. effective porosity, interstitial velocity or dispersion coefficient the analysis of BTCs produced from each column separately is an inherent control that the packing is reproducible. As stated above, the transport mechanism of the tracer is dominated by advection and hydrodynamic dispersion (Equation 2.1). Hydrodynamic dispersion leads to smearing of the tracer front, or in other words a wider band of tracer residence times with higher dispersion coefficients.

Table 2.1: *Hydraulic parameters of the packed columns. The spherical glass beads provide a slightly better packing in terms of eff. porosity than sand. The columns were characterised (Q = 3 mL min⁻¹) separately as well as in the later mounted serial configuration. The R² refers to nonlinear curve fitting to the analytical solution of Equation (2.1).*

Packing	Column	Velocity $[m\,s^{-1}]$	Dispersion coefficient $[m^2\,s^{-1}]$	Eff. porosity [1]	R^2
Glass beads	1	1.83E−4	1.77E−7	0.39	.998
	2	1.76E−4	0.99E−7	0.38	.995
	1+2	1.78E−4	2.99E−7	0.39	.986
Sand	1	1.79E−4	0.50E−7	0.40	.999
	2	1.72E−4	0.46E−7	0.40	.998
	1+2	1.76E−4	0.50E−7	0.40	.999

As the end concentration of thermo-sensitive tracers depend on the residence time in the system maximizing the Peclet number

$$Pe = \frac{vL}{D_0 + \alpha v} \tag{2.3}$$

is essential in order to ease the analysis. For the presented experimental system molecular diffusion can be neglected since D_0 is in the order of 1E−9 whereas αv is of order 1E−7. With a total of one meter column length the system is clearly advection dominated since *Pe* is in the order of 1000. Systems with high *Pe* numbers show a sharp and fast breakthrough with a small bandwidth of tracer residence time. This allows in turn estimating a mean residence time for the analysis of the BTC.

2.3.2 Isothermal experiment - Static batch experiments

The solute to be used in the column experiments contains phenyl acetate (c = 10 mg L⁻¹), uranine (c = 0.05 mg L⁻¹) and phosphate buffer (I = 0.014 mol L⁻¹, pH = 7). Note that the hydrolysis product of phenyl acetate is measured, since phenol has fluorescent properties but not its ester. Here uranine will be used as reference compound as it is stable and inert under the applied temperature conditions. The adjusted pH = 7 allows the comparison with the results from Nottebohm et al. (2012). Note that the kinetic parameters are extremely sensitive to the pH. For any decrease of pH by 1 unit, between pH = 6–8, the reaction rate of the reactive tracer reduces approximately one order of magnitude (Nottebohm et al., 2012). The buffer is used to maintain a constant pH of the solute, hence to maintain a stable dependency of reaction rate on temperature (Equation 2.2). The kinetic parameters, for the used pH of the solute where Ea = 77 kJ mol⁻¹ and ln A = 25.5 h⁻¹ (Nottebohm et al., 2012). These parameters
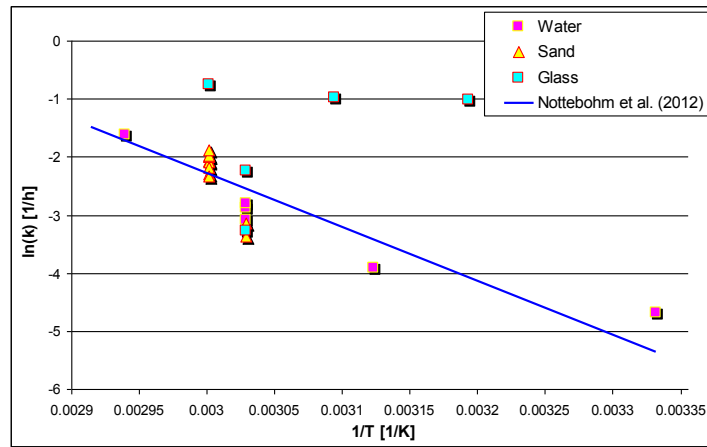
Figure 2.4:   The obtained reaction rates of the used tracer solute and tracer solute / sand mixture matches the values obtained from Nottebohm et al. (2012), in contrast reaction rates from the tracer solute / glass beads mixture are clearly of the line.

where verified again for the used tracer solute and packing material using batch experiments. For sand a small scattering around the values reported by Nottebohm et al. (2012) of the estimated reaction rates was obtained (Figure 2.4). This demonstrates the quality and robustness of the data set presented in Nottebohm et al. (2012). In addition to the sand as packing material glass beads of comparable size were also tested. Their spherical shape combined with their smooth surface leads to even better packing (Table 2.1) as well as reproducible hydraulic conditions between experiments. However, it turned out that the artificial material showed a higher reaction rate then natural materials (Figure 2.4). Therefore the data transferability to geothermal systems may be limited.

2.3.3 Isothermal experiment - Dynamic column experiments

Initially, isothermal experiments were conducted for system temperatures of 40, 50 and 60 °C with various pumping rates. Under these isothermal conditions it was possible to obtain the fundamental relationship of phenyl acetate concentration to tracer residence time according to the decay equation which states that for longer residence times more thermo-sensitive tracer reacts (Figure 2.5). Furthermore the temperature dependency is clearly seen, which states that for higher temperature, the reaction rate is higher and hence more thermo-sensitive tracer reacts. By applying Equation (2.2) the obtained tracer concentrations can be transformed into a system temperature estimate (Table 2.2). The system temperature estimates show a high accuracy and in the case of sand packing a very good reproducibility.
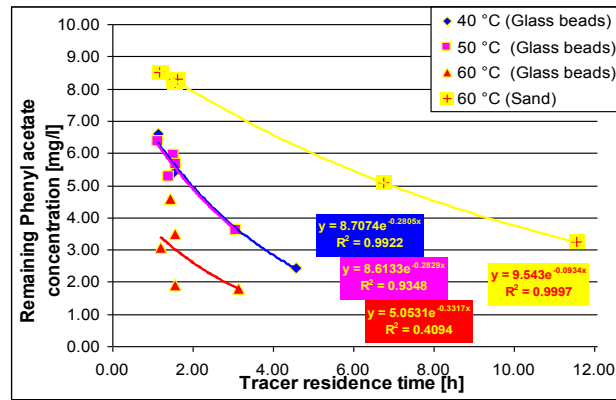
Figure 2.5: *Relation between residence time and tracer reaction for different isothermal temperatures*

Table 2.2: *Comparison of the estimated temperature with the applied temperature. The sand packing provides precise estimates for single experiments. Due to more scatter (Figure 2.5) the glass packing was analysed using mean values for the reaction rate (n = 3,5,4 for T = 40,50,60 °C).*

Packing	Q [mL min⁻¹]	residence time [h]	T estimated [°C]	T applied [°C]
Sand	0.4	11.56	59.7	60
	0.7	6.76	60.0	60
	3.0	1.57	62.8	60
	3.0	1.51	62.5	60
	3.0	1.62	61.5	60
	4.0	1.19	63.7	60
	4.0	1.18	63.6	60
	Mean value		62.0 ± 1.6	60
Glass beads	Mean values		40.5 ± 16	40
			48.5 ± 15	50
			63.0 ± 5	60

2.4 Conclusions

During the last decades, thermo-sensitive reactive tracers are considered as a method to obtain in-situ information about geothermal reservoir temperature and temperature evolution. In theory, the reaction rate is proportionally related to the temperature of the reservoir. Hence the measured concentrations are a function of temperature and residence time. Based on the relationship an evaluation of the thermal drawdown of geothermal reservoirs should be possible. This work contributes experimental results to the ongoing discussion.

This laboratory work is the first successful experimental trial, known so far, to validate the underlying theory in a flow system. The two main assumptions that for longer residence times and higher temperatures more thermo-sensitive tracer reacts are proven. Furthermore we obtain a high accuracy and good reproducibility of the estimated

system temperature. The outcome from the experiments has validated the proportionality of the reaction rate to the temperature of thermal sensitive tracers. The residence time alone was the driving factor that determined the end concentration, and thus the system temperature, when the system was operated under isothermal conditions. Furthermore it turned out that for a reliable analysis of thermo-sensitive tracers and therefore better understanding of the investigated systems, the simultaneous injection of an inert reference tracer is essential. The inert tracer provides comparable spatial and temporal information and hence the combined analysis allows an improved specification of influences e.g. dispersion, retardation, flow path heterogeneities, tracer loss etc. which are important for the analysis. Such influences must be considered and cannot be detected by tracer tests using only thermo-sensitive tracers.

The use of artificial material (glass beads) showed that the estimation of the system temperature is possible, but due to very different kinetic constants, possibly caused by catalytic effects from the glass beads, the transferability to geothermal systems is limited. The use of glass beads for testing thermo-sensitive tracers based on hydrolysis is not recommended. Further experiments will be conducted with sand filled columns.

The experimental setup allows examining the influencing processes on thermo-sensitive tracers as it provides known boundary conditions e.g. temperature, pumping rate, geometry and material properties. Next steps planned are the analysis of a wider temperature spectrum as well as the application of non-isothermal temperature fields. Additionally, the application of different compounds and multi-compound experiments is considered. Finally, the experimental setup aims to contribute solving questions about sensitivity in terms of temperature front estimation and interpretability of pumping and injection schemes (Push-Pull, Slug injection etc.).

2.5 References

Behrens, H., Ghergut, I., Sauter, M., Licha, T., 2009. Tracer properties and spiking results from geothermal reservoirs. In: Proceedings of the 31st Workshop of Geothermal Reservoir Engineering, Stanford University, Stanford, CA, USA, February 9–11, 2009, SGP-TR-187.

IPCC, 2011. IPCC Special Report on Renewable Energy Sources and Climate Change Mitigation. Prepared by Working Group III of the Intergovernmental Panel on Climate Change [O. Edenhofer, R. Pichs-Madruga, Y. Sokona, K. Seyboth, P. Matschoss, S. Kadner, T. Zwickel, P. Eickemeier, G. Hansen, S. Schlömer, C. von Stechow (eds)]. Cambridge University Press, Cambridge, United Kingdom and New York, NY, USA, 1075 pp.

Kwakwa, K.A., 1988. Tracer measurements during long-term circulation of the Rosemanowes HDR geothermal system. In: Proceedings of the 13th Workshop on Geothermal Reservoir Engineering, Stanford University, Stanford, CA, USA, January 19–21, 1988, SGP-TR-113.

Nottebohm, M., Licha, T., Ghergut, I., Nödler, K., Sauter, M., 2010. Development of Thermosensitive Tracers for Push-Pull Experiments in Geothermal Reservoir Characterization. Proceedings World Geothermal Congress 2010 Bali, Indonesia, 25−29 April 2010.

Nottebohm, M., Licha, T., Sauter, M., 2012. Tracer design for tracking thermal fronts in geothermal reservoirs. Geothermics, 43, 37−44.

O'Sullivan, M., Yeh, A., Mannington, W., 2010. Renewability of geothermal resources. Geothermics, 39, 314–320.

Plummer, M.A., Palmer, C.D., Hull, L.C., Mattson, E.D., 2012. Sensitivity of a reactive tracer based estimate of thermal breakthrough in an EGS to the properties of the reservoir and tracer. In: Proceedings of the 37th Workshop on Geothermal Reservoir Engineering, Stanford University, Stanford, CA, USA, February 1–3, 2012, SGP-TR-194.

Pruess, K., Doughty, C., 2010. Thermal single-well injection-withdrawal tracer tests for determining fracture-matrix heat transfer area. In: Proceedings of the 35th Workshop on Geothermal Reservoir Engineering, Stanford University, Stanford, CA, USA, February 1–3, 2010, SGP-TR-188.

Robinson, B.A., Tester, J.W. and Brown, L.F., 1984. Reservoir sizing using inert and chemically reacting tracers. Conference: 59. annual Society of Petroleum Engineers of AIME technical conference, Houston, TX, USA.

Schaffer, M., Maier, F., Licha, T., Sauter, M. (in press). A New Generation of Tracers for the Characterization of Interfacial Areas during Supercritical Carbon Dioxide Injections into Deep Saline Aquifers: Concept for Kinetic Interface-Sensitive Tracers (KIS Tracer). International Journal of Greenhouse Gas Control, doi: 10.1016/j.ijggc.2013.01.020.

Shook, G.M., 2001. Predicting thermal breakthrough in heterogeneous media from tracer tests. Geothermics, 30, 573–589.

Tester, J.W., Robinson B.A., Ferguson J.H., 1986. Inert and Reacting Tracers for Reservoir Sizing in Fractured, Hot Dry Rock Systems. In: Proceedings of the 11th Workshop on Geothermal Reservoir Engineering, Stanford University, Stanford, California, January 21−23, 1986, SGP-TR-93.

Tester, J.W., Robinson, B.A., Ferguson, J.H., 1987. The theory and selection of chemically reactive tracers for reservoir thermal capacity production. In: Proceedings of the 12th Workshop on Geothermal Reservoir Engineering, Stanford University, Stanford, CA, USA, January 20–22, 1987, SGP-TR-109.

3 Temperature Determination Using Thermo-Sensitive Tracers: Experimental Validation in an Isothermal Column Heat Exchanger

Friedrich Maier *, Mario Schaffer, Tobias Licha

Geoscience Centre, Dept. Applied Geology, University of Göttingen, Goldschmidtstr. 3, 37077 Göttingen, Germany

* Corresponding author

Abstract

The estimation of the thermal drawdown and its spatial and temporal evolution is a major challenge in the context of geothermal reservoir management. Column experiments were performed with the aim of assessing the potential of thermo-sensitive tracers to measure prevailing in-situ temperatures of the flowed-through medium. The results from 40 isothermal experiments with different residence times and temperatures using thermo-sensitive tracers are presented. The resulting precise temperature estimates were independent from the residence time and measured concentration. Considering pH, an accuracy of up to 1 K was achieved. The underlying theory was successfully verified and the general applicability proven.

3.1 Introduction

With an estimated technical potential of up to 5000 EJ per year, geothermal energy is considered as one of the largest renewable energy resources (WEA, 2000; IPCC, 2011). Due to its widespread distribution, the challenge lays in the technical ability to exploit this huge potential (WEA, 2000). While various factors can impact geothermal power generation efficiency, one of the biggest exergy losses can be attributed to the reinjection of geothermal fluids (Yari, 2010). This practice leads to a thermal drawdown in the injection region. It also includes a potential risk of early thermal breakthrough, since the extracted energy exceeds the natural heat flow in nearly all geothermal reservoirs (O'Sullivan et al., 2010). Nevertheless, reinjection can serve a beneficial role in reservoir management as it can provide for the safe disposal of the geothermal wastewater, the maintenance of reservoir pressures and the reduction of subsidence due to compaction (Stefansson, 1997). Consequently, there is a demand for new sophisticated reservoir tools that can help to guide management procedures and improve the efficiency of geothermal power generation.

In this context, the knowledge of the thermal front position in the geothermal reservoir would provide valuable information towards quantifying the thermal drawdown and estimating the risk of early thermal breakthrough. However, all currently available monitoring and characterization techniques, e.g., geophysical, borehole and/or tracer methods lack a direct in-situ measure for quantifying this drawdown. New chemical compounds may close this gap. Today, tracer tests are an established tool, which provides an increasing number of reservoir-relevant metrics. In addition to the classical evidence of hydraulic connections, further information can be gained such as reservoir size and recharge rates (Rose et al., 1999), mean residence times and reservoir volumes (Shook, 1998). Tracer methods have become an important characterization tool for the investigation of thermal drawdown (Axelsson et al., 2005). Commonly, the analysis is based on available analytical or numerical retardation relations linking the tracer front to the thermal front in porous media (e.g. Bodvarsson 1972, Pruess and Doughty, 2010; Shook, 2001; Suzuki et al., 2014). Recently, the possibility of using the temperature signal itself as a "tracer" was discussed (Maier and Kocabas, 2013; Jung and Pruess, 2013). All existing concepts have similarities with their analyses, in that they are based on idealized assumptions with regard to geometry and used parameters. Therefore, the

obtained solutions are usually non-unique (Axelsson et al., 2005). Shook (2001) concluded that tracer test data can only be reliably analyzed when considering these narrow restrictions. The recently introduced thermo-sensitive tracers (TSTs) from Nottebohm et al. (2010) have the potential to provide a new testing routine allowing the measurement of the thermal state of a geothermal reservoir. TSTs were proposed for the first time in the Mid-1980s (Robinson et al., 1984; Tester et al., 1986), but confirmation of the capability of TSTs is still pending. Previous laboratory (Robinson et al., 1984) and field (Kwakwa, 1988) experiments can be built upon with new compounds and measurement techniques. The thermal dependence of ester compounds, as the TST tested, is based on its pseudo-first order hydrolysis reaction (Nottebohm et al., 2010) in contact with water. In this investigation, phenol acetate (PhAc) was used, as it has well defined kinetic parameters and releases the fluorescent product, phenol, allowing for online measurement (Nottebohm et al., 2012). Results from the analysis of TST column experiments are presented, providing a valuable contribution in the currently ongoing theoretically/numerically based discussion (Behrens et al., 2009; Plummer et al., 2012) on the applicability and sensitivity of TST experiments. The main focus of this work is the experimental investigation of the general behavior of TSTs in isothermal flow fields under various temperatures and flow rates.

3.2 Material and methods

3.2.1 Experimental setup of the column heat exchanger

The experimental setup provided a controlled thermal flow environment. It was designed to reduce the number of occurring processes to the lowest possible extent. As a result of this idealization/simplification, well-defined, adjustable boundary conditions were guaranteed in order to obtain reliable results (Maier et al., 2013, Schaffer et al., 2013). Figure 3.1 shows the experimental setup of the double column heat exchanger. The core of the system was comprised of two columns (preparative HPLC column, Alltech Grom GmbH, Rottenburg-Haifingen, Germany), each with a length of 50 cm and a diameter of 3 cm. The columns were mounted coaxially in vertically positioned vented chambers, where connected thermostats (F40, Julabo GmbH, Seelbach, Germany) allow for heating/cooling of the columns between 0 and 100 °C (± 0.2 °C).
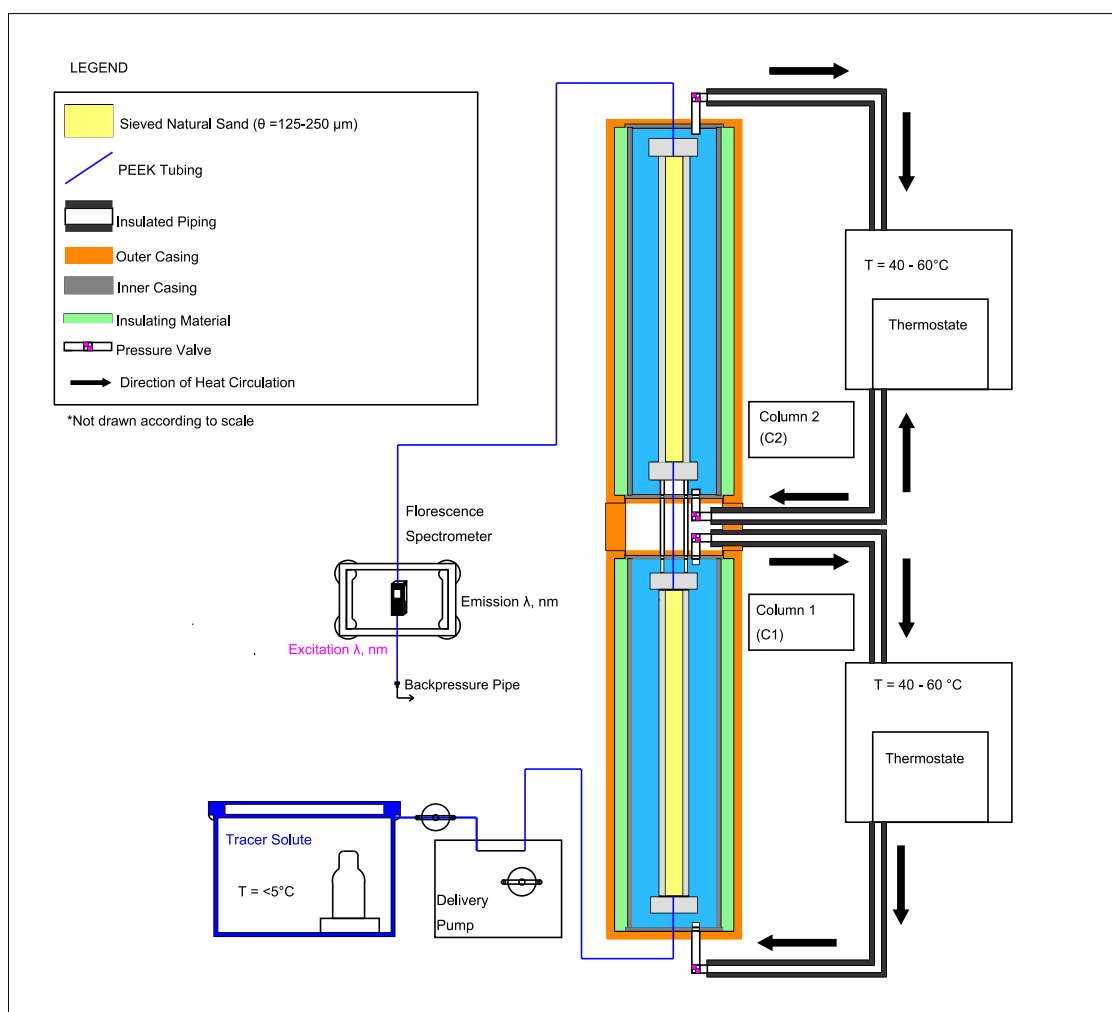
Figure 3.1: Sketch of the experimental setup.

The columns were filled with sand (Type S80, Euroquarz GmbH, Dorsten, Germany), which was sieved to grain sizes from 125–250 µm. Before filling, the sand was ultra-sonicated for several hours to reduce the turbidity and the initially alkaline sand (pH > 8) was titrated according to Niedbala et al. (2013) with an HCl solution until a neutral pH (pH = 7 at room temperature) was established. Polyether ether ketone (PEEK) tubing connected all parts of the experimental setup.

3.2.2 Chemicals

In the experiments, the carboxylic acid ester phenol acetate (PhAc) was used as a TST tracer. PhAc undergoes a hydrolysis reaction in aqueous media. A 0.01 M aqueous N,N-bis(2-hydroxyethyl)-2-aminoethanesulfonic acid (BES, CAS: 10191-18-1) buffer solution (pH = 7 at room temperature) containing 5 g L^{-1} NaCl was used as the working fluid. The addition of NaCl is intended to reduce microbial activity during the experiments. For the tracer experiments, 0.4 mg L^{-1} of the conservative reference tracer 2-OH-3,6-NDS (CAS: 135-51-3) (Nottebohm and Licha, 2012) purchased from TCI

Europe, Zwijndrecht, Belgium and 10 mg L^{-1} PhAc (CAS: 122-79-2) from Acros Organics, Geel, Belgium were added to the solution. PhAc was chosen as the TST because it meets the following requirements: well known reaction kinetics, availability of the corresponding kinetic parameters Ea and A, and suitable reaction speed for the dimensioning of the columns and experimental setup. After each TST experiment, the system was flushed with the buffer solution containing the biocide NaN$_3$ (5 g L^{-1}) to further inhibit potential microbially induced side reactions. Prior to each subsequent tracer test, the system was flushed for a short period with the buffer solution, void of tracer to avoid quenching of the fluorescence signal by the azide anion.

3.2.3 Concentration measurement

The tracer solution was stored in a cooled water bath with a maximum temperature of 5 °C to avoid significant PhAc hydrolysis prior to injection. The solutions were pumped through the system using a HPLC pump (Pro Star, Varian GmbH, Darmstadt, Germany), allowing variable flow rates between 0 and 5 mL min^{-1}. Tracer concentrations at the column outlet were measured with a fluorescence spectrophotometer (Cary Eclipse, Varian GmbH, Darmstadt, Germany) in a peltier-thermostated (± 0.1 °C) 80 µL flow-through cell (Type 583F flow through, Starna Scientific Limited, Hainault, England), allowing the simultaneous detection of multi-compound tracer solutions. Due to the fluorescent properties of 2-OH-3,6-NDS and the PhAc reaction product, phenol, the breakthrough curves (BTCs) can be recorded in real time. The constant tracer input allows for direct analysis after a constant concentration of the measured compounds at the column outlet is established (Figure 3.2) whereas dispersion must be considered for the analysis of pulse injections. Concentrations were measured at the effluent temperatures. Hence, to account for the different thermal dependencies of the fluorescence signal, the more robust signal ratio of the two tracers was calibrated. The reliability of TST experiments is significantly improved by using at least one conservative tracer as an internal reference standard. This has several advantages as it resolves secondary dilution processes, e.g. dispersion, allowing the estimation of the effective reservoir temperature (T_{eff}) from the difference between conservative tracer and TST concentrations.
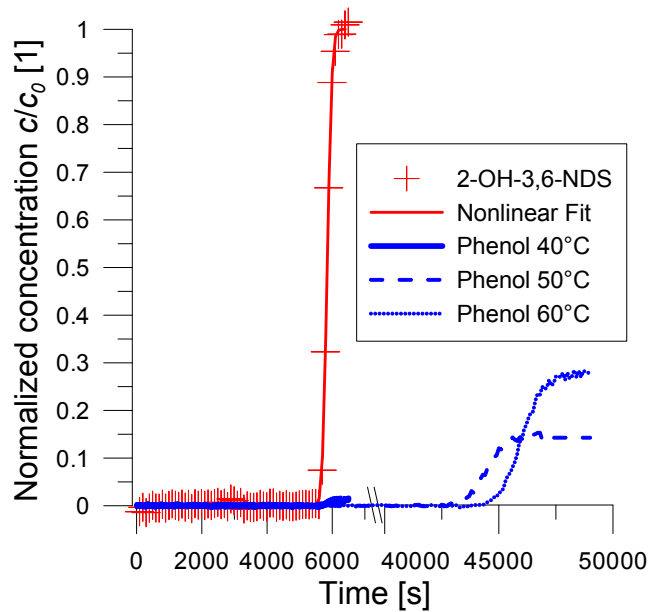
Figure 3.2: Breakthrough curve of a conservative tracer (red) for the hydraulic characterization with $Q = 3 \, mL \, min^{-1}$. The corresponding lowest obtained phenol concentration with $Q = 3 \, mL \, min^{-1}$ and $T = 40 \, °C$ is shown. For longer residence times, the resulting phenol concentrations for $Q = 0.4 \, ml \, min^{-1}$ and two different thermal setups are displayed. For the analysis of the continuous injection experiments, the mean residence time is derived at c(Phenol) = 0.5 and the concentration after reaching steady state conditions. Only every 10th recorded data point is plotted.

Initially, 21 isothermal continuous injection experiments at temperatures of 40 °C, 50 °C and 60 °C and different flow rates (0.2 – 3 mL min^{-1}) were conducted. To ensure repeatability, at least one replicate experiment was conducted for the same flow rate at each investigated temperature. The temperatures were chosen to ensure a reasonable range of detectable phenol concentrations. For the fastest experiments at 40 °C, on the one hand, the residence time was ~ 1.6 h, resulting in a phenol concentration slightly above the limit of detection (0.1 mg L^{-1}). On the other hand, the PhAc half-life was exceeded for the longest performed experiment at 60 °C with a residence time of ~27 h. The tracer residence time was controlled by the flow rates.

Since continuous injection experiments are usually not a feasible experimental design for field tracer tests in reservoirs where vast amounts of tracer solution would be required, 21 further experiments using tracer pulses were conducted. The pulses were again injected into 40 °C, 50 °C and 60 °C environments. The impact of pulse length and dilution due to hydrodynamic dispersion on the analysis of the resulting BTCs was examined. This was performed with a flow rate of Q = 3 mL min^{-1} and with tracer pulse lengths from 15 s to 64 min. The integral method was applied for the analysis of the tracer peaks (Käss et al., 1998). In this method, the ratio of the peak areas was used to estimate the absolute tracer concentrations and hence T_{eff}.

3.3 Governing equations and analysis of thermo-sensitive tracer experiments

3.3.1 Hydrolysis of thermo-sensitive tracers

PhAc reacts in the presence of water, forming acetic acid and phenol as daughter products. The hydrolysis of esters is a second order reaction where the rate-limiting step is the attack of OH^- (Sykes, 1988). The reaction can be reduced to a pseudo-first order reaction under constant pH-conditions (Nottebohm et al., 2012). The reaction speed is controlled by the ambient temperature following Arrhenius' law:

$$k = A \cdot e^{-\frac{E_a}{R \cdot T}} \tag{3.1}$$

where A is the pre-exponential factor, E_a is the activation energy, R is the universal gas constant, k is the reaction rate and T is the absolute temperature. The pH dependence of the reaction (e.g., Bender, 1960; Sykes, 1988) must be considered to account for the pH of the geothermal system being investigated. The pH of a geothermal reservoir can vary (Arnórsson et al., 1982; Adams, 1985; Durst and Vuataz, 2001; Andre et al., 2006), but geothermal reservoirs usually have a high buffer capacity due to dissolved minerals and CO2, providing stable pH conditions (e.g. Chiba, 1991; Pang and Reed, 1998).

3.3.2 Column flow and tracer transport

Due to the large length to diameter ratio of the serially connected columns (~ 33), tracer transport is assumed to be one-dimensional. Therefore, it can be described by means of the one-dimensional advection-dispersion-reaction-equation:

$$\frac{\partial c_i}{\partial t} = D_x \frac{\partial^2 c_i}{\partial x^2} - v \frac{\partial c_i}{\partial x} - R_i \tag{3.2}$$

where c_i is the tracer concentration, t the time, x the spatial coordinate, D_x the longitudinal dispersion coefficient, v the pore water velocity and R_i the sink/source term related to the kinetic reaction properties of the tracer/product. For the pseudo-first order TST reaction R_i in Equation (3.2) is described as:

$$R_i = \pm k c_i \tag{3.3}$$

For the conservative reference tracer Ri is neglected. The hydraulic characterization of the columns is based on the BTC of 2-OH-3,6-NDS. The obtained BTCs (Figure 3.2) were fitted to the analytical solution of Equation (3.2) using the nonlinear optimization

Table 3.1: *Hydraulic parameters of the packed single and serially connected columns.*

Column	α [mm]	n_e [1]
1	0.264 ± 0.012	0.413 ± 0.001
2	0.233 ± 0.014	0.414 ± 0.001
1+2	0.253 ± 0.057	0.412 ± 0.001

procedure of the CXTFIT code (Toride et al., 1995) implemented in the program package Stanmod (Version 2.08, Simunek et al., 1999). The resulting hydraulic parameters (effective porosity (n_e) and dispersivity (α)) are provided in Table 3.1. The scale independent results for single and double columns and the good fitting quality indicate that the packed sand (bulk density: 1.56 g cm^{-3}) provides a nearly isotropic flow domain.

For the serially connected columns with a total length of 1 m (L), a strongly advection-dominated flow pattern was observed, since the Peclet number:

$$Pe = \frac{L}{\alpha} \tag{3.4}$$

is on the order of 4000. Due to low hydrodynamic dispersion, the BTC has a sharp and virtually symmetrical shape. Consequently, with sufficient data resolution, the mean residence time (or center of mass) can be accurately estimated with:

$$t_{residence} = \begin{cases} t\left(\dfrac{c_{max}}{2}\right) \\ t(c_{max}) \end{cases} \quad \text{for} \quad \begin{array}{l} \text{continuous injection} \\ \text{pulse injection} \end{array} \tag{3.5}$$

3.3.3 Concept of effective temperature

The estimated effective temperature is defined here as a corresponding temperature, describing the state of the exploited reservoir assuming isothermal conditions in the analysis. The analysis is based on the solution of the decay equation, describing the pseudo-first order hydrolysis reaction. With two experimentally accessible parameters, namely duration of the experiment and the ratio of outflow/inflow concentrations, the effective reaction rate (k_{eff}) of the applied TST can be determined from the relationship:

$$k_{eff} = -\ln\left(\frac{c(t)}{c_0}\right)\frac{1}{t} \tag{3.6}$$

To account for dilution processes, the observed concentrations were referenced to the signal of the accompanied conservative tracer. The estimated k_{eff} can be transformed into the corresponding T_{eff} using Equation (3.1). For the estimation of T_{eff}, the kinetic parameters E_a and A are required. Nottebohm et al. (2012) published these parameters for selected TSTs, including PhAc in the pH range between 6 and 8. Since the ester hydrolysis reaction speed is pH dependent and the organic buffer solution applied in the column experiments to control the pH conditions shows a stronger pH dependence on temperature than inorganic buffers, such as the phosphate buffer applied by Nottebohm et al. (2012), their data cannot be used directly. However, they were used to derive pH correlation functions. In doing so, the kinetic parameters are assumed to be continuous over the considered pH range (Figure A1) and the data from Nottebohm et al. (2012) were fitted with a quadratic function (Maier at al. 2014). Running the system as an isothermal plug-flow-reactor allows direct comparison of the results with isothermal batch experiments published by Nottebohm et al. (2012) and verifies the data transferability from static to dynamic experiments (Maier et al., 2013).

3.4 Results and discussion

3.4.1 Continuous injection

For deriving the temperatures by (Equations (3.1) and (3.6)), a uniform pH of 7 was initially assumed. This pH also represents the pH of the tracer solution at room temperature, but obviously neglects the temperature dependence of the pH in the experimental system. However, the calculated temperature estimates show a high precision but a low accuracy compared to the applied temperatures (Figure 3.3). Furthermore, the systematic offset of the linear relationship between the estimated and applied temperatures allow already relative estimates of different system temperatures. To increase accuracy, the temperature dependence of the pH was measured in the effluent of the columns in a second step. A constant pH gradient of 0.015 K^{-1} was obtained, confirming the value of 0.016 K^{-1} from Good et al. (1966) for the BES buffer. The required kinetic parameters E_a and A in Equation (3.1) were adapted based on the pH correlation functions derived from the independent dataset in Nottebohm et al. (2012) (Maier et al., 2013; Figure A1). As a consequence, the accuracy could be improved and the resulting T_{eff} deviates only between 1.0 – 3.9 K (Table 3.2, Figure 3.3) from the applied temperatures.
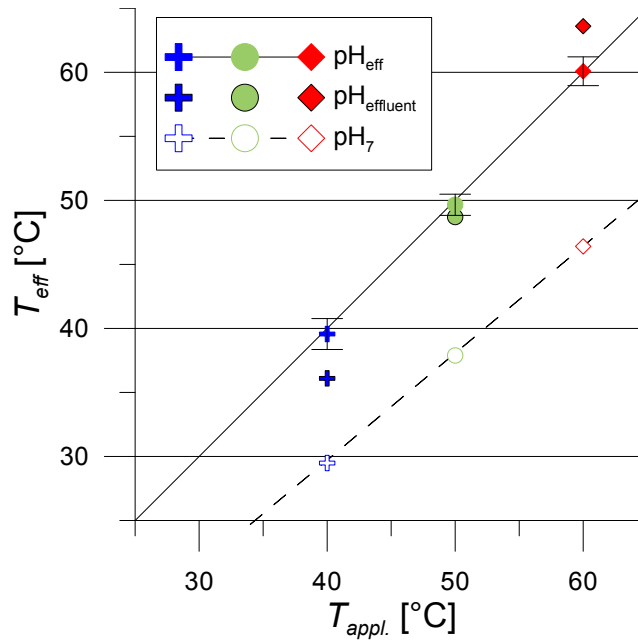
Figure 3.3: Relationship between the estimated and applied temperatures for the continuous injection experiments. While the initial temperature estimates for an assumed pH = 7 show a systematic offset, the applied pH correction results in accurate and precise absolute values. The error bars apply to all data points.

Table 3.2: Summarized results of the experiments. The pH_{eff} for 40 °C and 50°C was obtained from the optimization analysis (Equation 3.7). 60°C pH_{eff} is extrapolated from the resulting gradient between 40°C and 50°C. The SD of T_{eff} (pH_{eff}) applies to all temperature estimates.

Applied T [°C]	k_{eff} [h^{-1}]	T_{eff} (pH$_7$) [°C]	T_{eff} (pH$_{effluent}$) [°C]	T_{eff} (pH$_{eff}$) [°C]	# of Experiments [1]
Continuous Injection					
40	0.006 ± 0.001	29.5 (7)	36.1 (6,74)	39.0 ± 1.7 (6,60)	5
50	0.014 ± 0.001	37.9 (7)	48.7 (6,58)	49.5 ± 0.8 (6,56)	7
60	0.031 ± 0.003	46.4 (7)	63.6 (6,43)	60.4 ± 1.2 (6,52)	7
Pulse Injection					
40	0.007 ± 0.001	30.6 (7)	36,4 (6,74)	40.2 ± 0.8 (6,60)	8
50	0.015 ± 0.001	38.4 (7)	49.0 (6,58)	49.8 ± 0.9 (6,56)	7
60	0.029 ± 0.002	45.8 (7)	62.9 (6,43)	59.7 ± 1.0 (6,52)	6

For reservoirs, where the in-situ pH cannot be estimated due to dilution and degassing during production (Pang and Reed, 1998), the effective reservoir pH (pH$_{eff}$) can be inversely fitted. In this case, the average pH$_{eff}$ for the T range can be derived using an optimization procedure applied to the calculated ln(k_{eff}) against the inverse temperatures (Figure 3.4) using the relationship:

$$\ln(k) = \frac{E_a(pH_{eff})}{R} \cdot \frac{1}{T} + \ln(A)(pH_{eff}) \tag{3.7}$$

where $E_a(\text{pH}_{\text{eff}})$ and $\ln(A)(\text{pH}_{\text{eff}})$ are the correlation functions (Maier et al., 2013; Figure A1) derived from the data published by Nottebohm et al. (2012). Note that the measured reaction rates have a slightly different slope than the regression predicted for a constant pH (Figure 3.4). This tilt can be explained by the omission of the pH-T dependence when only one pH_{eff} is applied for all T values. Hence, the pH-T relation leads to relatively different reaction rates at lower and higher temperatures. The estimated (average) pH_{eff} of 6.56 coincides with the measured pH range of 6.74 – 6.43 (40 – 60 °C) in the effluents. For practical reservoir applications, therefore, the pH_{eff} could be estimated by interwell tracer tests in the weakly disturbed system prior to production and/or with push-pull measurements in the nearly isothermal vicinities of the used wells. As an extension to the inverse fitting, the pH_{eff} can be determined for different temperature setups. Consequently, individual pH_{eff}-T relationships can be calibrated. Using the 40 °C and 50 °C measurements in Equation (3.7), for example, a system specific damping of the pH gradient to -0.004 pH K^{-1} is obtained in this temperature range. This empirically derived pH_{eff} gradient was successfully extrapolated to account for the 60 °C experiments. Several influencing factors may cause the observed damping. First, the sand surfaces in the columns may locally influence the k_{eff} and the calculated pH_{eff} due to catalytic effects. Second, the results are sensitive to uncertainties in the kinetic data E_a and A used for the transformation of k_{eff} into T_{eff} (Figure 3.3). Hence, the identified pH_{eff}-T relationship takes all systematic errors into account. Therefore, its calibration provides an important basis for more complex experiments that consider, for example internal thermal gradients or other non-isothermal environments (Maier et al., 2014). As a result of the system-specific pH adaptions, very accurate estimates within ~1 K for all applied temperatures can be achieved (Table 3.2).For a single experiment, the temperature deviations commonly fluctuated up to ~2 K, while very few outliers showed a deviation of up to 4.5 K. (Figure 3.5) A statistical analysis of several independent experiments showed a reduction of the standard deviation (SD) to ~1 K with a rapid decrease in uncertainty for repeated experiments (Figure A2). The estimated temperatures are independent of the applied injection rates and tracer residence times (Figure 3.5). For the worst-case scenario (Figure A2), where the analyzed experiments are arranged by their deviation in descending order, an accurate value was always reached within three experiments. In contrast, the SD converges after four to five realizations. Based on this result, the realization of at least three independent TST experiments is recommended.
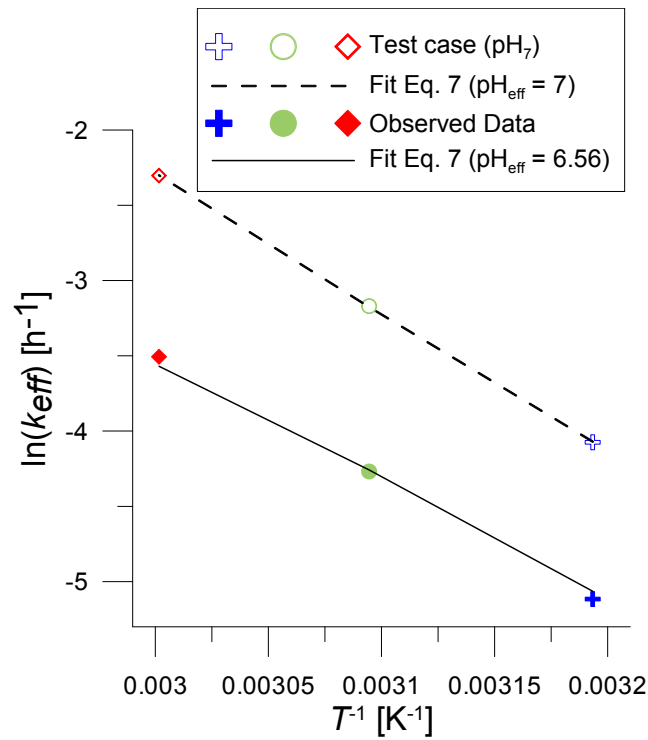
Figure 3.4: Fitting of the obtained logarithmic reaction rates against the inverse temperature. The reaction rates in the BES buffered system indicate precise results but with a systematic offset compared to an assumed test case. The calculated reaction rates are derived from the data of Nottebohm et al. (2012). The application of the dependent linear fit (Equation (3.7)) reveals the pH_{eff} shift to 6.56 due to the used BES buffer and thus enables the correction of the pH influence. The small tilt of the observed data compared to the dependent linear regression is hereby explained by a pH-T relation introduced with the used BES buffer.
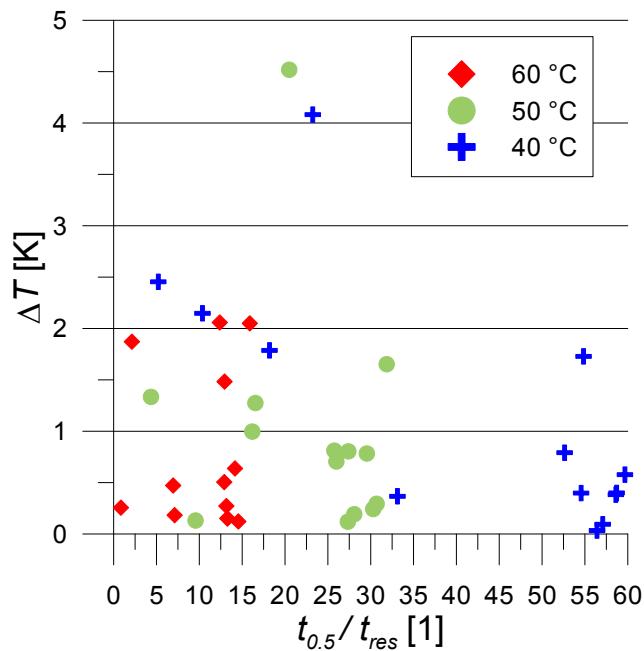
Figure 3.5: Absolute temperature deviation of all single experiments. The results show no dependence of the residence time or tracer concentration on the precision of the temperature estimates.

3.4.2 Pulse injection

Similar to the results from continuous injection experiments, the temperature estimates for single pulses varied by up to ~2 K from the expected temperature (Figure 3.6). Bias from the pH influence was also observed. The injection of several consecutive pulses from one tracer solution led to highly reproducible results. The observed fluctuations for the temperature estimates were always ≤1 K SD (Table 3.2). For very short injection lengths (t < 1 min), the decreasing signal to noise ratio resulted in slightly worse predictability of the temperature (Figure 3.6). This illustrates the possible wide range of the BTC analysis, only limited either for no or complete TST decay when neglecting secondary dilution processes. Reaching these limits, the relevant information is hidden in the background or saturation noise, respectively. With the injection of tracer pulses, in contrast to the continuous injection experiments, dispersion cannot be neglected in the BTC analysis. While dispersion introduces additional dilution (see Equation (3.2)), the analysis benefits from the increasing phenol concentration with longer residence times. The generation of the reaction product during the experiment results in an advantageous (higher) height-to-width ratio of the evaluated peak. This is in contrast to tracers, which are evaluated based on their declining signal (Rose and Clausen, 2014). The reproducibility of the dispersion coefficients was confirmed by a nonlinear optimization of the single BTC to the analytical solution of Equation (3.2).
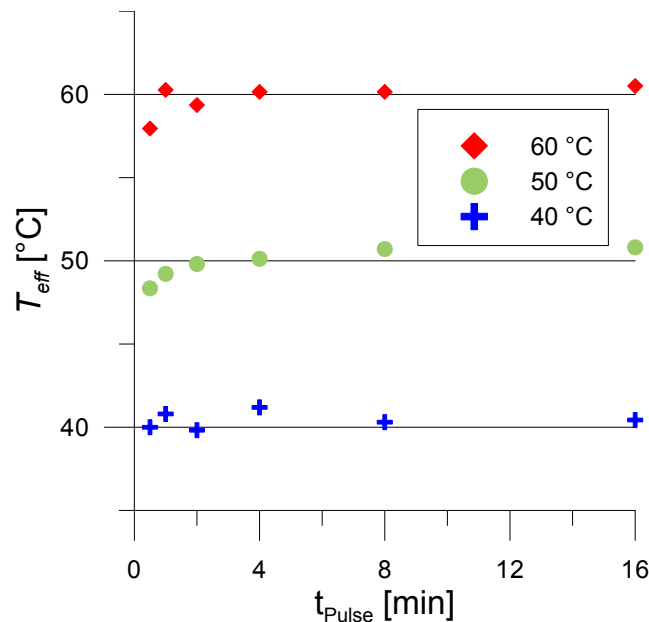
Figure 3.6: Temperature estimates of several tracer pulse injections. The relation of the pulse length, reaction speed and residence time must be sufficient to avoid inaccuracies due to a decreasing signal to noise ratio (compare first data point for a pulse length of 30 s at 50 and 60 °C).

Thus, the identical transport properties of PhAc, phenol and 2-OH-3,6-NDS in the flow field facilitate the analysis. Therefore, dispersion effects are inherently considered when the ratio of the corresponding signals is used in the analysis. For continuous injection with $Q = 3$ mL min^{-1}, a smearing of the tracer front width of up to ~9 min was observed. Consequently, a pulse length of $t > 16$ min led to a plateau, whereas for example, the injection of a 15 s pulse at 60 °C led to noisy data with no chance of their evaluation. In general, the single pulse injections show again a very good repeatability in duplicate experiments (Table 3.2).

3.5 Summary and conclusions

In the 1980´s, thermo-sensitive tracers (TSTs) were proposed for the first time. However, no successful laboratory or field scale applications have been reported. Thus, the underlying theory, based on the combination of ester hydrolysis and transport in porous media, and its utility has remained unproven. The results presented in this paper validate the proposed fundamental theory by means of using two different injection schemes. Replicate experiments in the laboratory under identical conditions show the chemical and physical stability of the experimental setup. TSTs were found to be able to precisely detect different temperatures in the context of reservoir cooling due to reinjection. The T_{eff} was identified as a suitable measure of the relative thermal state of geothermal reservoirs. Even in environments where the pH is unknown, T_{eff} provides reliable relative estimates and, thus, has a high potential as a thermal monitoring tool. The additional consideration of the thermal dependence of pH$_{eff}$ allows correcting the data and thus gives precise and accurate system temperatures. Pulse injection reveals the hydraulically equivalent behavior between all used tracer compounds and the possible separation of contributing dilution processes. Also, the limitations of phenol acetate used as TST, in terms of minimal and maximal tracer decay, are demonstrated for different experimental durations and temperatures (T = 40 – 60 °C). The observed fluctuations of the temperature for single measurements are in the order of ~2 K. In all cases, the arithmetic mean gives accurate values for the applied temperatures when three independent measurements were conducted.

From the presented investigation the following conclusions can be drawn:

•   The concept of TST was successfully transferred from static batch experiments to dynamic flow systems.

•   The analysis of T_{eff} for esters from k_{eff} is sensitive to inaccuracies of the used pH correlation function for estimating the Arrhenius parameters.

- The pseudo-first order reaction kinetics only depend on intensive quantities, e.g., pH, temperature and concentration. This enables the transfer of the results from batch experiments to dynamic laboratory systems and most likely to reservoir scale.

- The temperature estimates are independent of residence time and measured concentration.

- For unknown pH values, relative temperature differences can be estimated. In contrast, knowledge of pH improves the accuracy tremendously. The precision of the temperature estimates was around 1 K SD.

- The use of an inert tracer with the TST is essential as it allows identification of secondary processes, e.g. retardation, dilution, tracer loss, dispersion, measurement errors etc. in the analysis.

- For a given reservoir, an individual TST must be chosen based on the ambient temperature and pH conditions as well as the expected experimental duration of the tracer test.

Acknowledgements

3.6 References

Adams, M.C., 1985. Tracer stability and chemical changes in an injected geothermal fluid during injection-backflow testing at the East Mesa geothermal field. In Proceedings, 10th Workshop on Geothermal Reservoir Engineering, Stanford University, Stanford, CA. SGP-TR-84.

Andre, L., Spycher, N., Xu, T., Vuataz, F.D., Pruess, K., 2006. Modeling brine-rock interactions in an enhanced geothermal system deep fractured reservoir at Soultz-Sous-Forets (France): a joint approach using two geochemical codes: frachem and toughreact. LBNL-62357.

Arnórsson, S., Sigurdsson, S., Svavarsson, H., 1982. The chemistry of geothermal waters in Iceland. I. Calculation of aqueous speciation from 0° to 370 °C. Geochimica et Cosmochimica Acta, 46(9), 1513-1532.

Axelsson, G., Björnsson, G., Montalvo, F., 2005. Quantitative interpretation of tracer test data. In Proceedings, World Geothermal Congress 2010 Bali, Indonesia.

Behrens, H., Ghergut, I., Sauter, M., Licha, T., 2009. Tracer properties and spiking results (from geothermal reservoirs). In Proceedings, 34th Workshop on Geothermal Reservoir Engineering. Stanford University, Stanford, CA, SGP-TR-187.

Bender, M.L., 1960. Mechanisms of catalysis of nucleophilic reactions of carboxylic acid Derivatives. Chemical Reviews, 60(1), 53-113.

Bodvarsson, G., 1972. Thermal problems in the siting of reinjection wells. Geothermics, 1(2), 63-66.

Chiba, H., 1991. Attainment of solution and gas equilibrium in Japanese geothermal systems. Geochemical Journal, 25(4), 335-355.

Durst, P., Vuataz, F.D., 2001. Geochemical modelling of the Soultz-sous-Forêts Hot Dry Rock system. Brine-rock interactions in a deep hot fractured granite reservoir. In Proceedings, 26th Workshop on Geothermal Reservoir Engineering, Stanford University, Stanford, CA, SGP-TR-168.

Good, N.E., Winget, G.D., Winter, W., Connolly, T.N., Izawa, S., Singh, R.M., 1966. Hydrogen ion buffers for biological research. Biochemistry, 5(2), 467-477.

IPCC (2011), "IPCC Special Report on Renewable Energy Sources and Climate Change Mitigation." Prepared by Working Group III of the Intergovernmental Panel on Climate Change [O. Edenhofer, R. Pichs-Madruga, Y. Sokona, K. Seyboth, P. Matschoss, S. Kadner, T. Zwickel, P. Eickemeier, G. Hansen, S. Schlömer, C. von Stechow (eds)]. Cambridge University Press, Cambridge, United Kingdom and New York, NY, USA, 1075 pp.

Jung, Y., Pruess, K., 2013. Reply to comment by Maier and Kocabas on "A closed-form analytical solution for thermal single-well injection-withdrawal tests". Water Resources Research, 49(1), 644-646.

Käss, W., Behrens, H., Hötzl, H., 1998. Tracing technique in geohydrology (p. 581). Rotterdam: Balkema.

Kwakwa, K.A., 1988. Tracer measurements during long-term circulation of the Rosemanowes HDR geothermal system. In Proceedings, 13th Workshop on Geothermal Reservoir Engineering, Stanford University, Stanford, CA, SGP-TR-113.

Maier, F., Kocabas, I., 2013. Comment on "A closed-form analytical solution for thermal single-well injection-withdrawal tests" by Jung and Pruess. Water Resources Research, 49(1), 640-643.

Maier, F., Olloni, A., Licha, T., 2013. Controlled column experiments to determine the theory and sensitivity of thermo-sensitive tracers. In Proceedings, 38th Workshop on Geothermal Reservoir Engineering, Stanford University, Stanford, CA, SGP-TR-198.

Maier, F., Schaffer, M., Nur, Nnjie, S., Licha, T., 2014. Ability of thermo-sensitive tracers for precisely estimating system temperatures in column experiments with thermal gradient. In Proceedings, 39th Workshop on Geothermal Reservoir Engineering, Stanford University, Stanford, CA, SGP-TR-202.

Niedbala, A., Schaffer, M., Licha, T., Nödler, K., Börnick, H., Ruppert, H. Worch, E., 2013. Influence of competing inorganic cations on the ion exchange equilibrium of the monovalent organic cation metoprolol on natural sediment. Chemosphere, 90(6), 1945-1951.

Nottebohm, M., Licha, T., Ghergut, I., Nödler, K., Sauter, M., 2010. Development of thermosensitive Tracers for push-pull experiments in geothermal reservoir characterization. In Proceedings World Geothermal Congress 2010 Bali, Indonesia.

Nottebohm, M., Licha, T., 2012. Detection of naphthalene sulfonates from highly saline brines with high-performance liquid chromatography in conjunction with fluorescence detection and solid-phase extraction. Journal of chromatographic science, 50(6), 477-481.

Nottebohm, M., Licha, T., Sauter, M., 2012. Tracer design for tracking thermal fronts in geothermal reservoirs. Geothermics, 43, 37-44.

O'Sullivan, M., Yeh, A., Mannington, W., 2010. Renewability of geothermal resources. Geothermics, 39(4), 314-320.

Pang, Z.H., Reed, M., 1998. Theoretical chemical thermometry on geothermal waters: problems and methods. Geochimica et Cosmochimica Acta, 62(6), 1083-1091.

Plummer, M.A., Palmer, C.D., Hull, L.C., Mattson, E.D., 2012. Sensitivity of a reactive tracer based estimate of thermal breakthrough in an EGS to the properties of the reservoir and tracer. In Proceedings, 37th Workshop on Geothermal Reservoir Engineering, Stanford University, Stanford, CA, SGP-TR-194.

Pruess, K., Doughty, C., 2010. Thermal single-well injection-withdrawal tracer tests for determining fracture-matrix heat transfer area. In Proceedings, 35th Workshop on Geothermal Reservoir Engineering, Stanford University, Stanford, CA, SGP-TR-188.

Robinson, B.A., Tester, J.W., Brown, L.F., 1984. Reservoir sizing using inert and chemically reacting tracers. Conference: 59. annual Society of Petroleum Engineers of AIME technical conference, Houston, TX, USA.

Rose, P., Goranson, C., Salls, D., Kilbourn, P., 1999. Tracer testing at Steamboat Hills, Nevada, using fluorescein and 1,5-naphthalene disulfonate. In Proceedings, 24th Workshop on Geothermal Reservoir Engineering, Stanford University, Stanford, CA, SGP-TR-162.

Rose, P., Clausen, S., 2014. The use of Amino G as a thermally reactive tracer for geothermal applications. In Proceedings, 39th Workshop on Geothermal Reservoir Engineering, Stanford University, Stanford, CA, SGP-TR-202.

Schaffer, M., Maier, F., Licha, T., Sauter, M., 2013. A new generation of tracers for the characterization of interfacial areas during supercritical carbon dioxide injections into deep saline aquifers: Kinetic interface-sensitive tracers (KIS tracer). International Journal of Greenhouse Gas Control, 14, 200-208.

Shook, G.M., 1998. Prediction of reservoir pore volume from tracer tests. In Transactions of the Geothermal Resources Council 22, 477–480.

Shook, G. M., 2001. Predicting thermal breakthrough in heterogeneous media from tracer tests. Geothermics, 30(6), 573-589.

Simunek, J., van Genuchten, M.Th., Sejna, M., Toride, N., Leij, F. J., 1999. The STANMOD computer software for evaluating solute transport in porous media using analytical solutions of convection-dispersion equation, versions 1.0 and 2.0. U.S. Salinity Laboratory, USDA, ARS, Riverside, California.

Stefansson, V. Ð., 1997. Geothermal reinjection experience. Geothermics, 26(1), 99-139.

Suzuki, A., Niibori, Y., Fomin, S.A., Chugunov, V.A., Hashida, T., 2014. Analysis of water injection in fractured reservoirs using a fractional-derivative-based mass and heat transfer model. Mathematical Geosciences, 1-19.

Sykes, P., 1988. A guidebook to mechanism in organic chemistry. 6th ed. Longman, London (Chapter 8.6).

Tester, J.W., Robinson B.A., Ferguson J.H., 1986. Inert and reacting tracers for reservoir sizing in fractured, hot dry rock systems. In Proceedings, 11th Workshop on Geothermal Reservoir Engineering, Stanford University, Stanford, CA, SGP-TR-93.

Toride, N., Leij, F.J., van Genuchten, M.Th., 1995. The CXTFIT code for estimating transport parameters from laboratory or field tracer experiments. Version 2.0." Research Report No. 137, U. S. Salinity Laboratory, USDA, ARS, Riverside, CA, 1995.

WEA, 2000. World energy assessment: energy and the challenge of sustainability. Prepared by UNDP, UN-DESA and the World Energy Council United Nations Development Programme, New York. 508pp.

Yari, M., 2010. Exergetic analysis of various types of geothermal power plants. Renewable Energy, 35(1), 112-121.

4 Determination of temperatures and cooling fractions in differentially heated media by means of hydrolysable thermo-sensitive tracers

Friedrich Maier *, Mario Schaffer, Tobias Licha

Geoscience Centre, Dept. Applied Geology, University of Göttingen, Goldschmidtstr. 3, 37077 Göttingen, Germany

* Corresponding author

Abstract

This work presents the development of improved tracer techniques for monitoring applications with the objective of estimating internal temperatures and cooling fractions in water saturated porous media. The analysis is based on reactive chemical compounds whose hydrolysis reaction allow for accurate temperature measurements. Initially, the investigated (thermo-sensitive) tracers are designed for the application in geothermal reservoir management procedures. However, other technical applications are also conceivable. Thermo-sensitive tracers are found to provide valuable information about the thermal state of the examined permeable media. This is demonstrated by means of sand packed column laboratory experiments. The special heating/cooling setup provides a defined internal temperature distribution. In this study, 70 independent experiments were performed in total. The experiments examine the tracer sensitivity and practical limitations in three different experimental schemes: flow through, moving thermal front and push pull. The results show that thermo-sensitive tracers are able to determine temperatures and cooling fractions with a high precision and accuracy.

4.1 Introduction

The efficient exploitation of geothermal energy plays an increasing role in the context of climate change (Arvizu et al., 2011). Hereby, a preferred reservoir management strategy to enhance geothermal energy extraction efficiency is the reinjection of the heat-exploited geothermal waters. Because the heat extraction usually exceeds the natural heat flow (O'Sullivan et al., 2010) the cold water injection leads to a cooling of the reservoir with the potential risk of thermal short-circuiting (Stefansson, 1997). Thus, there is a direct need for methods enhancing reservoir monitoring and characterization in order to control and mitigate this risk (Goldstein et al., 2011). One possibility are physical methods, e.g. with heat as tracer (temperature as state variable), to measure and forecast thermal drawdown (e.g. Kocabas, 2005; Maier and Kocabas, 2013). However, due to the slow propagation of the thermal front either very large injection volumes are needed or the result is only representative for the vicinity of the injection well (e.g. Ghergut et al. 2011). In contrast, chemical methods, based on the intentional injection of organic molecules, benefit from the faster mass than heat transport in porous media. For systems with a known linear relationship between solute and heat transport a relative retardation factor can be derived (Bodvarsson, 1972). Hence, with chemical tracers, showing a conservative behaviour (e.g. Rose et al. 2001), it is theoretically possible to gain early information of the thermal flow properties (e.g. Shook, 2001; Pruess and Doughty, 2010).

A very promising approach in improving reservoir management by gaining a deeper insight into the reservoir cooling state, is the use of a new and specifically developed tracer group. It would be advantageous, if they are based on already established conservative dye tracers, but their tracer properties are expanded by the incorporation of a reactant group susceptible to a known temperature-dependent hydrolysis reaction, while preserving their other advantageous properties, such as fluorescence, conservative transport and stability (e.g. Nottebohm et al., 2010). These recently developed and studied thermo-sensitive tracers (TSTs) have the potential to detect *in-situ* temperature and temperature distributions (Maier et al., 2013, 2014a, 2014b). The underlying theory of TSTs was deduced in the mid 1980s (Robinson et al., 1984; Tester et al., 1986) and led afterwards with the increasing relevance of geothermal energy to an intensive numerical/theoretical discussion (e.g. Behrens et al., 2009; Plummer et al., 2012). However, the conclusions and deductions from the governing equations describing energy (advection and conduction) and mass transport (advection and dispersion) as

well as relevant couplings in a dynamic flow system lacked of an experimental validation (e.g. Plummer et al., 2010). First experiments, applying phenol acetate (PhAc), as the TST tested, proofed the transferability of the results from isothermal static batch tests (Nottebohm et al., 2012) to isothermal dynamic flow experiments (Maier et al., 2013). A high precision and accuracy of the temperature estimates within ~2 K was obtained (Maier et al., 2014b).

Therefore, the objective of the presented work is the investigation of the tracer behaviour in non-isothermal environments under controlled laboratory conditions. The performed laboratory experiments are inspired by common field tracer test designs (continuous, pulse, and push-pull injections). A defined thermal front position was applied in order to explore the feasibility and limitations of the proposed tracer methods by a differentially heated setup. As a result, the general ability of TSTs to estimate system temperatures and cooling fractions can be assessed and valuable implications for future field tests can be derived.

4.2 Material and methods

4.2.1 Experimental design

A modified version of a previously described laboratory column setup (Maier et al. 2014b) allows examining tracer behaviour in isothermal/non-isothermal flow environments with only a minor influence of the porous matrix. The system comprises of two serially connected stainless steel columns which are filled with sieved sand (fraction between 125–250 μm) providing a homogeneous flow field. Each column is individually mounted in an insulated and vented chamber, which is connected to a thermostat. Therefore, each column can be heated individually between 0–100 °C (when using water as operating fluid) enabling a controlled temperature distribution throughout the whole system. Additional to the setup described in Maier et al. (2014b), a switching valve was installed to enable reversed flow inside the two columns. Hence, different operation modes for various tracer applications can be investigated. In the experiments, solutions containing always a conservative and a thermo-sensitive tracer were injected into the column system. All used tracers have fluorescent properties allowing online recording at the respective column outlet.

4.2.2 Chemicals

For preparing the thermo-sensitive tracer solution phenol acetate (PhAc, CAS: 122-79-2) from Acros Organics, Geel, Belgium with a concentration c of 10 mg/L was used. PhAc was chosen because it reacts relatively fast at temperatures below 100 °C resulting in reasonable experimental durations ranging from 2–24 h for each experiment. Furthermore, an extensive dataset on the hydrolysis reaction kinetcs of PhAc is available in Nottebohm et al. (2012). For internal referencing, PhAc was accompanied with $c = 0.4$ mg/L of the tracer 2-naphthol-3,6-disulfonic acid (2-OH-3,6-NDS, CAS: 135-51-3) (Nottebohm and Licha, 2012) purchased from TCI Europe, Zwijndrecht, Belgium. Sulfonic acids are known non-reactive and conservative tracers (Schaffer et al., 2013). Both tracers were dissolved in a buffered (pH = 7 at room temperature) aqueous solution containing 0.01 M aqueous N,N-bis(2-hydroxyethyl)-2-aminoethanesulfonic acid (BES, CAS: 10191-18-1) (Good et al, 1966) and 5 g/L NaCl.

4.2.3 Governing equations

The reactive transport of (thermo-sensitive) tracers in non-isothermal porous media flow can be described with a set of coupled partial differential equations. While the transport of the tracers follows the advection-dispersion-reaction-equation,

$$\frac{\partial c_i}{\partial t} = \nabla \cdot \left(D \nabla c_i \right) - \frac{\boldsymbol{u}}{\varphi} \cdot \nabla c_i + R \tag{4.1}$$

where c_i is the tracer concentration, t the time, ∇ the nabla operator, D the dispersion coefficient, $\boldsymbol{u}$ the Darcy velocity vector, φ the porosity and R a sink/source term. The temperature sensitivity is given by a (pH dependent) pseudo-first order hydrolysis reaction contributing to Equation (4.1) as follows

$$R = \begin{cases} -kc_i \\ 0 \end{cases} \quad \text{for} \quad \begin{array}{l} \text{thermo sensitive tracer} \\ \text{conservative tracer} \end{array} \tag{4.2}$$

Here k is the reaction rate expressed by Arrhenius law,

$$k = Ae^{-\frac{E_a}{RT}} \tag{4.3}$$

where A the pre-exponential factor, E_a is the activation energy, R the ideal gas constant and T the temperature. Hence, R enables the coupling of Equation (4.1) with the equation for the energy transport

$$\left(\varphi_{\mathrm{S}}\rho_{\mathrm{S}}c_{\mathrm{S,p}} + \varphi\rho c_{\mathrm{p}}\right)\frac{\partial T}{\partial t} = \nabla \cdot \left(k_{we}\nabla T\right) - \rho c_{\mathrm{p}}\mathbf{u} \cdot \nabla T + Q \tag{4.4}$$

where ρ is the fluid density, c_{p} the fluid heat capacity at constant pressure, k_{we} is the weighted thermal conductivity and Q is the heat sink/source. The subscript S denotes the solid parameters. While k_{we} is related to the conductivity of the solid, k_{S} and to the conductivity of the fluid, k_{L} by

$$k_{we} = \varphi_{\mathrm{S}}k_{\mathrm{S}} + \varphi\, k_{\mathrm{L}} \tag{4.5}$$

with the solid material's volume fraction φ_{S} related to φ by

$$\varphi_{\mathrm{S}} + \varphi = 1 \tag{4.6}$$

For the presented experiments with an applied thermal distribution the temperature is in steady state and, thus, the term on the left-hand side of Equation (4.4) disappears. Note that minor couplings due to temperature dependent material parameters etc. are not discussed.

4.2.4 *Hydrolysis of thermo-sensitive tracers*

The used TST PhAc is an ester undergoing a hydrolysis reaction in contact with water. In the first hydrolysis step under the relevant conditions existing in georeservoirs, PhAc reversibly forms an intermediate complex under the catalytic influence of OH^-. This complex irreversibly reacts in a second step with water yielding an alcohol and acid (Nottebohm et al., 2012). Due to the excess of water and at constant pH, this second order reaction (Sykes, 1988) reduces to a pseudo first-order reaction with the reaction rate expressed by Equation (4.3) (Nottebohm et al., 2012). Note that the rate limiting step of the total reaction is the formation of the intermediate complex (Bender, 1960; Sykes, 1988), which makes the reaction pH dependent. For taking this dependence into account, Maier et al. (2014b) derived pH correlation functions based on an optimization procedure applied to the obtained effective reaction rates (k_{eff}), which are defined as

$$k_{eff} = -\ln\left(\frac{c(t)}{c_0}\right)\frac{1}{t}. \tag{4.7}$$

where c_0 is the input concentration.

4.2.4.1 Concept of equivalent temperature

While in isothermal systems the possible temperature concepts are virtually identical with the applied temperatures (Maier et al., 2014b) the analysis of data with the applied non-isothermal temperature field requires the differentiation of two temperature concepts. In the first concept, k_{eff} can be simply used for the determination of the equivalent temperature T_{eq} applying Arrhenius' law (Equation (4.1))

$$T_{eq} = -\ln\left(\frac{A}{k_{eff}}\right)\frac{E_a}{R} \, . \tag{4.8}$$

This concept uses the fact that for a given input/output concentration and experimental length one equivalent isothermal temperature can be determined for the whole system. The assumption of isothermal conditions is obviously a violation of the actual non-isothermal state. Nevertheless, T_{eq} globally describes the thermal state of the considered domain and is independent from additional influences. For the evaluation of Equation (4.8), Nottebohm et al. (2012) published the required pH dependent kinetic parameters (E_a and A).

4.2.4.2 Concept of cooling fraction and mean temperature

In contrast to T_{eq}, the derivation of the mean temperature (T_{mean}) provides additional information about the spatial temperature distribution. Initially, k_{eff} is transformed into an estimate of the cooling fraction χ, relatively quantifying the cooler part of the investigated reservoir region, by applying a two temperature domain model

$$\chi = 1 - \left(A \cdot \exp(-\frac{E_a}{RT_{eff}}) - k_1\right)\frac{1}{k_2 - k_1} = 1 - \frac{k_{eff} - k_1}{k_2 - k_1} \tag{4.9}$$

with k_i the bounding reaction rates, the indices $1,2$ denote the different temperature domains (or columns in our specific experimental set-up), respectively. Note the linear dependency in Equation (4.9) of k_{eff} with the propagation of the thermal front. T_{mean} can then determined by multiplying χ with the observed injection and abstraction temperatures, respectively. Also two additional isothermal experiments may be required for determining the isothermal reaction rates $k_{1,2}$. These can be performed e.g. with fast
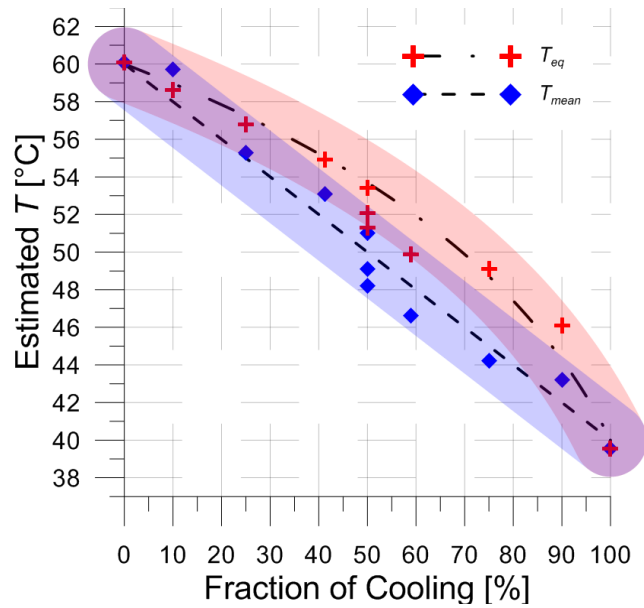
Figure 4.1: *Development of T_{eq} and T_{mean} with the fraction of cooling χ. The symbols are the obtained values and the lines represent the theoretical target. The shaded curves have a half thickness of 2 K representing the expectable temperature fluctuations of single measurements.*

Push-Pull experiments in the vicinity of the respective wells. This procedure would reduce the occurring limitations due to the pH dependency of the hydrolysis reaction. In theory, when the temperature/pH dependent reaction rates are unknown it is also possible to estimate the required isothermal reaction rates from Equation (4.3). Nevertheless, measuring $k_{1,2}$ *in-situ* leads to an inherent correction of the pH. Hence, the derived T_{mean} are automatically in the right order of magnitude.

Both temperature concepts are differently related to the fraction of cooling. Since the reaction rate is exponentially related to the determined T_{eq} of non-isothermal systems, it is shifted towards higher temperatures when compared with T_{mean} (Figure 4.1).

4.2.5 Performed tracer test experiments

In general, two main types of field tracer experiments can be distinguished: single well injection withdrawal (push-pull) and inter well experiments. For the first type, the tracer is injected and pumped back through the same well. Usually, an additional shut-in phase is placed between injection and abstraction. For the latter type, at least one additional abstraction/monitoring well is required, which is hydraulically connected to the injection well. Therefore, three general experimental and relevant operation modes were investigated in the laboratory column studies in order to address the practical applicability of thermo-sensitive tracer experiments:

1. A differential heating of the two columns with temperatures of 40 °C/50 °C, 50 °C/60 °C and 40 °C/60 °C was applied to demonstrate the applicability of the two concepts T_{eq} and T_{mean}, in non-isothermal regimes. For these, three thermal setups, 24 flow-through experiments with continuous tracer injection and 25 experiments with pulse injections were performed. These temperature differences were chosen since they provide a practical approach for the experimental set-up in a good relation between experimental time and output concentrations (Maier et al. 2014b). Further, they are in the common range of applied reinjection temperatures in German geothermal plants. For each investigated temperature distribution at least two replicate experiments were performed.

2. Additional experiments with 7 different fractions of cooling were performed in the 40 °C/60 °C setup. Here, the geometrically fixed front position was virtually moved by stopping the flow in order to simulate different fractions of cooling. For each investigated fraction of cooling two replicate experiments were performed.

3. Finally, the application of thermo-sensitive tracers in push-pull injection schemes is demonstrated. The experiments were performed with the same temperature distribution of 40 °C/60 °C. A series of three consecutive pulses, each with durations of 10 min, were injected into the first (cooler) column. Only the first two peaks reached the second (hotter) column. Additional experiments with shut-in phases of different durations, ranging between 1–512 min, compared to 20–200 min flow time of the single pulses, show their influence on the interpretation of the obtained breakthrough curves (BTCs). Again, two replicate experiments for each experiment were performed.

4.3 Results and discussion

4.3.1 Flow-through experiments

The analysis of the performed flow-through experiments with continuous injection results in precise temperature estimates (Table 4.1). The comparison of the derived temperature estimates for T_{eq} with the expected temperatures shows a systematic deviation when an arbitrary but constant pH = 7, which is also the pH of the tracer solute under room temperature conditions, is initially assumed (Figure 4.2). This is in

analogy to the findings in Maier et al. (2014b) for isothermal systems. Hence, TST experiments allow a reliable relative T_{eq} estimate even when the exact pH is unknown. Applying an effective pH gradient (-0.004 K^{-1}) obtained from independent isothermal system calibration experiments in the applied temperature range from 40–60 °C (Maier et al., 2104b) in a next step leads to accurate absolute T_{eq} results. In contrast, the estimates for T_{mean} directly provide the correct temperatures since the pH dependence is considered inherently (Figure 4.2). The obtained results from single measurements show a scattering up to 2 K, which is comparable to the isothermal results (Maier et al. 2014b).

Repeating the experiments with tracer pulses of different duration instead of continuously injecting the tracer also results in stable estimates of the two evaluated temperature concepts (Table 4.1). After considering the pH, precise estimates of T_{eq} with even smaller fluctuations than in the continuous injection case were obtained. Note that the possible discrimination of the contributing dilution processes (here reaction and dispersion, cf. Equation (4.1)) eases the analysis of the peak area ratios (Maier et al. 2014b).
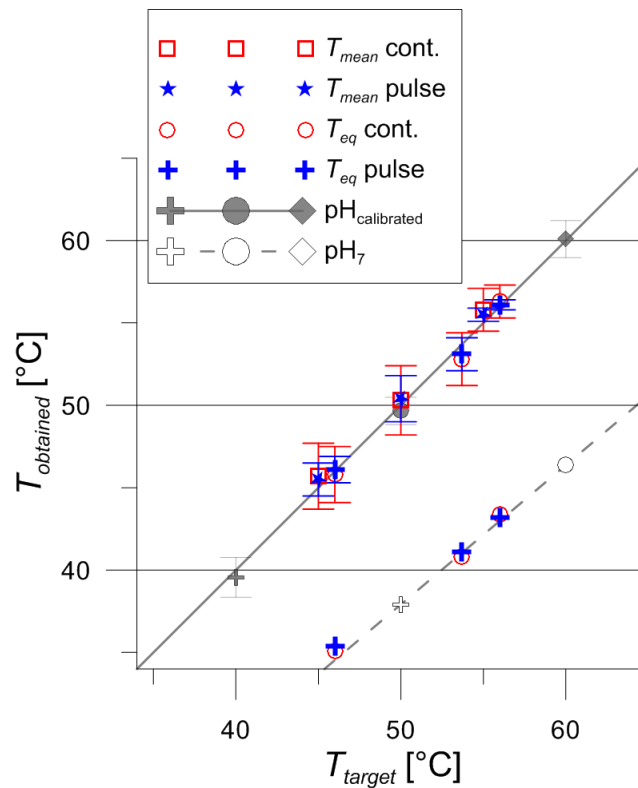
Figure 4.2: Modified plot of the obtained versus the target temperatures from Maier et al. (2014b) in grey shades. For the initial analysis of T_{eq} a pH = 7 was assumed, resulting in precise estimates with a correct systematic. The pH calibration after Maier et al. (2014b) leads to accurate estimates. In contrast, T_{mean} gives directly accurate results since the pH dependency is inherently considered (cf. Equation (4.9)).

Table 4.1: Results of the flow-through experiments for all applied temperature differences.

Applied T [°C]	Target T_{eq}/T_{mean} [°C/°C]	k_{eff} [h^{-1}]	T_{eq} [°C]	T_{mean} [°C]	χ [%]	# of Experiments [1]
Continuous Injection						
40/50	46.0/45.0	0.011 ± 0.002	45.8 ± 1.7	45.7 ± 2.0	43 ± 20	6
40/60	53.7/50.0	0.018 ± 0.003	52.8 ± 1.6	50.3 ± 2.1	46 ± 10	10
50/60	56.0/55.0	0.023 ± 0.002	56.3 ± 1.0	55.8 ± 1.3	42 ± 13	8
Pulse Injection						
40/50	46.0/45.0	0.011 ± 0.001	46.1 ± 0.8	45.5 ± 1.0	45 ± 10	10
40/60	53.7/50.0	0.019 ± 0.002	53.1 ± 1.0	50.4 ± 1.4	48 ± 07	10
50/60	56.0/55.0	0.023 ± 0.001	56.1 ± 0.3	55.5 ± 0.4	45 ± 04	5

The additionally required reaction rates of the isothermal boundaries in the estimation of χ and T_{mean} where used from the data published in Maier et al. (2014b). In further applications this can be realised by means of two push-pull experiments in the abstraction/injection well or calculated by applying Arrhenius' law using the kinetic parameters published e.g. in Nottebohm et al. (2012). Due to the additionally needed quantities/parameters, which introduce additional error sources, the evaluated T_{mean} show slightly larger deviations compared to the estimates for T_{eq} (Table 4.1). Nonetheless, the analysis for T_{mean} is suggested as it provides in addition to the information about the global thermal state of the reservoir further a measure for χ.

For the estimation of χ, two trends are found. Due to the virtually constant standard deviation (SD) of the obtained k_{eff} (Table 4.1), the uncertainty of the temperature estimates decreases slightly for higher temperatures and for larger temperature differences. Therefore, the SD of χ ranges from 04%–20% for the two injection schemes, with a slight decrease towards hotter temperatures and larger temperature differences (Table 4.1). This result is remarkable considering that the feasible precision of 2 K which is 20% or 10% of the applied small temperature differences (10 K or 20 K) promise an even higher accuracy for the larger temperature differences existing in geothermal reservoirs.

4.3.2 Moving thermal front

Initially, the obtained experimental data were modelled with Comsol Multiphysics[®] (Version 4.4; Comsol, 2013) by solving Equations (4.1) and (4.4) and using the finite element method (Figure 4.3). This simulation allows the verification of the stop flow procedure to achieve a virtually moving front (Figure 4.4). For doing so, the results

were compared with a second model, which has a spatially moving thermal front position at steady flow conditions. It reveals that there are differences of the obtained BTCs. This can be assigned to the ongoing and thus additional dispersive smearing in the latter continuous flow case compared to the stop flow case (neglecting diffusion). Nevertheless, the ratio of the peak areas which is the relevant metric in the analysis however, is equal to the experimentally achieved virtually moving front position when a stop flow is applied (Figure 4.4). As a consequence, the identical hydraulic transport properties of the used tracers (Maier et al., 2014b) allow the application of a pump stop phase to extend the residence time of the tracer in specific parts of the thermal system and thus mimic different thermal front positions. For χ a deviation of up to 7% from the expected value was obtained (Table 4.2). This deviation is within the ability of PhAc to detect system temperatures with an accuracy within 2 K, which is a tenth of the applied temperature difference of 20 K (Figure 4.1). The results also confirm the expected linear relation (cf. Equation (4.10)) between the obtained k_{eff} and χ (Figure 4.5).
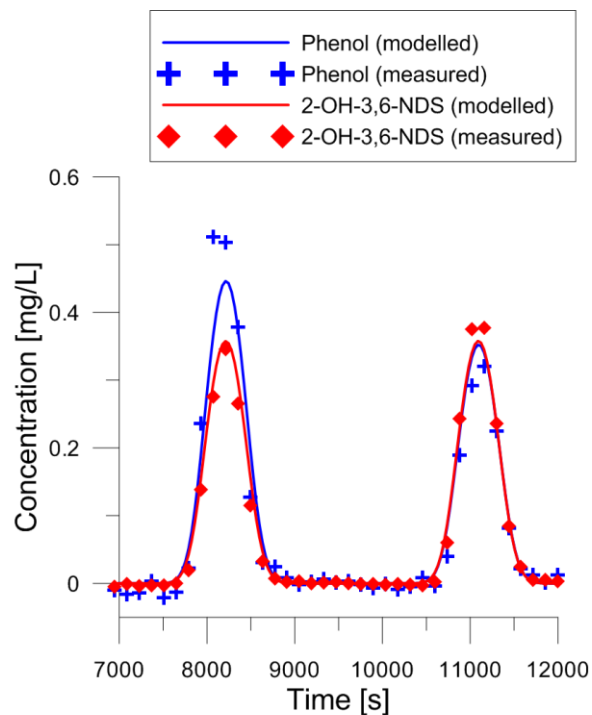
Figure 4.3: *Comparison of obtained BTC with the results of the numerical simulation. The experiment was performed with a thermal gradient between 40°C and 60°C. The first pulse was longer in the hotter column (χ = 40%) than the second pulse (χ = 60%) resulting in a higher phenol signal. Note that the signal of the inert tracer (2-OH-3,6-NDS) is equal for both pulses since the total residence time is equal.*
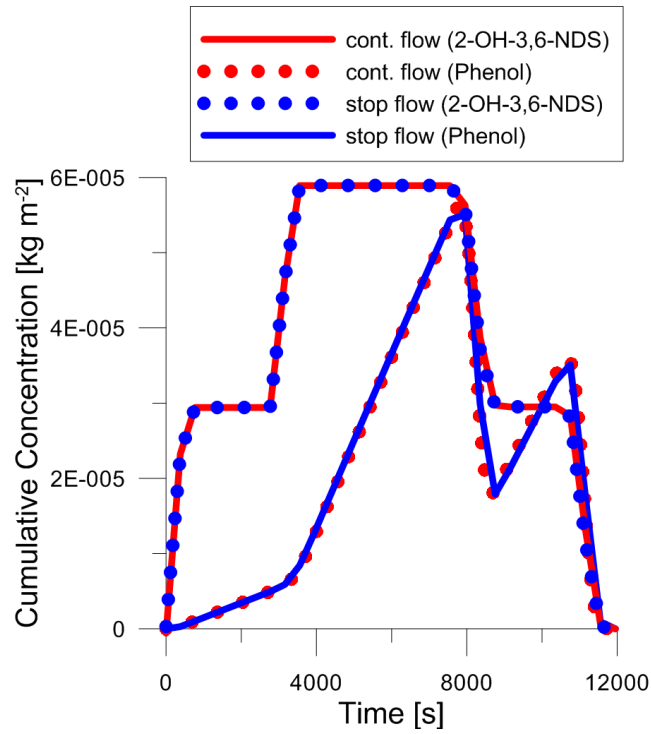
Figure 4.4: *Comparison of the cumulative concentrations of two injected pulses along the entire column length. The concentrations are shown for two different injection schemes. The data for 'stop flow' represent the performed experiment shown in Figure 4.3, while 'cont. flow' refers to a numerically simulated experiment with an identical total residence time. In contrast to the virtual movement of the thermal front in the performed stop flow experiment the second model applies a spatially moved thermal front with χ of 60% and 40%, respectively*
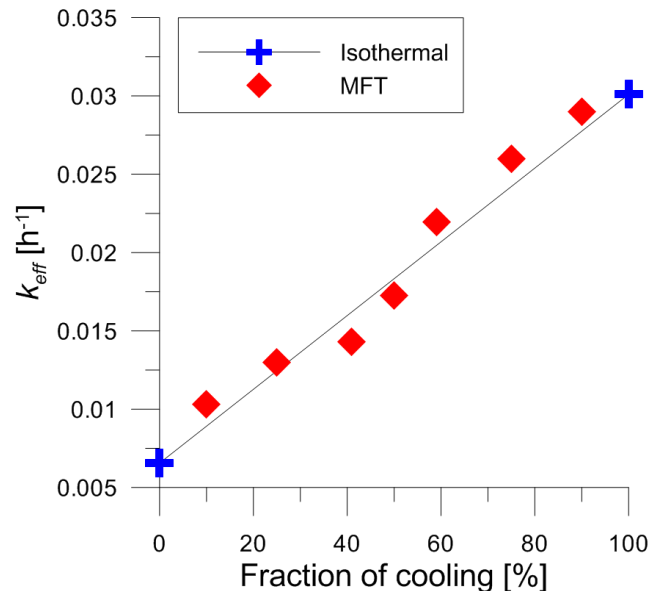
Figure 4.5: *Obtained k_{eff} for different cooling fractions (MFT). The data confirm the expected linear relation. (cf. Equation (4.9)). The limiting k_{eff} for a cooling fraction of 0 and 100% are obtained in Maier et al. (2014b).*

Applied χ [%]	k_{eff} [h^{-1}]	T_{eq} [°C]	T_{mean} [°C]	χ [%]
10	0.029	58.4	59.3	3
25	0.026	56.8	55.3	23
40	0.022	54.9	53.1	41
60	0.014	49.9	46.6	59
75	0.013	49.1	44.2	79
90	0.010	46.1	43.2	84

4.3.3 Push-Pull

From the results with a reversed flow direction it can be clearly seen which temperature zones were reached by the respective tracer pulses (Figure 4.6). The first two injected pulses reached the hotter column. The highest temperature estimates were derived for the first injected volume indicating the longest relative residence time in the hotter column. In contrast, the last of the three injected tracer pulses remained entirely in the cooler column, which is nicely reflected by the obtained temperatures in Table 4.3. Considering the additional stop flow phase, two further conclusions can be drawn. On the one hand, detailed information on the extension and position of the thermal front can be deduced from the differences in the obtained χ for the injections with short shut-in phases. On the other hand, the position between which pulse the thermal front is located can be better defined for longer shut-in phases (Figure 4.6). The analysis of the obtained BTCs was done following Equations (4.7), (4.8) and (4.9) under the assumption of a two temperature block model. Nevertheless, the scenario where the tracer is initially injected into the cold part of a reservoir and then flowing alternately through hot and cold areas (like in push-pull experiments) is different. Here, the resulting concentrations are given by

$$c_1(t_1) = c_0 e^{-k_{cold}t_1} \rightarrow c_2(t_2) = c_1 e^{-k_{hot}(t_2)} \rightarrow \ldots \qquad (4.10)$$

where the indices 1,2,... indicate the respective domains (cold/hot) of the reservoir. By rearranging Equation (4.10) to

$$c_{end}(t_{end}) = c_0 e^{-k_{cold}\sum t_{cold}} e^{-k_{hot}\sum t_{hot}} \qquad (4.11)$$

it becomes possible to apply again a two block model for the analysis. The results show that tracer flow through different temperature zones is independent from the actual

distribution of the temperature blocks. Consequently, all domains having the same temperature can be summarised and simply expressed as one block.

4.4 Conclusions

Independent from pH and knowledge of the internal flow geometry, T_{eq} was identified as a suitable relative measure for the thermal state of geothermal reservoirs. The used pH calibration from Maier et al. (2014b) leads to precise absolute temperature estimates.

Table 4.3: Results of the push-pull experiments. Column 1 has a temperature of 40 °C and column 2 of 60 °C. While the first two pulse reached both columns the last injected pulse 3 was only in the first, cooler column. Listed are the temperature estimates and the corresponding fraction in the cooler column.

Pump Stop [min]	Pulse 1 ($T_{eq}/T_{mean}/\chi$) [°C/°C/%]	Pulse 2 ($T_{eq}/T_{mean}/\chi$) [°C/°C/%]	Pulse 3 ($T_{eq}/T_{mean}/\chi$) [°C/°C/%]
1	52.5/49.7/52	48.3/45.1/75	41.0/40.0/100
20	52.3/49.3/53	49.1/45.8/71	39.2/39.1/104
128	53.3/50.7/46	53.7/51.3/43	40.2/39.6/102
256	56.5/55.8/21	55.5/54.0/30	41.0/40.0/100
512	57.0/56.7/17	55.9/54.7/26	43.3/41.2/94
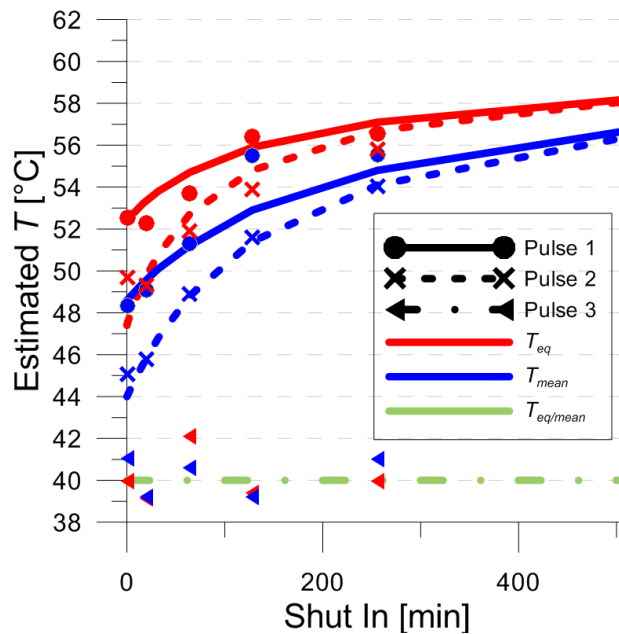
Figure 4.6: *Effect of an applied shut in of the injection pump on the obtained temperature estimates (symbols). The lines show the theoretical target temperatures. Three pulses were consecutively injected into a system with thermal distribution of 40 °C and 60 °C. After a shut-in phase of different duration the flow was reversed. While the first two injected pulses reaches the hotter column the third pulse solely remains in the cooler column.*

In contrast, from the obtained T_{mean} of the moving front and push pull experiments it becomes possible to obtain information on the thermal distribution in the considered system. For T_{mean} it was found that the results were not biased. The major advantage of the T_{mean} concept is that the information about χ is directly provided. The required reaction rates can either be measured *in-situ* by additional experiments, e.g. push-pull experiments or estimated from literature data.

The observed fluctuations of the two temperature concepts for single measurements are in the order of 2 K. Hence, with a temperature difference of 20 K the estimate for χ from push pull and moving front experiments could be estimated and is confirmed to be within 10% deviation from the true value.

From the presented work the following conclusions can be drawn:

- The concept of thermo-sensitive tracers was successfully transferred from a dynamic isothermal system to dynamic non-isothermal systems with an applied thermal distribution by differentially heated columns.

- The high precision of the estimated temperatures within 2 K indicates the potential to measure in-situ temperatures with a suitable accuracy.

- While the general thermal state of a reservoir could be determined from a single experiment using the concept of Teq, the appropriate isothermal reaction rates are required to quantify the fraction of cooling and Tmean.

- The linear scaling of the obtained keff for different thermal front positions was experimentally confirmed.

- The application of push pull experiments shows the potential to obtain fast and reliable data on the thermal state of reservoir parts. The introduction of a shut-in phase allows the adjustment on the desired target metrics.

- For push-pull applications with long shut-in phases, the resulting temperature estimates are dominated by the ambient temperature of the stop position. Also the interpretability is improved since the signal intensity increases due to the ongoing reaction but stopped hydromechanic dispersion (no additional dilution).

- The used PhAc is a suitable thermo-sensitive tracer for low temperature domains and at the laboratory scale. For the geothermal application it may be useful in

the cooled vicinity around the injection well, low temperature reservoirs or in fast experiments with low residence times, e.g. push-pull (t ≤ day).

- In principle, the characterisation of temperature distributions in water-saturated permeable media by means of thermo-sensitive tracers is conceivable for various applications in natural, medical or engineering sciences. Thermo-sensitive tracers provide a non-destructive method to probe the thermal flow systems of interest. Hence applications e.g. in chemical reactors, monolithic catalytic converters or for sensible energy storage are also imaginable.

Acknowledgements

4.5 References

Arvizu, D., T. Bruckner, H. Chum, O. Edenhofer, S. Estefen, A. Faaij, M. Fischedick, G. Hansen, G. Hiriart, O. Hohmeyer, K. G. T. Hollands, J. Huckerby, S. Kadner, Å. Killingtveit, A. Kumar, A. Lewis, O. Lucon, P. Matschoss, L. Maurice, M. Mirza, C. Mitchell, W. Moomaw, J. Moreira, L. J. Nilsson, J. Nyboer, R. Pichs-Madruga, J. Sathaye, J. Sawin, R. Schaeffer, T. Schei, S. Schlömer, K. Seyboth, R. Sims, G. Sinden, Y. Sokona, C. von Stechow, J. Steckel, A. Verbruggen, R. Wiser, F. Yamba, T. Zwickel (2011). Technical Summary. In IPCC Special Report on Renewable Energy Sources and Climate Change Mitigation [O. Edenhofer, R. Pichs-Madruga, Y. Sokona, K. Seyboth, P. Matschoss, S. Kadner, T. Zwickel, P. Eickemeier, G. Hansen, S. Schlömer, C. von Stechow (eds)], Cambridge University Press, Cambridge, United Kingdom and New York, NY, USA.

Behrens, H., Ghergut, I., Sauter, M. Licha, T., 2009. Tracer properties and spiking results from geothermal reservoirs,. In Proceedings of the Thirty-first Workshop of Geothermal Reservoir Engineering, Stanford University, Stanford, CA, USA, February 9–11, 2009, SGP-TR-187.

Bender, M.L., 1960. Mechanisms of catalysis of nucleophilic reactions of carboxylic acid derivatives. Chemical Reviews, 60(1), 53-113.

Bodvarsson, G., 1972. Thermal problems in the siting of reinjection wells. Geothermics, 1(2), 63-66.

COMSOL 2013. COMSOL Multiphysics® Version 4.4: User's Guide and Reference Manual. COMSOL Inc., Burlington, MA.

Ghergut, I., Behrens, H., Maier, F., Karmakar, S., Sauter, M., 2011. A note about "heat exchange areas" as a target parameter for SWIW tracer tests. In Proceedings of the thirty-sixth Workshop on Geothermal Reservoir Engineering, Stanford University, Stanford, California. January 31 - February 2, 2011, SGP-TR-191

Goldstein, B., Hiriart, G., Bertani, R., Bromley, C., Gutiérrez-Negrín, L., Huenges, E., Muraoka, H., Ragnarsson, A., Tester, J., Zui V., 2011. Geothermal Energy. In IPCC Special Report on Renewable Energy Sources and Climate Change Mitigation [O. Edenhofer, R. Pichs-Madruga, Y. Sokona, K. Seyboth, P. Matschoss, S. Kadner, T. Zwickel, P. Eickemeier, G. Hansen, S. Schlömer, C. von Stechow (eds)], Cambridge University Press, Cambridge, United Kingdom and New York, NY, USA.

Good, N.E., Winget, G.D., Winter, W., Connolly, T.N., Izawa, S., Singh, R.M., 1966. Hydrogen ion buffers for biological research. Biochemistry, 5(2), 467-477.

Kocabas, I., 2005. Geothermal reservoir characterization via thermal injection backflow and interwell tracer testing. Geothermics, 34(1), 27-46.

Maier, F. Schaffer, M., Licha, T., 2014b. Temperature determination using thermo-sensitive tracers: experimental validation in an isothermal column heat exchanger Geothermics (submitted, pending minor revisions)

Maier, F., Kocabas, I., 2013. Comment on "A closed- form analytical solution for thermal single- well injection- withdrawal tests" by Jung and Pruess. Water Resources Research, 49(1), 640-643.

Maier, F., Olloni, A. Licha, T., 2013. Controlled column experiments to determine the theory and sensitivity of thermo-sensitive tracers. In Proceedings of the Thirty-Eighth Workshop on Geothermal Reservoir Engineering, Stanford University, Stanford, CA, February 11-13, 2013, SGP-TR-198

Maier, F., Schaffer, M., Nur, Nnjie, S., Licha, T., 2014a. Ability of thermo-sensitive tracers for precisely estimating system temperatures in column experiments with thermal. In Proceedings of the Thirty-ninth Workshop on Geothermal Reservoir Engineering, Stanford University, Stanford, CA, SGP-TR-202.

Nottebohm, M., Licha, T., 2012. Detection of naphthalene sulfonates from highly saline brines with high-performance liquid chromatography in conjunction with fluorescence detection and solid-phase extraction. Journal of Chromatographic Science, 50(6), 477-481.

Nottebohm, M., Licha, T., Ghergut, I., Nödler, K., Sauter, M., 2010. Development of thermosensitive tracers for push-pull experiments in geothermal reservoir characterization.In Proceedings World Geothermal Congress 2010 Bali, Indonesia, 25−29 April 2010.

Nottebohm, M., Licha, T., Sauter, M., 2012. Tracer design for tracking thermal fronts in geothermal reservoirs. Geothermics, 43, 37-44.

O'Sullivan, M., Yeh, A., Mannington, W., 2010. Renewability of geothermal resources. Geothermics, 39(4), 314-320.

Plummer M.A., Palmer C.D., Hull L.C., Mattson E.D., 2010. Sensitivity of a reactive-tracer based estimate of thermal breakthrough in an EGS to properties of the reservoir and tracer. In Proceedings of the thirty-fifth Workshop on Geothermal Reservoir Engineering, Stanford University, Stanford, CA, SGP-TR-188.

Plummer, M.A., Palmer, C.D., Hull, L.C., Mattson, E.D., 2012. Sensitivity of a reactive tracer based estimate of thermal breakthrough in an EGS to the properties of the reservoir and tracer. In Proceedings of the Thirty-seventh Workshop on Geothermal Reservoir Engineering, Stanford University, Stanford, CA, USA, February 1–3, 2012, SGP-TR-194.

Pruess, K., Doughty, C., 2010. Thermal single-well injection-withdrawal tracer tests for determining fracture-matrix heat transfer area. In Proceedings of the thirty-fifth Workshop on Geothermal Reservoir Engineering, Stanford University, Stanford, CA, USA, February 1–3, 2010, SGP-TR-188.

Robinson, B.A., Tester, J.W., Brown, L.F., 1984. Reservoir sizing using inert and chemically reacting tracers. In Conference: 59. annual Society of Petroleum Engineers of AIME technical conference, Houston, TX, USA.

Rose, P.E., Benoit, W.R., Kilbourn, P.M., 2001. The application of the polyaromatic sulfonates as tracers in geothermal reservoirs. Geothermics, 30(6), 617-640.

Schaffer, M., Maier, F., Licha, T., Sauter, M., 2013. A new generation of tracers for the characterization of interfacial areas during supercritical carbon dioxide injections into deep saline aquifers: Kinetic interface-sensitive tracers (KIS tracer). International Journal of Greenhouse Gas Control 14, 200–208.

Shook, G.M., 2001. Predicting thermal breakthrough in heterogeneous media from tracer tests. Geothermics, 30(6), 573-589.

Stefansson, V.Ð., 1997. Geothermal reinjection experience. Geothermics, 26(1), 99-139.

Sykes, P., 1988. A guidebook to mechanism in organic chemistry. 6th ed. Longman, London (Chapter 8.6).

Tester, J.W., Robinson B.A., Ferguson J.H., 1986. Inert and reacting tracers for reservoir sizing in fractured, hot dry rock systems. In Proceedings of the Eleventh Workshop on Geothermal Reservoir Engineering, Stanford University, Stanford, California, January 21−23, 1986, SGP-TR-93.

5 A new generation of tracers for the characterization of interfacial areas during supercritical carbon dioxide injections into deep saline aquifers: Kinetic interface-sensitive tracers (KIS tracer)

Mario Schaffer*, Friedrich Maier, Tobias Licha, Martin Sauter

Geoscience Centre, Dept. Applied Geology, University of Göttingen, Goldschmidtstr. 3, 37077 Göttingen, Germany

* Corresponding author

Abstract

The storage of supercritical carbon dioxide in deep saline aquifers requires new techniques to assess plume spreading, storage efficiencies and operational strategies after and during injections. In this work, a new class of reactive tracers (KIS tracers) planned to be used for the characterization of interfacial areas between supercritical CO_2 and formation brine is presented. The implementation of a time-dependent hydrolysis reaction at the interface enables to investigate the development of the CO_2/brine interface. Besides the basic concept for these novel tracers and the methodology for a suitable target molecular design, the desired tracer properties as well as the exemplary synthesis of first promising compounds are presented here. Additionally, the first experimental results of an analogue study in a static two-phase batch system are shown and evaluated with a newly developed macroscopic model. Subsequently, the numerical forward modelling of different functions for the interfacial area change is described. The first results are promising and show the potential for new applications of KIS tracers after further research.

Graphical abstract
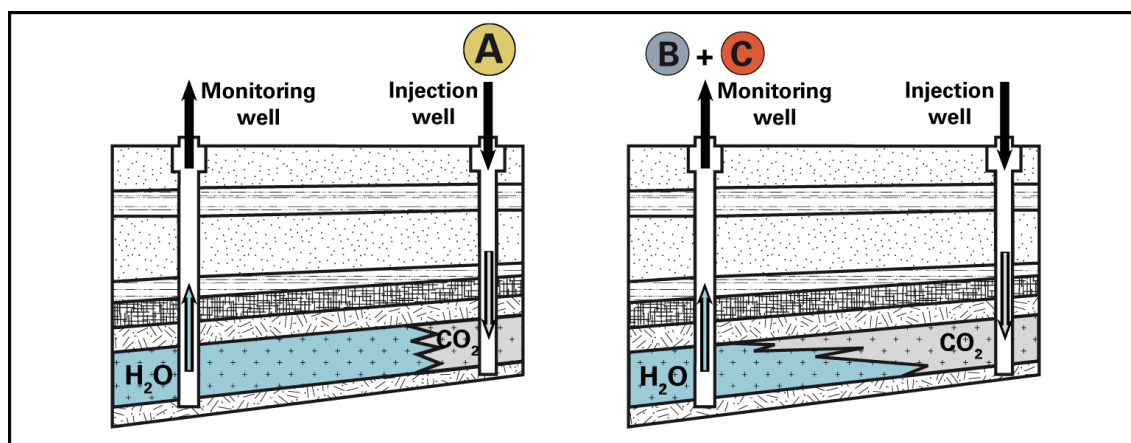
Nomenclature

c	concentration of reaction product in water phase
c_0	initial concentration of reaction product in water phase
c_a	tracer concentration in $scCO_2$
c_i	tracer concentration at interface
$c_{i,\mathrm{max}}$	tracer concentration at saturated interface
k_1	hydrolysis reaction rate constant in water (one-phase system)
k_a	effective hydrolysis reaction rate constant (two-phase system)
m	slope of a line
p	pressure
p_c	pressure at critical point
pH	pH value
pK_a	logarithmic acid dissociation constant
q	specific mass flux across interface
$scCO_2$	supercritical carbon dioxide
t	time
A	interfacial area size
A_{eff}	effective interfacial area
A_{scCO2}	reactive Tracer in $scCO_2$ phase (reactant)
B_{H2O}	reaction product 1 in water phase
C_{H2O}	reaction product 2 in water phase
D	diffusion coefficient

D_{H2O} diffusion coefficient in water

D_{scCO2} diffusion coefficient in scCO$_2$

D_{OW} pH-dependent n-octanol/water distribution coefficient

$E_T(30)$ empirical solvent polarity indicator (based on solvatochromism)

K_L Langmuir sorption coefficient

K_{OW} n-octanol/water distribution coefficient

NAPL   non-aqueous phase liquid

T temperature

T_c temperature at critical point

V volume of water phase

λ fluorescence: excitation wavelength $\rightarrow$ emission wavelength

5.1 Introduction

The storage of CO_2 into geological formations, such as unmineable coal beds, depleted oil or gas reservoirs, sedimentary basins and deep saline aquifers is recently one of the most promising technologies to mitigate anthropogenic greenhouse gas emissions into the earth's atmosphere (Lackner, 2003; Bachu and Adams, 2003; IPCC, 2005, 2007). Deep saline aquifers are considered as the most potential sequestration sites of CO_2 due to their large storage capacities and wide presence compared with other geological sequestration alternatives (Lackner, 2003; IPCC, 2005). The global storage capacity of these aquifers is estimated to be in the order of up to 10 teratons (IEA, 2001; Bachu and Adams, 2003).

When CO_2 is injected as supercritical fluid ($scCO_2$) above its critical point ($p_c = 7.39$ MPa, $T_c = 31.1$ °C) it has a lower density than the formation brine. Therefore, it is buoyant with respect to the brine and flows unevenly upwards until it reaches the top of the aquifer, usually represented by overlying and sealing caprocks. At this point the CO_2 is able to continue the migration only in lateral direction. Here, four trapping mechanisms play a major role (IPCC, 2005): (1) structural and stratigraphic trapping: hindrance of vertical CO_2 migration by impermeable caprock (static trapping) or very slow CO_2 migration over long distances in open systems (hydrodynamic trapping); (2) capillary or residual trapping: retention of CO_2 by capillary forces as immobile phase in the pore space, disconnection from initial plume at the edges; (3) solubility trapping: dissolution of CO_2 in brine, decreasing solubility with increasing temperature and salinity of brine (20–60 g L^{-1}); (4) geochemical trapping: reaction of dissolved CO_2 in reservoir leads to formation of HCO_3^{-}/CO_3^{2-} species (ionic trapping) or precipitation of carbonate minerals at rock surfaces (mineral trapping) at higher pH.

Due to the different time scales ($t_{(1)} = t_{(2)} < t_{(3)} << t_{(4)}$) dissolution and mineral trapping processes can be neglected during and shortly after the injection (IPCC, 2005; Juanes et al., 2007; Ide et al., 2007). Therefore, several authors assume sharp interfaces for the existing three-phase system $scCO_2$/brine/rock in their modelling approaches (Juanes et al., 2007; MacMinn and Juanes, 2009; Dentz and Tartakovsky, 2009). This approximation appears to be plausible from the physicochemical point of view, since as a result of the low solubility between the phases a very high concentration gradient exists between them. More concisely, a several angstroms thick interphase is formed due to the diffusion of $scCO_2$ into the brine phase (Tewes and Boury, 2005).

To assess the fate of CO_2 during and after injection into these aquifers, an understanding of spreading, mixing and plume migration is fundamental. Particularly, knowledge on the size, the amount, and the shape of the injected CO_2 plume is important to provide more information on the trapping effectiveness in the formation.

Dissolution of $scCO_2$ into the brine is limited by the interfacial area. Thus, numerous subsequent chemical processes (e.g., mineral dissolution, precipitation) are also directly affected. Therefore, the extent of the interfacial area between injected $scCO_2$ and brine is of great interest. The larger the interface, the larger is the reacted or dissolved mass. In most cases, it is desired to maximize this area to increase the storage effectiveness in terms of long-term trapping. During injections the interfacial area increases with time due to mixing, spreading and dispersive processes (Dentz and Carrera, 2005; Dentz and Tartakovsky, 2009). Therefore, novel tracers, which are able to describe and to characterize the spatial and temporal development of the plume and its interface in the reservoir, are required.

Up to now, such time-dependent tracers for reservoir studies are not available. Current studies are limited to equilibrium tracers. On the one hand, volume-sensitive partitioning tracers are used to quantify the amount or the saturation of immiscible hydrophobic phases (e.g., NAPLs or $scCO_2$) in porous multiphase systems under equilibrium conditions. Frequently used compounds are (Noordman et al., 2000): alcohols (Dwarakanath and Pope, 1998), gases (e.g., SF_6 and Kr; Vulava et al., 2002), fluorinated hydrocarbons (McCallum et al., 2005; Wells et al., 2007) and naturally occurring isotopes (e.g., [222]Rn; Hunkeler et al., 1997). On the other hand, so-called "interfacial tracers" exist (Saripalli et al., 1998; Setarge et al., 1999; Annable et al., 1998). Anionic surfactants, such as linear alkylbenzenesulfonates (Saripalli et al., 1998; Kim et al., 1999), which adsorb exclusively on the interface between the water and the non-aqueous phase are applied. Hence, these tracers are interface-sensitive. But similarly to conventional partitioning tracers, a thermodynamic equilibrium between water and liquid/liquid-interface is assumed. Therefore, the application is only useful in static time-independent systems. Furthermore, these tracers are dissolved in the water phase and cannot be injected together with the $scCO_2$ phase.

The work presented provides first insight into the development of novel reactive tracers, termed as kinetic interface-sensitive tracers (KIS tracer). These tracers have the potential to overcome above-mentioned deficits by describing the plume and interface

development with time. This is obtained by the implementation of an intended and well studied hydrolysis reaction of the tracer molecule, which allows an irreversible chemical reaction at the scCO$_2$/water interface. Due to the reaction kinetics controlling the phase transfer a time-dependent component is integrated. In CO$_2$ sequestration reservoirs, the tracers may help to provide additional information on the following issues:

- Effect of pressure stimulation on mixing

- Plume spreading, characterization of interfacial area and area change

- Identification of fingering effects

- Estimation of residual scCO$_2$ saturation

- Assessment of storage capacity and effectiveness

- Optimization of operational strategies, management of injection wells

5.2 Theory – conceptual model

5.2.1 Application of KIS tracers during CO$_2$ injections

Before the CO$_2$ injection, the KIS tracer (A_{scCO2}) is dissolved in supercritical or mixed with liquid CO$_2$. Afterwards, the mixture is injected simultaneously through the injection well into the brine saturated aquifer. The tracer reacts at the brine/scCO$_2$ interface to highly water soluble reaction products B_{H2O} and C_{H2O}. Subsequently, these products are measured in the water phase over time (monitoring well). Due to the spreading of the scCO$_2$ plume, the interfacial area increases with time (Figure 5.1).
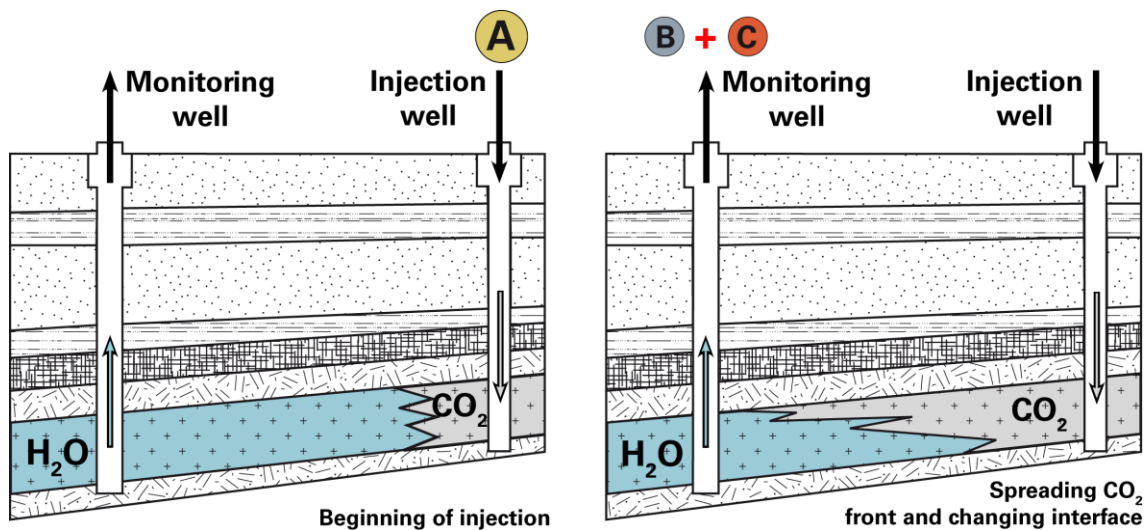
Figure 5.1 Injection well: Injection and spreading of scCO$_2$ together with dissolved KIS tracer. Monitoring well: Measurement of KIS tracer reaction products in the brine.

The larger the interface (reaction surface) between both phases, the higher is the mass of the reaction products in the water phase. The high water solubility leads to negligible back-partitioning of the reaction products into the scCO$_2$ phase. Because of the implemented interface-sensitive hydrolysis reaction with known kinetic parameters, it is possible to establish a correlation between time, concentration in water phase, and interfacial area size for given reservoir conditions (T, p, pH). For the field evaluation and interpretation of the time-dependent interface development, these correlations may be integrated as specific reaction terms into a flow and transport model of the reservoir.

5.2.2 Underlying processes

The basis of KIS tracers is an interface-sensitive hydrolysis reaction at the scCO$_2$/brine interface. Here, the tracer substance A_{scCO2} reacts irreversibly into two reaction products B_{H2O} and C_{H2O} in the presence of water (H$_2$O) at the interface:

$$A_{scCO_2} \quad + \quad H_2O \quad \xrightarrow{k_1} \quad B_{H_2O} \quad + \quad C_{H_2O} \tag{5.1}$$
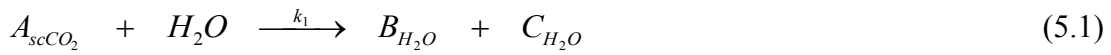
The parameter k_1 depends on the physical and chemical conditions (e.g., T and pH) at the point of reaction and expresses the reaction rate constant of the hydrolysis reaction. Due to the presence of two mobile phases, several underlying physicochemical processes influencing the mass transfer from scCO$_2$ to the brine phase and the reaction speed have to be taken into account as well (Figure 5.2):

(1.) Dissolution of tracer in scCO$_2$ and diffusion toward the interface. A_{scCO2} is dissolved and evenly distributed into the scCO$_2$ phase. This assumption is reasonable because the diffusion coefficients in scCO$_2$ are one order of magnitude higher than in water (e.g., for phenol $T = 35–55$ °C: $D_{scCO2} = 1–3\text{E}{-}08$ m^2 s^{-1} (Lai and Tan, 1995) and $D_{H2O} = 0.5–2\text{E}{-}09$ m^2 s^{-1} (Niesner and Heintz, 2000)). Thus, a fast transport without limitations (small transport resistance) to the interface is expected.

(2.) Adsorption at the interface. The surface active tracer molecules A_{scCO2} are assumed to accumulate at the interface (energy minimization) and saturate the interface after an initial time. This adsorption process normally follows a non-permeable mono-layer isotherm type, such as a Langmuir or Frumkin isotherm (Benjamin, 1997). The absolute amount of adsorbed molecules depends linearly on the interfacial area. Due to an excess of dissolved A_{scCO2} in the supercritical phase, the interface is assumed to be permanently saturated. Therefore, the concentration of A_{scCO2} at the interface can be expected to remain constant.

(3.) Reaction at the interface. After adsorption at the interface, A_{scCO2} reacts in contact with water. The envisaged hydrolysis reaction (see Section 5.3.1) of an ester with water follows a (pseudo)-first order kinetics (Nottebohm et al., 2012). Due to the constant interface concentration, the reaction kinetics simplifies to (pseudo)-zero order kinetics with linear behavior. Thus, the reaction kinetics is the limiting step for phase transfer across the interface.

(4.) Phase transfer. The highly water soluble reactions products B_{H2O} and C_{H2O} are distributed into the brine due to diffusion and thus away from the interface. Therefore, the concentrations of B_{H2O} and C_{H2O} increase proportionally to the decrease of A_{scCO2} and can be measured in the water phase. In addition to the interface-sensitive part of mass transfer across the interface, partitioning between both phases also has to be taken into account. Despite the low polarity and water solubility of A_{scCO2} small amounts of A_{scCO2} may partition into the brine phase. The resulting reaction in the water phase follows first order kinetics and would lead to an exponential increase of B_{H2O} and/or C_{H2O} in the water phase. Hence, the superposition of interface reaction and partitioning results in a non-linear function. *Vice versa*, a low back-partitioning of the polar and highly water soluble reaction products B_{H2O} and C_{H2O} into the scCO$_2$ phase may also occur. Because of the increasing complexity, it is desirable to be able to neglect or to minimize partitioning effects within the data evaluation. To estimate and compare the
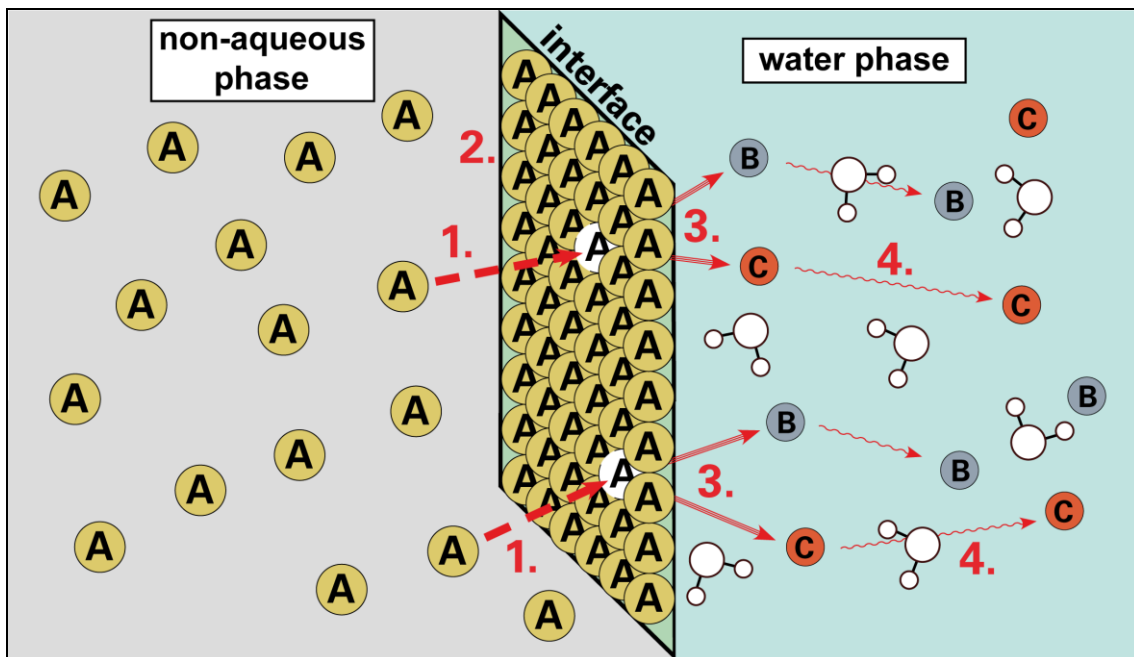
Figure 5.2 Schematic representation of all involved processes at the scCO₂/water interface during KIS tracer application.

tendency for partitioning between both phases at reservoir conditions the n-octanol/water distribution coefficient K_{OW} was used as a model parameter due to similar solvent hydrophobicities of n-octanol and $scCO_2$ (log $K_{OW(scCO2)}$ = 2.85 (50 °C, 143 bar; Nakaya et al., 2001), log $K_{OW(n\text{-}octanol)}$ = 2.88 (25 °C, 1 bar; SciFinder, 2012). Furthermore, Timko et al. (2004) showed for non-acidic compounds, such as the KIS tracers, that the log K_{OW} is correlated to the $scCO_2$/water partitioning behaviour.

5.3 KIS tracer design

Molecular target design has been established as a methodology for producing molecules with desired properties or effects especially in the field of pharmaceutical, biochemical (Kuntz et al., 1994) and material sciences (Kang and Zhang, 2000). Due to the exploitation and combination of well studied structural elements and molecular properties (e.g., functional groups, substructures, and homologs) novel tailor-made compounds with controlled structures and properties are conceivable and can be synthesized for a magnitude of applications. During the molecular design quantitative structure-property relationships (QSPR) can be used as a tool for predicting molecule properties for the molecule selection/modification and to transfer their chemical behavior to unknown systems. In this work for instance, the relation of the molecule structure to the log K_{OW} value was used to estimate the water/$scCO_2$ partitioning behavior of the synthesized esters (see Section 5.3.2).

Up to now, the molecular design of tracer substances for environmental studies has not yet been considered. This also applies to challenging tracer tests in CO_2. Published tracer tests are limited to classical hydrogeological and thus commercially available tracer compounds. For example, Freifeld et al. (2005) and McCallum et al. (2005) applied several perfluorocarbons and noble gases (Kr, SF_6) for the determination of CO_2 travel times and the CO_2 saturation within the formation. Identical compounds were used from Wells et al. (2007) and Hortle et al. (2011) to detect CO_2 leakage. For the same purpose, Bachelor et al. (2008) proposed the spiking of injected CO_2 with radioactive isotopes (^{14}C and [222]Rn).

Due to the limitations of conventional tracers, the general applicability of molecular design for geoscientific problems is shown here with KIS tracers as an example, especially developed for CO_2 injections into deep saline aquifers.

5.3.1 Tracer requirements

A prior consideration of the KIS tracer requirements is essential for a successful target design of potential tracer substances. For describing interfacial areas between scCO₂ and brine a defined reaction of the tracer with water is required. Splitting reactions with water as nucleophilic reagent belong to hydrolysis reactions as a subgroup of solvolysis. Hydrolysable substances are alcoholic and phenolic esters, acid chlorides, acid amides, and nitriles. Due to the comparably easy synthesis, different phenol esters were suggested and used in this work. The simplified hydrolysis reaction scheme is the following:

$$Ester\ (A_{scCO_2}) + H_2O\ \xrightarrow{\ k_1\ }\ Acid\ (B_{H_2O}) + Alcohol\ /\ Phenol\ (C_{H_2O}) \qquad (5.2)$$
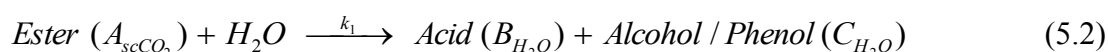
The esters are dissolved in scCO₂ (A_{scCO_2}) and should show minimal partitioning into the polar water phase. Since scCO₂ is an excellent solvent for non-polar compounds (Luque de Castro and Tena, 1996), the applied esters should also have non-polar substructures (e.g., linear *n*-alkyl chains, aromatic rings) with corresponding high log K_{OW} values.

In contrast, at least one of the hydrolysis reaction products has to be highly polar, water soluble and mobile in order to determine it in the water phase. For this purpose, the formed acids can be exploited (B_{H2O}). Their ability of deprotonation is very convenient, since anions are formed depending on pH. Thus, especially the esters of strong organic acids with very low logarithmic acid dissociation constants pK_a seem to be the most promising compounds.

The requirements for the second reaction product (C_{H2O}) are not so strict. The formed alcohols or phenols can be polar or even non-polar. If the product is medium polar with suitable distribution coefficients between the brine and scCO₂ phase, it may even be used as additional partitioning tracer. However, the major task of the alcohol or phenol, respectively, is the adjustment of the KIS tracer properties during the molecular design. Beside the modification of the tracer polarity, the alcohols or phenols used for esterification have a large influence on the hydrolysis reaction rate constant k_1. This rate constant can be modified and adapted to reservoir conditions (T, pH) as well as for experimental durations. Steric hindrance, mesomeric and inductive effects are only some reasons for different hydrolysis kinetics and can be considered during synthesis (Nottebohm et al., 2012).

Regarding the practicability for field applications, the concentrations of reaction products should preferably be measured with standard equipment in a high temporal resolution, a high selectivity, and with a low detection limit. Therefore, the synthesis of the target compounds was focused on compounds with fluorescence properties.

5.3.2 Tracer design / synthesis

As a consequence of the prior emphasized requirements, the esterification of naphthalenesulfonic acids is most promising. Because of $pK_a < 1$, these acids are deprotonated at even very low pH levels and therefore, very water soluble permanent anions are formed. Thus, no significant retardation can be expected for organic acids at $pH > pK_a + 2$ (Schaffer et al., 2012). This also applies for naphthalenesulfonates, which are established conservative, non-sorptive tracers for geothermal applications, very stable at high temperatures and anaerobic conditions (Rose et al., 2001; Rose et al., 2002; Nottebohm et al., 2010). Furthermore, a back-partitioning of the anions into the scCO$_2$ phase can be excluded. For reservoirs, which are already contaminated with these compounds different constitutional isomers can be prepared to make the identification of the tracer unique. Furthermore, naphthalenesulfonates are highly fluorescent with a detection limit in the low $\mu g\,L^{-1}$ range. Pre-concentration and subsequent chromatographic separation lowers the detection limit by around one order of magnitude and enables the determination of different isomers even in highly saline matrices (Nottebohm and Licha, 2012).

Additional analytical problems might occur in sequestration reservoirs that contain significant residuals of hydrophobic aromatic compounds (e.g., depleted petroleum reservoirs), such as polycyclic aromatic hydrocarbons, since the dissolution of these substances in scCO$_2$ can be expected during the injection. The leached compounds accumulate at the scCO$_2$/brine interface and might cause fluorescence interferences with the tracer reaction products. Thus, online measurements would be no longer possible and chromatographic systems have to be used again for sample clean-up and compound separation prior to fluorescence analysis.

If mononaphthalenesulfonic acids are applied, the esterification of the sulfo group leads to non-polar esters. In dependence of the deployed alcohol or phenol the ester properties can further be modified. For example, the esterification with linear aliphatic alcohols leads to non-polar but also non-fluorescent esters whereby the measurement of these compounds is more complicated. For this reason, aromatic alcohols (phenols, naphthols)
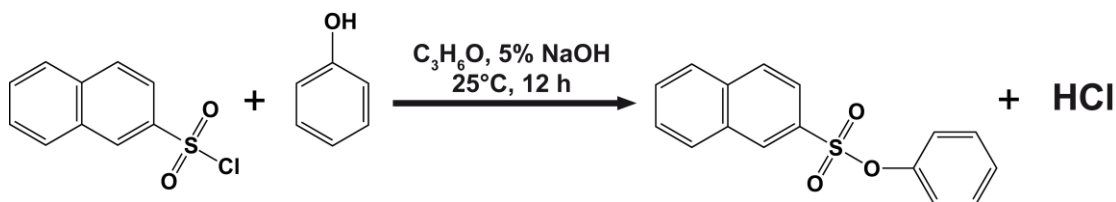
Figure 5.3 Synthesis of phenyl naphthalene-2-sulfonate from naphthalene-2-sulfonyl chloride and phenol.
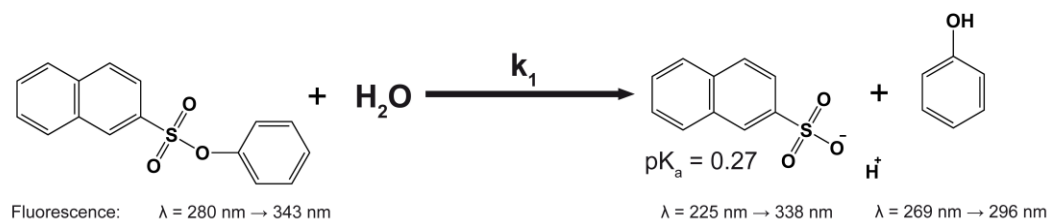
Figure 5.4 Hydrolysis reaction of phenyl naphthalene-2-sulfonate with water and the fluorescent properties of the reagent and the reaction products.

can be used for the esterification of the naphthalenesulfonic acids (Figure 5.3). The resulting fluorescent esters are hydrophobic (log K_{OW} > 4). For the modification of the hydrophobic properties, different esters were synthesized by esterification of naphthalene-2-sulfonic acid (2-NSA) with different methyl substituted phenols. The more non-polar the employed phenol, the more non-polar is the resulting ester (Table 5.1). The esterification of chlorophenols therefore leads to more hydrophobic esters. However, the higher toxicity of these compounds should be also taken into account when used in field studies. The ester compounds were synthesized on the basis of naphthalene-2-sulfonyl chloride and the respective phenol under alkaline catalyzed conditions (Figure 5.3) in a slightly modified procedure according to Vennila et al. (2008). Instead of 4 mL acetone 6 mL were used. The identity and purity of the esters were confirmed by [1]H-Nuclear Magnetic Resonance (^{1}H-NMR) spectroscopy. The purity was >95%. The hydrolysis reaction results in 2-NSA and the respective phenol homologues (Table 5.1). The reaction scheme and the fluorescent properties for the phenyl ester are shown in Figure 5.4.

Table 5.1 Properties of synthesized KIS tracer compounds, phenyl acetate and their respective reaction products.

Ester (Abbreviation)	$\rightarrow$	Acid	+	Alcohol / Phenol	
	log K_{OW}*				log K_{OW}*
Phenyl naphthalene-2-sulfonate (2-NSAPh) CAS 62141-80-4	4.29	Naphthalene-2-sulfonic acid (2-NSA) log K_{OW}* = 0.63 pK_a* = 0.27 log D_{OW} (pH > 5)* = −2.87		Phenol	1.54
p-tolyl naphthalene-2-sulfonate (2-NSA-4-Ph) CAS 108980-59-2	4.48			4-methylphenol (*p*-cresol)	2.07
3,5-dimethylphenyl naphthalene-2-sulfonate (2-NSA-3,5-Ph) CAS 889803-73-0	5.13			3,5-dimethylphenol (3,5-xylenol)	2.55
Phenyl acetate (PhAc) CAS 122-79-2	1.65	Acetic acid		Phenol	1.54

* SciFinder predicted values, calculated using Advanced Chemistry Development (ACD/Labs) Software (1994–2012).

5.4   Experiments and modelling

5.4.1   Lab experiments

5.4.1.1 Analogue approach

Due to the necessity of high pressure cells to generate scCO$_2$ for identifying and quantifying the expected involved processes the new tracers cannot be tested easily under reservoir conditions. Available pressure cells and scCO$_2$ reactors are limited in size and in their setup variability. Furthermore, direct online measurements in the water phase cannot easily be employed and a sampling over time is not possible due to small cell volumes of only a few millilitres. Therefore, the use of pressure cells seems to be feasible only for a limited number of fundamental static batch experiments, such as the determination of solubilities, partitioning coefficients, further thermodynamic equilibrium parameters, and the inertness of the tracer in mixture with other compounds.

In order to overcome these limitations, to investigate and to interpret the tracer behaviour in defined systems at larger scale, the scCO$_2$ was replaced with another solvent. Particularly, organic solvents, which are immiscible with water, are expected to show a similar behaviour and allow the process identification and separation at the interface on a larger scale without special equipment. For this purpose, different non-

polar solvents were selected and tested with respect to density, polarity, inertness, and solubility in water.

The alkane *n*-octane has proven most suitable as $scCO_2$ analogue. Table 5.2 compares some selected properties of $scCO_2$ at reservoir conditions with *n*-octane at atmospheric conditions. Density of $scCO_2$ depends strongly on temperature. In contrast, the density of *n*-octane is almost constant but lies in the same range. The solubility of $scCO_2$ in water under equilibrium conditions is higher than that of *n*-octane. Due to the timescale of $scCO_2$ dissolution (non-equilibrium), the salinity of the brine, and the presence of further dissolved gases (e.g., methane) a significantly lower water solubility can be assumed (IPCC, 2005). Therefore, *n*-octane develops analogously to $scCO_2$ a sharp interface to the water phase (see Section 5.1). For the comparison of the solvent polarity, which influences the tracer solubility and the partitioning between both phases, two different parameters were selected. On the one hand the $\log K_{OW}$ value, which depends for $scCO_2$ strongly on the pressure (Nakaya et al., 2001), and on the other hand the $E_T(30)$ value as empirical solvent polarity indicator (Reichardt, 1994) were used. As desired, these values lie for *n*-octane in the same range as for $scCO_2$. Additional advantages of *n*-octane are the low cost as well as the comparable low toxicity and vapor pressure. Therefore, the handling is uncomplicated and the compound can be used in larger amounts. All obtained values for kinetic rate constants, interface adsorption parameters, mass fluxes and mass transfer coefficients in the *n*-octane/water system can be transferred and adapted later to $scCO_2$ based on calibrated process models.

Table 5.2 Comparison of physical and chemical properties between $scCO_2$ with* n-*octane as analog compound.

Parameter	$scCO_2$	*n*-octane
Density [g cm^{-3}]	0.52 (150 bar, 65 °C)[a] 0.75 (150 bar, 40 °C)[a]	0.67 (1 bar, 65 °C)[b] 0.69 (1 bar, 40 °C)[b]
$E_T(30)$ [kcal mol^{-1}]	28.5 (150 bar, 40 °C)[c]	31.1 (1 bar, 25 °C)[d]
$\log K_{OW}$ [-]	3.14 (150 bar, 50 °C)[e] 4.87 (180 bar, 50 °C)[e]	4.78 (1 bar, 25 °C)[b]
Solubility [mg L^{-1}]	20–60E+03[f]	1.3[b]

[a] Calculated after Stryjek and Vera (1986) (www.criticalprocesses.com).
[b] SciFinder predicted values, calculated using Advanced Chemistry Development (ACD/Labs) Software (1994–2012).
[c] Eberhardt et al. (1997).
[d] Reichardt (1994).
[e] Nakaya et al. (2001).
[f] IPCC (2005).

As an analog for the aqueous brine phase (buffer) solutions with different pH values can be used. This allows investigating the effects of different hydrolysis rate constants due to their direct relation to the pH value. The hydrolysis rate changes by about one order of magnitude per one pH unit increase (Nottebohm et al., 2012).

5.4.1.2 Experimental setup

For identifying, verifying, and separating the processes relevant for the developed novel KIS tracer application, major effort was made to simplify the experimental setup. The reason is that a profound knowledge of processes controlling the tracer interface sensitivity is fundamental to all consecutive investigations and the process modeling. Thus, an undisturbed (closed) system with fixed boundary conditions (constant interfacial area size, phase volume ratio, T, pH) and high temporal resolution measurements are necessary.

For this reason, static batch experiments were conducted directly in sealed small-volume fluorescence spectroscopy cuvettes ($V = 4$ mL). This approach has the advantage that the concentrations of the reaction products and the possibly partitioned tracer can be measured in short time intervals without mass loss and without disturbing the closed system by sampling. Furthermore, it is possible to adjust certain temperatures and stirring rates in the cells to avoid unwanted temperature changes and diffusive effects.

After providing 3 mL deionized or buffered and degassed water in the cuvette, 1 mL of n-octane containing the dissolved (KIS) tracer (2-NSAPh or PhAc) was carefully added above the water phase. The interfacial area was constant ($A = 1$ cm²). Consecutively, the concentration increase of the respective reaction products (2-NSA or phenol) in the water phase was recorded every minute for several thousand minutes by using fluorescence spectroscopy.

The resulting concentration curves of the measured compounds were used to determine the mass flux across the interface and to calibrate the numerical model that was developed in parallel to the experiments.

5.4.2 Numerical modelling

To understand the relationship between interface development and resulting concentration curves of the reaction products in the water phase, a numerical modeling approach using the finite element method was implemented. The problem can be

described as a heterogeneous reaction of the KIS tracer at the $scCO_2$/water interface. The KIS tracer in the $scCO_2$ migrates to the interface and reacts here with the water in a hydrolysis reaction. In this study, a macroscopic model with averaged quantities was developed.

5.4.2.1 Model description

The comprehensive problem consists of the two different immiscible phases ($scCO_2$ or analog solvent and water) and of the allocation of the KIS tracer with its reaction products. Since the reaction at the interface is the limiting step in the mass transfer across the interface and due to high diffusion rates and the excess of tracer in the $scCO_2$ phase, the interface is permanently saturated. Here, a Langmuir (Langmuir, 1918) isotherm is assumed for the adsorption process onto the interface:

$$c_i = \frac{K_L \cdot c_{i,max} \cdot c_a}{1 + K_L \cdot c_a}$$

(5.3)

K_L is the Langmuir sorption coefficient. For high tracer concentrations c_a in the $scCO_2$ phase the interface concentration c_i is approximately equal to the maximum concentration of the saturated interface $c_{i,max}$. The assumption includes that the hydrolysis at the interface and the migration of the reaction products into the water phase take place within one time step. It is additionally assumed that the reacted small fraction of tracer Δc_i at the interface is instantaneously replaced from the $scCO_2$ bulk due to large diffusion coefficients. Consequently, due to the interface limited transfer the KIS tracer decay in the non-aqueous phase follows the linear zero order reaction kinetics of the hydrolysis reaction. The effective reaction rate constant k_a of the limiting step can be expressed as a specific constant mass flux q of the reaction products into the water phase:

$$q = k_a = \frac{\Delta c_i}{\Delta t}$$

(5.4)

This allows the reduction of the numerical model to a single-phase problem. The model geometry follows the cuvette used in the lab experiment (see Section 5.4.1.2) with a base area $A = 1$ cm². The height depends on the volume and therefore the filling level of water. The upper model boundary is equal to the interfacial area. The constant q of tracer products into the water phase, which is represented by the model domain, is

defined as boundary condition. All other boundaries are no-flow boundaries (Figure 5.5).

For the ionic tracer reaction product 2-NSA no back-partitioning into the scCO$_2$ phase is assumed. Hence, the concentration curve is only allowed to rise or to level at a constant value. The distribution of the product across the water volume is described through a diffusion process:

$$\frac{\partial c}{\partial t} = -D\frac{\partial^2 c}{\partial x^2}$$

(5.5)

Therefore, a steady-state concentration increase establishes in the model region (observation point) for a given constant interfacial area size.
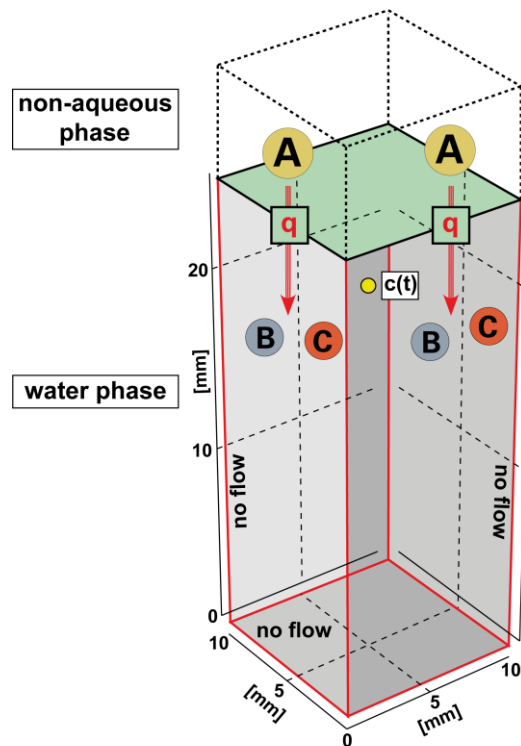
Figure 5.5 Sketch of the numerical model domain: The yellow dot at 20 mm height represents the observation point where the fluorescence signal is measured. Red boundaries are no flow boundaries. On the upper green boundary the flux q is defined, where the reaction products flow into the water.

5.4.2.2 Relation between concentration curve and interfacial area size

As stated above, the concentration of KIS tracer reaction product depends only on the interface size and time. The zero order kinetics of the hydrolysis reaction results for a constant interfacial area in a linear concentration curve $c(t)$:

$$c(t) = c_0 + q\frac{A}{V}t \qquad (5.6)$$

Where A is the interfacial area, V the volume and c_0 the initial concentration in the water phase. From linear regression analysis the mass transfer rate q can be determined with:

$$q = m\frac{V}{A} \qquad (5.7)$$

Here, m is the slope of the concentration curve. For the case of a time-dependent variable interfacial area $A(t)$ a decomposition ansatz is applied:

$$A(t) = f_A(t) \cdot A_{max} \qquad (5.8)$$

A dimensionless time-dependent function $f_A(t)$ is used to scale a constant maximum area A_{max}. The function $f_A(t)$ must be equal to one when A_{max} establishes and has some additional properties:

$$f_A(t) \in [0\ 1] \quad \text{and} \quad \exists \hat{t} \in [0\ t_{max}] \quad \text{with} \quad f_A(\hat{t}) = 1 \qquad (5.9)$$

The application of the ansatz in Equation (5.8) in Equation (5.6) leads to:

$$\frac{dc}{dt} = \frac{A_{max}}{V}q \cdot f_A(t) \quad \text{and} \qquad (5.10)$$

$$c(t) = c_0 + \frac{A_{max}}{V}q \cdot \int f_A(t)\,dt \qquad (5.11)$$

For the determination of A_{max} a case-by-case analysis of $c(t)$ has to be carried out:

$$(1) \quad \exists \ddot{c}(\hat{t}) = 0 \quad \Rightarrow \quad f(\hat{t}) = 1 \qquad \text{if} \qquad c(\hat{t}) = max\{\dot{c}(\hat{t})\} \qquad (5.12)$$

$$(2) \quad \exists! \ddot{c}(\hat{t}) = 0 \quad \Rightarrow \quad f(\hat{t}) = 1 \qquad \wedge \qquad A(\hat{t}) = A_{max} \qquad (5.13)$$

$$(3) \quad \neg\exists \ddot{c}(\hat{t}) = 0 \quad \Rightarrow \quad f(t_{max}) = 1 \qquad \vee \qquad f(0) = 1 \qquad \text{with}$$

$$A(T) = A_{max} \quad \vee \quad A(0) = A_{max} \tag{5.14}$$

Hence, A_{max} can be calculated with:

$$A_{max} = \frac{(c(\hat{t}) - c_0) \cdot V}{q} \quad \cdot \quad \frac{1}{\int\limits_0^{\hat{t}} f_A(t)\, dt} \tag{5.15}$$

At this point it can clearly be seen that the time-dependent function $f_A(t)$ and consequently A_{max} are highly dependent on the sampling rate and detection limit of the reaction products.

5.4.3 First results from static batch experiments

Initially, the lab experiments were conducted with phenyl acetate (PhAc) as well as with the potential KIS tracer compound phenyl naphthalene-2-sulfonate (2-NSAPh) (Table 5.1). PhAc is the phenyl ester of acetic acid. Due to the significantly lower log K_{OW}, the KIS tracer can be compared with a more hydrophilic compound as a reference. Thus, it is more likely that PhAc shows a stronger partitioning into the water phase than the more hydrophobic 2-NSAPh. The resulting concentration curves of the respective hydrolysis reaction products phenol (reactant: PhAc) and naphthalene-2-sulfonate (reactant: 2-NSAPh) are shown in Figure 5.6. As expected, the desired hydrolysis reactions went on and both products could be measured online in the water phase by fluorescence spectroscopy. But obviously, both compounds developed a completely different curve shape. As mentioned above, a considerable partitioning additional to the interface sensitive part of mass transfer across the interface leads to an exponential increase of the phenol concentration curve for PhAc. Therefore, the interface sensitivity is lost and the compound is not suitable as KIS tracer. In contrast, 2-NSA showed a very promising curve shape. After an initial start up phase of around 2,000 min, a steady state condition established in the concentration change and the concentration increase became linear. The start-up phase might be caused by the initial saturation of the interface, partitioning of ester impurities (2-NSA) and the final establishment of constant diffusion gradients. Furthermore, the linear slope of the concentration curve seems to confirm the expected reduction of first order to zero order kinetics and indicates a negligible partitioning of the ester between both phases.
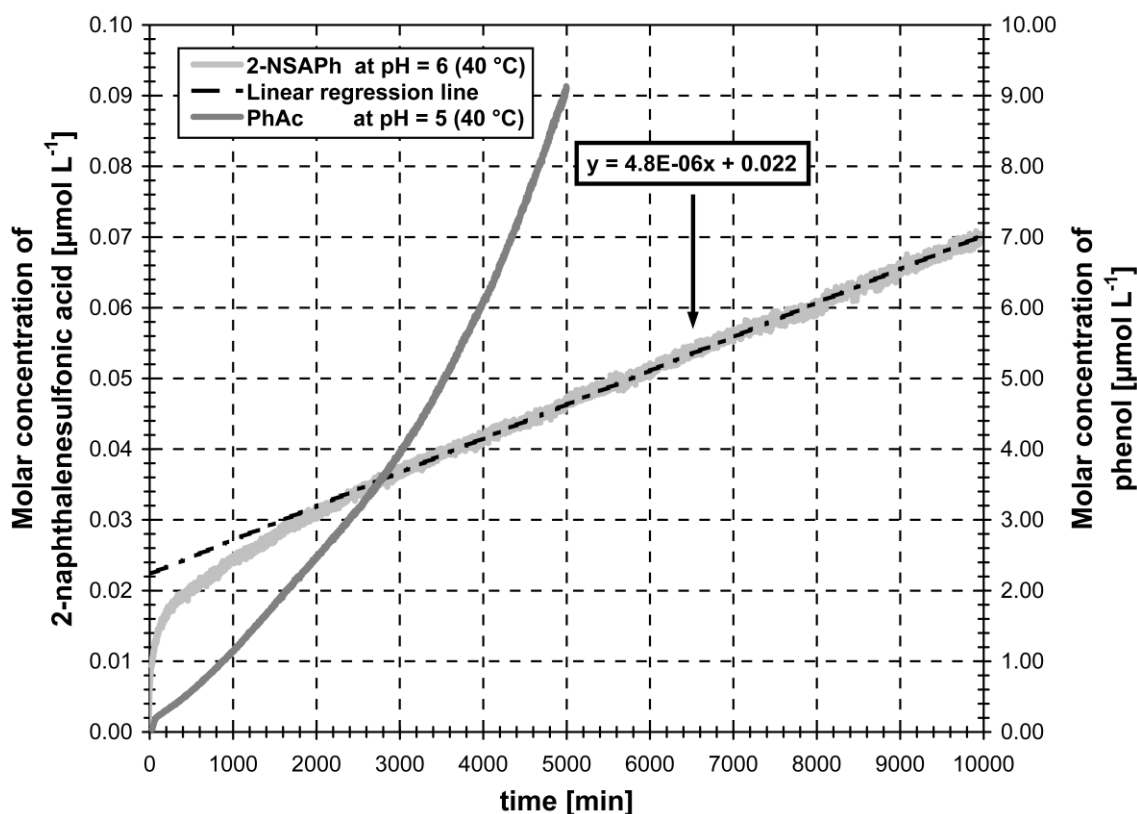
Figure 5.6 Comparison of measured concentration curves for the hydrolysis reaction products of phenyl acetate (PhAc) and phenyl naphthalene-2-sulfonate (2-NSAPh).

For the evaluation of the interface sensitivity, a linear regression analysis was carried out for the values $t > 2,000$ min (Figure 5.6, $R^2 = 0.99$). By applying the obtained slope $m = 4.8\text{E}{-}06$ µmol L^{-1} $\min^{-1}$, and the given values $A = 1$ cm², $V = 3$ mL for the cuvette in Equation (5.7), q was calculated with $2.4\text{E}{-}06$ µmol m^{-2} s^{-1}. The fitted m depends directly on k_1 of the hydrolysis reaction and is only valid for the given conditions. Conceivable changes in T, pH and the molecule structure would lead to different k_1 and thus to different m and q, respectively (see Sections 5.3.1 and 5.4.1.1). During CO_2 injections, the pH is lower in the vicinity of the $scCO_2$/water interface than for the experiments conducted in this study. Therefore, k_1 and q are also expected to be lower under field conditions.

The numerical model was calibrated using the observed m from the static batch experiment and a constant interfacial area of $A = 1$ cm² (Figure 5.7). Additionally, three different classical test functions $A(t)$ with properties according to Equation (5.8) were applied and the resulting concentration curves were modelled to gain further insight into the behaviour of KIS tracers. The concentrations are proportional to the integrated $A(t)$ which represents an effective area A_{eff}:

$$c(t) \propto \int_0^t A(t)\ dt = A_{eff} \tag{5.16}$$

Furthermore, the model allows the distinction between different functions for $A(t)$ even when A_{eff} and thus also the total amount of reacted tracer is equal (Fig. 5.7). Hence, A_{eff} is one of the main target parameters for proving the effectiveness of $scCO_2$ injections.

5.5   Summary and conclusions

The interfacial area between $scCO_2$ and brine is an important parameter for the evaluation of CO_2 storage in deep saline aquifers, since numerous relevant trapping mechanisms and physicochemical processes are directly dependent on this reactive interface. Up to now, these interfacial areas and their development during injection cannot be studied directly. In this work, a methodology for the design of kinetic-interface sensitive tracers (KIS tracers) was presented. These tracers are believed to have the potential to close the existing gaps for field experimental interpretation by implementing an interface-sensitive reaction. Here, the idea and the theoretical concept for these novel tracers were presented. After defining the tracer requirements and
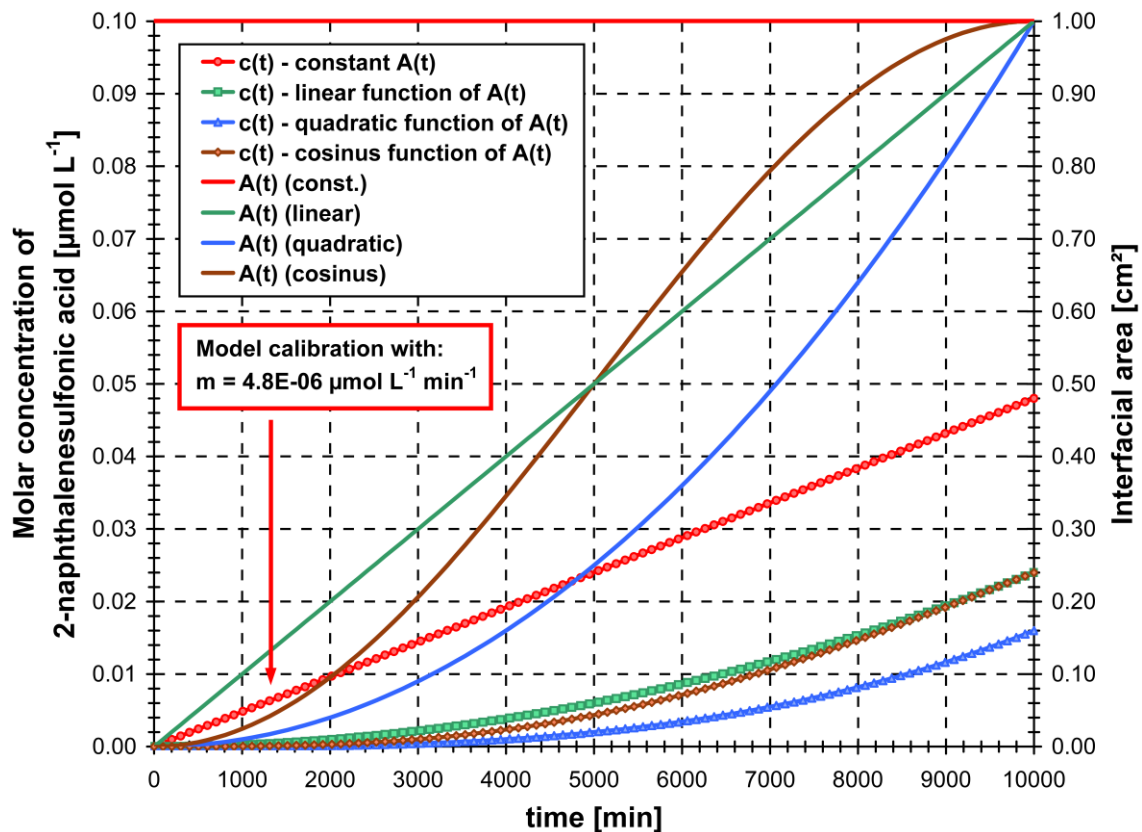
Figure 5.7 Comparison of different modelled scenarios: Concentration curves are modelled based on different functions for A(t). For the model calibration (red line) the constant A from the experiment was used.

showing possibilities for a tailor-made molecular design, several compounds were successfully synthesized. An analogue approach was proposed for testing the tracer behaviour by replacing the non-aqueous $scCO_2$ phase with organic solvents. Additionally, a relationship between measured concentration curves and interfacial area was derived and a first model for the tracer evaluation in static batch systems was presented.

The results show, that molecular target design is a suitable method to develop these kinds of new tracers. As expected, the tested esters 2-NSAPh and PhAc confirmed the combination of mass transfer across the interface and hydrolysis reaction. The respective reaction products 2-NSA and phenol were detected in the water phase by fluorescence spectroscopy. However, in contrast to the newly synthesized potential KIS tracer compound 2-NSAPh, which demonstrated the expected linear increase of the reaction product 2-NSA in the water phase and thus interface sensitivity, PhAc showed no interface sensitivity due to a too strong partitioning behaviour. The linear concentration increase of 2-NSA is very promising and supports the theoretically derived zero order reaction kinetics at the interface. Thus, a constant mass flux across the interface could be determined. Based on this flux, the new macroscopic numerical model was calibrated and different scenarios were calculated. The model demonstrated the interface sensitivity of KIS tracers and showed the possibility for evaluating the from lab experiments obtained concentration curves. In contrast to conventional equilibrium tracers (partitioning or interfacial tracers), KIS tracers are injected together with the non-aqueous phase and their reaction kinetics (non-equilibrium) is exploited to gain information on the temporal interface or plume development.

Future works will include additional process studies and modelling to describe the relevant processes, dependencies and mechanisms. Furthermore, the experiments will be extended to dynamic systems with a variable interface as well as repeated with additional compounds with regard to their possible application as KIS tracer. The influence of a third phase (rock material) on the tracer behaviour will also be investigated. In parallel, the existing model will be extended and adapted according to the experimental progress. Hence, it is planned to use the model as forecast tool for more complex dynamic systems. Finally, when all relevant physicochemical processes are completely understood, it should be possible to implement the model in a reservoir simulator.

Acknowledgment

5.6 References

Annable, M.D., Jawitz, J.W., Rao, P.S.C., Dai, D.P., Kim, H., Wood, A.L., 1998. Field evaluation of interfacial and partitioning tracers for characterization of effective NAPL-water contact areas. Ground Water 36 (3), 495–502.

Bachelor, P.P., McIntyre, J.I., Amonette, J.E., Hayes, J.C., Milbrath, B.D., Saripalli, P., 2008. Potential method for measurement of CO_2 leakage from underground sequestration fields using radioactive tracers. Journal of Radioanalytical and Nuclear Chemistry 277 (1), 85–89.

Bachu, S., Adams, J.J., 2003. Sequestration of CO_2 in geological media in response to climate change: capacity of deep saline aquifers to sequester CO_2 in solution. Energy Conversion and Management 44 (20), 3151–3175.

Benjamin, I., 1997. Molecular structure and dynamics at liquid-liquid interfaces. Annual Review of Physical Chemistry 1997 (48), 407–451.

Dentz, M., Carrera, J., 2005. Effective solute transport in temporally fluctuating flow through heterogeneous media. Water Resources Research 41 (8), 1–20.

Dentz, M., Tartakovsky, D.M., 2009. Abrupt-interface solution for carbon dioxide injection into porous media. Transport in Porous Media 79 (1), 15–27.

Dwarakanath V., Pope, G.A., 1998. New approach for estimating alcohol partition coefficients between nonaqueous phase liquids and water. Environmental Science and Technology 32 (11), 1662–1666.

Eberhardt, R., Löbbecke, S., Neidhart, B., Reichardt, C., 1997. Determination of ET(30) values of supercritical carbon dioxide at various pressures and temperatures. Liebigs Annalen 1997 (6), 1195–1199.

Freifeld, B.M., Trautz, R.C., Kharaka, Y.K., Phelps, T.J., Myer, L.R., Hovorka, S.D., Collins, D.J., 2005. The U-tube: A novel system for acquiring borehole fluid samples from a deep geologic CO_2 sequestration experiment. Journal of Geophysical Research B: Solid Earth 110, B10203.

Hortle, A., de Caritat, P., Stalvies, C., Jenkins, C., 2011. Groundwater monitoring at the Otway Project site, Australia. Energy Procedia 4, 5495–5503.

Hunkeler, D., Hoehn, E., Höhener, P., Zeyer, J., 1997. 222Rn as a partitioning tracer to detect diesel fuel contamination in aquifers: Laboratory Study and Field Observations. Environmental Science and Technology 31 (11), 3180–3187.

Ide, S.T., Jessen, K., Orr, F.M., 2007. Storage of CO_2 in saline aquifers: Effects of gravity, viscous, and capillary forces on amount and timing of trapping. International Journal of Greenhouse Gas Control 1 (4), 481–491.

IEA Greenhouse Gas R&D Programme: Davison, J., Freund, P., Smith, A. (Eds.), 2001. Putting carbon back into the ground, http://www.ieaghg.org/docs/general_publications/putcback.pdf. Accessed 10th October 2011.

IPCC: Metz, B., Davidson, O.R., de Coninck, H. C., Loos, M., Meyer, L.A. (Eds.), 2005. IPCC special report on carbon dioxide capture and storage, Cambridge University Press, Cambridge and New York.

IPCC: Metz, B., Davidson, O.R., Bosch, P.R., Dave, R., Meyer, L.A. (Eds.), 2007. Summary for policymakers. In: Climate change 2007: Mitigation, Cambridge University Press, Cambridge and New York.

Juanes, R., MacMinn, C.W., Szulczewski, M.L., 2010. The footprint of the CO2 plume during carbon dioxide storage in saline aquifers: storage efficiency for capillary trapping at the basin scale. Transport in Porous Media 82 (1), 19–30.

Kang, E.T., Zhang, Y., 2000. Surface modification of fluoropolymers via molecular design. Advanced Materials 12 (20), 1481–1494.

Kim, H., Suresh, P., Rao, P.S.C., Annable, M.D., 1999. Consistency of the interfacial tracer technique: experimental evaluation. Journal of Contaminant Hydrology 40 (1), 79–94.

Kuntz, I.D., Meng, E.C., Shoichet, B.K., 1994. Structure-based molecular design. Accounts of Chemical Research 27 (5), 117–123.

Lackner, K.S., 2003. A guide to CO2 sequestration. Science 300 (5626), 1677–1678.

Lai, C.-C., Tan, C.-S., 1995. Measurement of molecular diffusion coefficients in supercritical carbon dioxide using a coated capillary column. Industrial and Engineering Chemistry Research 34 (2), 674–680.

Langmuir, I., 1918. The adsorption of gases on plane surfaces of glass, mica, and platinum. Journal of the American Chemical Society 40 (9), 1361–1403.

Luque de Castro, M.D., Tena, M.T., 1996. Strategies for supercritical fluid extraction of polar and ionic compounds. TrAC Trends in Analytical Chemistry 15 (1), 32–37.

McCallum, S.D., Riestenberg, D.E., Cole, D.R., Freifeld, B.M., Trautz, R.C., Hovorka, S.D., Phelps, T.J., 2005. Monitoring geologically sequestered CO2 during the Frio Brine pilot test using perfluorocarbon tracers. In: Proceedings of the 4th Annual Conference on Carbon Capture and Sequestration, Alexandria, USA.

MacMinn, C.W., Juanes, R., 2009. Post-injection spreading and trapping of CO2 in saline aquifers: impact of the plume shape at the end of injection. Computational Geosciences 13 (4), 483–491.

Nakaya, H., Miyawaki, O., Nakamura, K., 2001. Determination of log P for pressurized carbon dioxide and its characterization as a medium for enzyme reaction. Enzyme and Microbial Technology 28 (2–3), 176–182.

Niesner, R., Heintz, A., 2000. Diffusion coefficients of aromatics in aqueous solution. Journal of Chemical and Engineering Data 45 (6), 1121–1124.

Noordman, W.H., de Boer, G.J., Wietzes, P., Volkering, F., Janssen, D.B., 2000. Assessment of the use of partitioning and interfacial tracers to determine the content and mass removal rates of nonaqueous phase liquids. Environmental Science and Technology 34 (20), 4301–4306.

Nottebohm, M., Licha, T., Ghergut, I., Nödler, K., Sauter, M., 2010. Development of thermosensitive tracers for push-pull experiments in geothermal reservoir characterization. In: Proceedings of the World Geothermal Congress, Bali, Indonesia.

Nottebohm, M., Licha, T., Sauter, M., 2012. Tracer design for tracking thermal fronts in geothermal reservoirs. Geothermics 43, 37–44.

Nottebohm, M., Licha, T., 2012. Detection of naphthalene sulfonates from highly saline brines with high-performance liquid chromatography in conjunction with fluorescence detection and solid-phase extraction. Journal of Chromatographic Science 50 (6), 477–481.

Reichardt, C., 1994. Solvatochromic dyes as solvent polarity indicators. Chemical Reviews 94 (8), 2319–2358.

Rose, P.E., Benoit, W.R., Kilbourn, P.M., 2001. The application of the polyaromatic sulfonates as tracers in geothermal reservoirs. Geothermics 30 (6), 617–640.

Rose, P.E., Johnson, S.D., Kilbourn, P.M., Kasteler, C., 2002. Tracer testing at Dixie Valley, Nevada using 1-naphthalene sulfonate and 2,6-naphthalene disulfonate. In: Proceedings of the 27th Workshop on Geothermal Reservoir Engineering, Stanford, USA, SGP-TR-171.

Saripalli, K.P., Rao, P.S.C., Annable, M.D., 1998. Determination of specific NAPL-water interfacial areas of residual NAPLs in porous media using the interfacial tracers technique. Journal of Contaminant Hydrology 30 (3–4), 375–391.

Schaffer, M., Boxberger, N., Börnick, H., Licha, T., Worch, E., 2012. Sorption influenced transport of ionizable pharmaceuticals onto a natural sandy aquifer sediment at different pH. Chemosphere 87 (5), 513–520.

Setarge, B., Danzer, J., Klein, R., Grathwohl, P., 1999. Partitioning and interfacial tracers to characterize non-aqueous phase liquids (NAPLs) in natural aquifer material. Physical Chemistry of the Earth, Part B: Hydrology, Oceans and Atmosphere 24 (6), 501–510.

Stryjek, R., Vera, J.H., 1986. PRSV: An improved Peng-Robinson equation of state for pure compounds and mixtures. The Canadian Journal of Chemical Engineering 64 (2), 323–333.

Timko, M.T., Nicholson, B.F., Steinfeld, J.I., Smith, K.A., Tester, J.W., 2004. Partition coefficients of organic solutes between supercritical carbon dioxide and water: experimental measurements and empirical correlations. Journal of Chemical and Engineering Data 49 (4), 768–778.

Tewes, F., Boury, F., 2005. Formation and rheological properties of the supercritical CO2-water pure interface. The Journal of Physical Chemistry B 109 (9), 3990–3997.

Vennila, J.P., Kavitha, H.P., Thiruvadigal, D.J., Manivannan, V., 2008. Phenyl naphthalene-2-sulfonate. Acta Crystallographica Section E 64, o2304.

Vulava, V.M., Perry, E.B., Romanek, C.S., Seaman, J.C., 2002. Dissolved gases as partitioning tracers for determination of hydrogeological parameters. Environmental Science and Technology 36 (2), 254–262.

Wells, A., Diehl, J., Bromhal, G., Strazisar, B., Wilson, T., White, C., 2007. The use of tracers to assess leakage from the sequestration of CO2 in a depleted oil reservoir, New Mexico, USA. Applied Geochemistry 22 (5), 996–1016.

6 Comment on "A closed-form analytical solution for thermal single-well injection-withdrawal tests by Jung and Pruess, Water Res. Research, published 3 March 2012."

Friedrich Maier[1,]* Ibrahim Kocabas[2]

[1]University of Göttingen, Geoscience Centre, Dept. Applied Geology, Goldschmidtstr. 3, 37077 Göttingen, Germany

[2]Izmir Katip Celebi University, Faculty of Engineering and Architecture, Cigli Main Campus, Cigli/Izmir, Turkey

* Corresponding author

The authors Jung and Pruess (2012) are highly commended for addressing two important issues in the context of the inverse problem of heat transport in discrete fractures, i.e., thermal injection-shut-in-backflow tests and thermal injection shut in tests. Specifically, the modelling of thermal injection-shut-in-backflow tests is an important extension of the simpler thermal injection-backflow tests as they are important simulations of sensible energy storage in aquifers (Palmer et al., 1992; Sauty et al., 1978, 1982). The injection shut-in tests solutions, on the other hand, are valuable since they serve as modelling tools for those geothermal wells exhibiting good injectivity but very poor productivity. For poorly productive wells, backflow rates are low, and hence the injection shut-in solutions serve as the most convenient tools of modelling. In their thorough literature review, the authors cited several publications focusing on analytical (e.g. Kocabas, 2005, 2010) and numerical solutions (Pruess and Doughty, 2010) for single-well injection-withdrawal tests (SWIW) using temperature as tracer.

There are four issues pointed out in Jung and Pruess (2012), which we would like to address. First point is related to the efficiency of the solution method as '' ... *the analytical solution (15) for SWIW tests involving injection, quiescent, and withdrawal phases includes a six-dimen- sional improper integral ...* '' and '' ... *the solution (16), which is for SWIW tests with no quiescent period, .. . requires numerical integration only in two and three dimensions.*'' Second, in their discussion of the literature review, they pointed out the typographical errors in derivation process and final equations of Kocabas (2005, 2010). Third issue they addressed is the independence of return profiles from injection flow rate: '' ... *for the withdrawal phase is that the variation of fluid return temperatures with time will be independent of the flow rate.*'' Finally, they discussed the computational efficiency of the analytical and numerical solutions stating ''*For the case of no quiescent time, the analytical solution evaluation is much faster than TOUGH2 (<10 min versus several hours), but with a rest period, TOUGH2 becomes much faster than the analytical solution evaluation. The solution (15) converges extremely slowly, and it takes up to 1 week for computing one point.*''

First, we would like to discuss concerns regarding the *efficiency of solution methods*. The Jung and Pruess (2012) real-space closed-form solution, which includes a shut-in period, is a considerable improvement to that of Kocabas (2005, 2010) developed for injection-backflow tests only. However, to develop the analytical solutions, the solution method employed by Jung and Pruess (2012) appears to be significantly less efficient

than the iterated Laplace trans form (De Smedt and Wierenga, 1981; De Smedt et al., 2005; Kocabas., 2011) employed by Kocabas (2010) and Kocabas and Kucuk (2011). To verify this statement, one should consider Equation (11a) of Jung and Pruess (2012) and Equation (6.1) that we developed using the double and iterated Laplace transform as the injection shut-in solution:

$$T_D = \exp(\theta\, t_{sD})\, erfc\left(\sqrt{\theta\, t_{sD}}\right) H(t_D - x_D)\, erfc\left(\frac{\sqrt{\theta}\, x_D}{2\sqrt{t_D - x_D}}\right) +$$

$$\sqrt{\theta}\ \int\limits_0^\infty H(t_D - x_D)\ erfc\left(\frac{\sqrt{\theta}\, x_D + \eta}{2\sqrt{t_D - x_D}}\right)\ \exp\left(\sqrt{\theta}\,\eta\right)\exp(\theta\, t_{sD})\ erfc\left(\sqrt{\theta\, t_{sD}} + \frac{\eta}{2\sqrt{t_{sD}}}\right)\ d\eta \qquad (6.1)$$

Apparently computational speed of Equation1 which has a semi-infinite integral will be much higher than the Equation (11a) in Jung and Pruess (2012) which contains a two dimensional integral.

In their review, Jung and Pruess (2012) stated "However, the earlier analytical solutions unfortunately include several typographical errors in their derivation process and final equations…". We would like to clarify that the final solutions in Kocabas (2005, 2010) have indeed small typing errors and to avoid any future confusion, the correct equation in Kocabas (2010) reads:

$$T_D = \int\limits_0^{\min(1,\frac{t_n}{\lambda})} \left(\frac{\lambda^2 \sqrt{\alpha}\,\omega}{2(t_n - \lambda\omega)} + \lambda\sqrt{\alpha}\right) \frac{\exp\left(-\dfrac{\lambda^2 \alpha \omega^2}{4(t_n - \lambda\omega)}\right)}{\sqrt{\pi(t_n - \lambda\omega)}}\ erfc\left(\frac{\sqrt{\alpha}\,\omega}{2\sqrt{(1-\omega)}}\right) d\omega +$$

$$\int\limits_0^1 \int\limits_0^{\min\left(1-\eta,\frac{t_n+\eta}{\lambda}\right)} \left(\frac{\lambda^2 \alpha\omega}{t_n + \eta - \lambda\omega} - \frac{\lambda\alpha\omega}{1-\eta-\omega}\right) \frac{\exp\left(\dfrac{-\alpha\omega^2}{4(1-\eta-\omega)}\right)}{\sqrt{\pi(1-\eta-\omega)}} \frac{\exp\left(\dfrac{-\lambda^2 \alpha\omega^2}{4(t_n + \eta - \lambda\omega)}\right)}{2\sqrt{\pi(t_n + \eta - \lambda\omega)}} d\omega\, d\eta \qquad (6.2)$$

Equation (6.2) assumes a simple injection and backflow test with injection to backflow rate ratio equal to λ. For equal injection to backflow rates, i.e. $\lambda = 1$, Equation (6.2) reduces to the correct solution for Kocabas (2005).

Shortly after publication of Kocabas (2010), we worked out that the same solution can be put into a much simpler expression, which is also valid for radial flow geometry (Kocabas and Kucuk, 2011). The new and simpler form is reproduced below for the discussion that follows below and future referencing.

$$T_D = \int_0^{\min(1,\frac{t_n}{\lambda})} erfc\left(\frac{\sqrt{\alpha}\,\tau}{2\sqrt{(1-\tau)}}\right) G(\tau)\ d\tau + \lambda \int_0^{\infty} \sqrt{\alpha} \int_0^{\min(1,\frac{t_n}{\lambda})} erfc\left(\frac{\sqrt{\alpha}\tau + \omega}{2\sqrt{(1-\tau)}}\right) F(\omega)d\tau\,d\omega \quad (6.3)$$

where

$$G(\tau) = \frac{\lambda^2 \sqrt{\alpha}\,\tau}{2\sqrt{\pi(t_n - \lambda\tau)^3}} \exp\left(-\frac{\lambda^2 \alpha\tau^2}{4(t_n - \lambda\tau)}\right)$$

$$F(\omega) = \frac{\lambda\sqrt{\alpha}\tau + \omega}{2\sqrt{\pi(t_n - \lambda\tau)^3}} \exp\left(\frac{-(\lambda\sqrt{\alpha}\tau + \omega)^2}{4(t_n - \lambda\tau)}\right)$$

$$(6.4)$$

with $\alpha = \theta\, t_{Di}$ and $\lambda = \dfrac{u}{u_b}$ $\qquad\qquad$ (6.5)

Note that Equation (6.3) is the solution for a simple injection-backflow test where the ratio of injection rate to backflow rate is λ. Also note that, while Equation (6.2) was developed by using direct inversion of double Laplace transform, we additionally employed the iterated Laplace transform to reach Equation (6.3). Mathematically Equation (6.2) and Equation (6.3) become identical for $\lambda = 1$ (Figure 6.1 and Figure 6.2). While computing time of Equation (6.3) was several times faster than that of Equation (6.2) in Matlab programming, it was at least 10 times faster in Fortran programming.
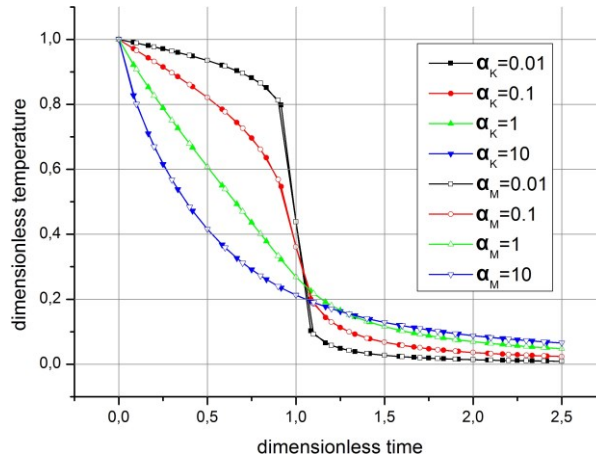
Figure 6.1: Comparison of the results from I. Kocabas (Equation (6.2), subscript K, Fortran) and the results from F. Maier (Equation (6.3), λ = 1, subscript M, Matlab) for α variation.
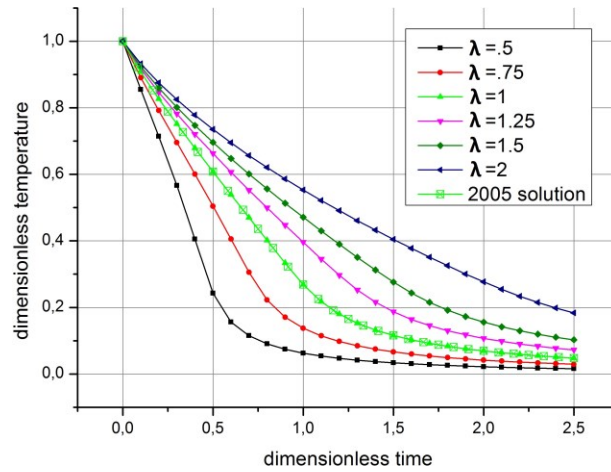
Figure 6.2: Comparison of Equation (6.2) (α = 1) with Equation (6.3) (α = 1, various λ). For λ = 1 the results are identical.

Considering the influence of flow speed allows extension of the illuminative discussion given by Jung and Pruess (2012) for SWIW with a fixed injection/withdrawal rate. Pumping rates are directly connected to the transport equation as they determine the flow velocity in a given fracture system. Equation (6.3) above allows considering different flow velocities for injection and withdrawal expressed by λ. The conclusion that the break through curve (BTC) is independent of flow velocity is given for the special case λ = 1. That implies that the pumping rate equals the injection rate and that the fracture geometry remains stationary during the SWIW. The more generalised case λ ≠ 1 is able to account for two basic processes namely a change in the pumping rates or a change in the fracture geometry. Both result in a change of flow velocity during the runtime of SWIW, where only the latter case could overcome the discussed insensitivity using SWIW as a universal tool to detect enhancing fracture-matrix interface area. While for static reservoirs, during a SWIW, the only changing geometry parameter which could be assessed at the injection/withdrawal well with consecutive SWIWs is the fracture width.

By expanding the solution to *different injection and production rates* more information can be extracted from the BTC. A closer look at Figure (6.3) shows that the BTCs could be split into two parts. The early times, for which $\lambda * t_{pump} < t_{inject}$, and the late times where $\lambda * t_{pump} > t_{inject}$. The BTC varies most during early times, while for late times all curves are more or less equal and not distinguishable should noise in experimental data also be considered. By applying a lower pumping rate we are able to gain more early times data points (by the factor of λ) and therefore the resulting BTC can be interpreted better and more uniquely.
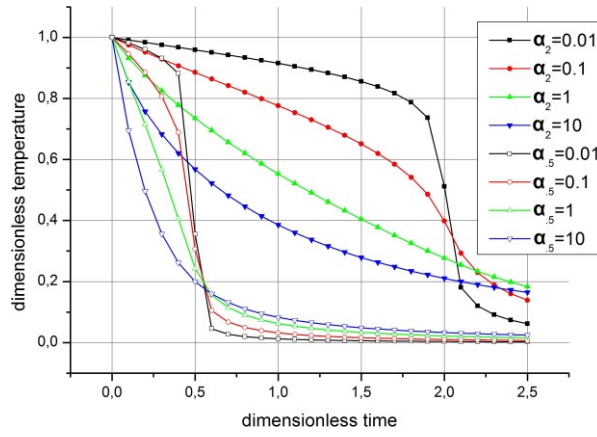
Figure 6.3: Influence of λ on the BTC, Subscripts indicate λ = 2 and λ = 0.5. For a given experimental time and sampling rate we obtain more early times data for higher λ values.

Furthermore, for the rare case when a nearby observation well is located directly along the flow path it is possible to expand the iterated Laplace solution which now allows computing both spatial and temporal distributions of temperature:

$$
T_D = \int_0^{\min(1-x_{Dn}, \frac{t_n}{\lambda})} erfc\left(\frac{\sqrt{\alpha}\,(\tau + x_{Dn})}{2\sqrt{(1-\tau-x_{Dn})}} \right) G(\tau)\ d\tau +
$$

$$
\lambda \int_0^\infty \sqrt{\alpha} \int_0^{\min(1-x_{Dn}, \frac{t_n}{\lambda})} erfc\left(\frac{\sqrt{\alpha}\,(\tau + x_{Dn}) + \omega}{2\sqrt{(1-\tau-x_{Dn})}} \right) F(\omega)d\tau\,d\omega
$$

$$(6.6)$$

Where $G(\tau)$ and $F(\omega)$ are given by Equation (6.4) above respectively. Note that Equation (6.6) above and Equation 16 in Jung and Pruess paper represent the same simple injection backflow tests with the former being more efficient computationally. The introduction of a third dimensionless number x_{Dn} (dimensionless distance) in the solution will give us the opportunity to investigate the influence of the monitoring location (distance from the injection well) on the return profiles at well as well as the direct influence of flow speed which is included in x_{Dn}. In addition, the problem description via two dimensionless numbers α (measure for fracture aperture) and λ (measure for flow velocity ratio) provides the opportunity to examine physically more versatile configurations.

The next issue concerns the *computational efficiency*. Equation (6.3) or Equation (6.6) contain only single and double integrals, and hence, computing Equation (6.3) is several orders of magnitude faster than computing Equation (16) in Jung and Pruess (2012) which involves double and triple integrals. We achieved a significant reduction in computational time from <10 min stated by Jung and Pruess (2012) to few seconds on a

state-of-the-art desktop computer. Hence the solutions given by Equation (6.3) and Equation (6.6) are quite suitable for the nonlinear regression procedures employed for parameter estimation (Figure 6.4). The discussed analytical solutions were cross checked with Finite Element simulations using Comsol Multiphysics®. The simulated BTC was compared with the analytical solution as well as used to test an optimization tool (Figure 6.4). The performance of the whole parameter estimation was in the order of only 10 seconds.

In conclusion Equation (6.3) and Equation (6.6) are the proposed improvements over resolving three issues raised by Jung and Pruess (2012). They are simple in mathematical terms and computationally more efficient compared to Equation 16 in Jung and Pruess (2012). They also avoid the return profile being independent of flow rate by considering different injectivity and productivity for the test well which is a common problem in almost all reservoirs. Finally Equation (6.6) allows to explore the influence of distance between observation and injection well during backflow period.
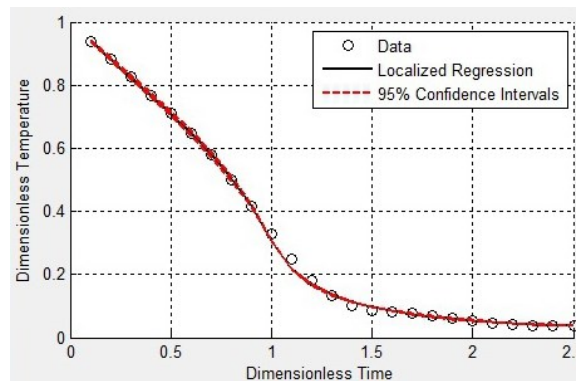
Figure 6.4: Plot section of the optimization tool written in Matlab®. Data originate from FE-Modeling using Comsol Multiphysics®. The synthetic data is for α = 0.36 and the 95% confidence interval of regression is 0.35 < α < 0.39

6.1   References

De Smedt, F., Wierenga, P. J., 1981. A generalized solution for solute flow in soils with mobile and immobile water. Water Resources. Res. Vol. 15,No. 5, pp. 1137-1141.

De Smedt, F., Brevis, W. Debels, P., 2005. Analytical solution for solute transport resulting from instantaneous injection in streams with transient storage. Journal of Hydrology, Vol. 315, pp. 25-39.

Jung, Y., Pruess, K., 2012. A closed-form analytical solution for thermal single-well injection-withdrawal tests. Water Resources Research, 48(3).

Kocabas, I., 2005, Geothermal reservoir characterization via thermal injection backflow and interwell tracer testing. Geothermics, 34, 27–46.

Kocabas, I., 2010. Designing thermal and tracer injection backflow tests. World Geothermal Congress 2010, Bali, Indonesia.

Kocabas, I., 2011. Application of iterated Laplace transformation to tracer transients in heterogeneous porous media. J. Franklin Institute, Volume 348, Issue 7, Sept. 2011, 1339-1362.

Kocabas, I., Kucuk, I., 2011. Modeling Sensible Energy Storage in Aquifers. The 2011 International Conference on Water, Energy and the Environment to in Nov. 14-17, 201 AUS, Sharjah, UAE

Palmer, C.D., Blowes, D.W., Frind, E.O., Molson, J.W., 1992. Thermal energy storage in an unconfined aquifer: 1. Field injection experiment. Water Resources Research, 28(10), 2845-2856.

Pruess, K., Doughty C., 2010. Thermal single-well injection-withdrawal tracer tests for determining fracture-matrix heat transfer area. In: Proceedings of the 35th Workshop on Geothermal Reservoir Engineering Stanford University, Stanford, California, February 1-3, 2010, SGP-TR-188

Sauty, J.P, Gringarten, A., Landel, P.A. 1978.The effect of thermal dispersion on injection of hot water in aquifers. Proc. The Second Invitational Well Testing Symposium, Div. Of Geothermal Energy, U.S. Dept. of Energy. Berkeley CA., 122-131

Sauty, J.P., Gringarten, A., Menjoz, A., Landel, P.A., 1982. Sensible energy storage in aquifers: 1. Theoretical study. Water Resources Research, 18(2), 245-252.

7 Efficient analytical solution for parameter estimation of push shut-in pull experiments in an idealized single fracture system

Friedrich Maier[1], Ibrahim Kocabas[2]

[1]University of Göttingen, Geoscience Centre, Dept. Applied Geology, Goldschmidtstr. 3, 37077 Göttingen, Germany

[2]Izmir Katip Celebi University, Faculty of Engineering and Architecture, Cigli Main Campus, Cigli/Izmir, Turkey

* Corresponding author

Abstract

To estimate efficiency of geothermal energy recovery knowledge of reservoir characteristics and thermal transport parameters is a prerequisite. Recently, heat has emerged as a useful type of tracer in which thermal transients have been monitored and temperature is employed as the state variable. The temperature return profile of thermal injection shut-in backflow test is analyzed to identify the equivalent fracture width or more precisely heat transport rate in a single fracture embedded in a low permeable matrix configuration. The developed computationally high efficient analytical solution is obtained using the method of iterated Laplace transform. Beside the heat transport rate the solution also accounts for temporal changes in the applied pumping/injection rates, which is a common problem in the design of thermal injection shut-in backflow test. Furthermore spatial information in the return profile of the idealized fracture/matrix system is provided by the introduction of a third dimensionless number in the presented solution. The derived spatial and temporal profiles are applied in a nonlinear regression tool written in Matlab®. The new analytical models are an extension of previous work allowing a more comprehensive insight into the collective roles of the parameters controlling heat transport in a single fracture/matrix system.

Nomenclature

b	half fracture width, m
c_m	specific heat of the matrix, J/kg.$^{\circ}$C
c_r	specific heat of fractured zone, J/kg.$^{\circ}$C
c_s	specific heat of reservoir rock, J/kg.$^{\circ}$C
c_w	specific heat of geothermal water, J/kg.$^{\circ}$C
k_m	thermal conductivity of the matrix, W/m.$^{\circ}$C
x	distance along flow direction, m
x_D	dimensionless distance along flow direction
x_{DL}	dimensionless distance of convective front at total injection time
T	temperature in the fractured zone, $^{\circ}$C
T_i	temperature of the injected fluid, $^{\circ}$C
T_0	initial reservoir temperature, $^{\circ}$C
T_D	dimensionless temperature of fracture
T_m	temperature of the matrix, $^{\circ}$C
T_{mD}	dimensionless temperature of matrix
t	injection period time variable, hr
t_D	dimensionless time for injection period
t_{iD}	dimensionless total injection time
t_d	characteristic time for dispersive transport, hr
t_i	total injection time, hr
t_n	backflow period time normalized by total injection time, t_p/t_i

t_p	time variable during backflow period, hr
t_{pD}	dimensionless time during backflow period
t_s	shut-in period time variable, hr
t_{sD}	dimensionless time during shut-in period
s	Laplace transform variable of injection time.
q	Laplace transform variable of shut-in time.
p	Lapace transform variable of backflow time.
q	injection rate, m3/hr
u	interstitial flow velocity, m/hr
z	distance normal to flow direction, m
z_D	dimensionless distance normal to flow direction
θ	ratio of the heat storage capacity of matrix to that of fracture
τ	convolution variable
τ_s	convolution variable for shut in time
ε, ω	dummy integral variables
η	dummy variable
φ	fracture porosity
φ_m	matrix porosity
ρ_m	bulk density of the matrix, kg/m^3
ρ_r	bulk density of the fracture, kg/m^3
ρ_s	density of the reservoir rock, kg/m^3
ρ_w	density of the geothermal water, kg/m^3

7.1 Introduction

The energy stored in geothermal reservoirs is considered to be a major potential energy source (IPCC, 2011). For an efficient exploitation of this resource, a profound knowledge of these reservoirs is essential. However, estimating of reservoir fluid flow characteristics and thermal properties of these reservoirs constitutes a major challenge. Tracer testing provides a valuable instrument to gain significant insides. Beside the well-established chemical tracers, recently heat has emerged as a useful type of tracer. Since temperature is employed as the state variable in thermal test, non-isothermal injection tests can easily extend the classical tracer test domain, which in turn provides a more comprehensive and valuable dataset (Kocabas, 2010). For the analysis of the tracer/temperature return profiles one can apply numerical methods (Pruess and Doughty, 2010; Maier et al., 2012). In case of well-known reservoirs geometries analytical solutions can provide reliable estimates for the parameter of interest (e.g. Haggerty et al., 1998). Recently significant discussions appeared on the inverse problem of heat transport in discrete fractures (Jung and Pruess, 2012, 2013; Maier and Kocabas, 2013). The closed form solutions for thermal injection shut-in backflow test (Jung and Pruess, 2012) and thermal injection backflow test (Maier and Kocabas, 2013) provide a tool for simulations of heterogeneous geothermal reservoirs. Specifically considering the shut-in phase is of interest in the modelling efficiency of sensible energy storage in aquifers (Palmer et al., 1992; Sauty et al., 1978, 1982). The dimensionless heat transfer rate parameter obtained from the temperature profile allows the estimation of thermal properties as well as the width of the energy storage aquifer or fracture transport zone of geothermal reservoirs.

Nonlinear regression analysis serves as a convenient tool to estimate parameter values from experimental data (Dogru et al., 1977). A prerequisite in nonlinear regression analysis is an efficient analytical solution of the describing mathematical model. In the optimization process, which is commonly iterative, several realizations of the analytical solution were derived.

7.2 Injection shut-in backflow tests

Thermal injection shut-in backflow tests could be easily performed in combination with a chemical tracer test. To combine a thermal and a tracer test one has to dilute the tracer in tempered water. The first tempered tracer slug is then followed by continuous injection of tempered water which is used as a driving fluid. Mostly in sensible energy

storage, and in some cases in a geothermal reservoir test prior to the backflow period the system is shut-in. The backflow could be done with an adjusted pumping rate to meet the energy demand or increase the reliability of the thermal tracer test. During the backflow period the state variables of the feed zone namely temperature and tracer concentration is monitored at the well. While the tracer return profile is analyzed for hydraulic properties; the parameters controlling the heat transfer can be estimated from the temperature profile. Minimum testing time is determined by the yield of the injected tracer and/or when the temperature reaches the reservoir temperature.

7.3 Mathematical modeling

describes two different concepts. First it accounts for a single fractured zone of infinite length and constant but significantly large width located in a matrix block. The fracture zone is replaced with the actual aquifer in sensible energy storage experiments. The injected water flows through the fracture zone and is heated by the adjacent matrix walls. In the low porosity matrix advection is neglected. The concept is described in Cartesian coordinates (Figure 7.1). The second concept of sensible energy storage in an aquifer is described by a radial flow geometry with origin at the well. It considers a high porosity/high permeability reservoir with considerable thickness. The reservoir is confined by two impermeable layers. Both concepts assume a uniform lateral temperature in the flow system, with conductive heat transfer into the adjacent layers. Also thermal equilibrium is assumed between rock and water.
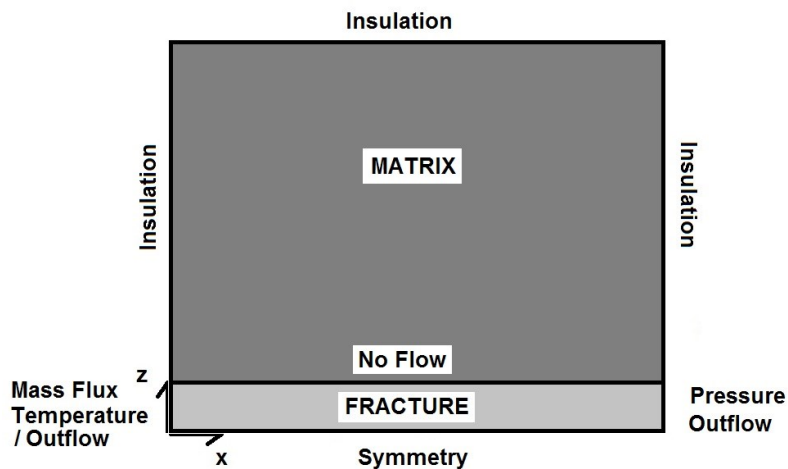
Figure 7.1:   Sketch of the idealized single fracture/matrix configuration.

Although the two scenarios are described by the same dimensionless mathematical model the first represent a fractured geothermal reservoir (Kocabas and Horne, 1990), while the second applies in sensible energy storage aquifers (Sauty et. al., 1978; Sauty et. al., 1982). In the last three decades few authors develop analytical solutions of injection (shut-in) backflow tests. Several authors focus on chemical tracer tests (Kocabas and Horne, 1987; Falade et al., 1987; Falade and Brigham, 1989; Haggerty et al., 1998). Furthermore heat could also applied as an useful tracer (Kocabas and Horne, 1990; Kocabas, 2005; Jung and Pruess, 2012; Maier and Kocabas, 2013). Recently the most comprehensive analytical solution for thermal injection shut-in backflow test in the above mentioned fracture/matrix system was developed (Jung and Pruess, 2012), but whose applicability is limited due to very long computational times. This work presents a new solution to the same injection shut-in backflow tests using triple Laplace transform and employing the powerful iterated Laplace transform theory which provides computationally far superior solutions (Maier and Kocabas, 2013).

7.3.1 Model development

The mathematical model describes an idealized single fractured zone in an infinite matrix system (Figure 7.1). For a radial flow field in sensible energy storage aquifer the same governing dimensionless equations are valid (Kocabas, 2005). In lateral direction we assume a constant thermal conductivity in the matrix, whereas for the fracture it is infinite. Heat conduction and/or dispersion in flow direction is neglected. The governing equations for the heat transport during the injection phase reads:

$$\rho_f c_f \frac{\partial T}{\partial t} + \rho_w c_w \phi u \frac{\partial T}{\partial x} - \frac{k_m}{b} \frac{\partial T_m}{\partial z} \Big]_{z=0} = 0 \tag{7.1}$$

$$\rho_m c_m \frac{\partial T_m}{\partial t} - k_m \frac{\partial^2 T_m}{\partial z^2} = 0 \tag{7.2}$$

Note that the origin of the transverse distance coordinate is located at the fracture matrix boundary. The concerning initial and boundary conditions are given by:

$$T = T_m = T_0 \quad \text{at} \qquad t = 0 \tag{7.3}$$

$$T = T_i \text{ at} \qquad x = 0 \tag{7.4}$$

$$T = T_m \text{ as} \qquad z = 0 \tag{7.5}$$

$$T_m \to 0 \qquad \text{as} \qquad z \to \infty \tag{7.6}$$

Defining the following dimensionless variables:

$$T_D = \frac{T_o - T}{T_o - T_i}, \quad T_{mD} = \frac{T_o - T_m}{T_o - T_i} \tag{7.7}$$

$$x_D = \frac{k_m x}{\rho_w c_w \phi b^2 u}, \qquad t_D = \frac{k_m u t}{\rho_r c_r b^2} \tag{7.8}$$

$$z_D = \frac{z}{b}, \qquad \text{and} \qquad \theta = \frac{\rho_m c_m}{\rho_r c_r} \tag{7.9}$$

Using the above dimensionless variables yields:

$$\frac{\partial T_D}{\partial t_D} + \frac{\partial T_D}{\partial x_D} - \frac{\partial T_{mD}}{\partial z_D}\bigg]_{z_D=0} = 0 \tag{7.10}$$

$$\theta \frac{\partial T_{mD}}{\partial t_D} - \frac{\partial^2 T_{mD}}{\partial z_D^2} = 0 \tag{7.11}$$

The dimensionless initial and boundary conditions become:

$$T_D = T_{mD} = 0 \quad \text{at} \qquad t_D = 0 \tag{7.12}$$

$$T_D = 1 \qquad \text{at} \qquad x_D = 0 \tag{7.13}$$

$$T_{mD} = T_D \qquad \text{at} \qquad z_D = 0 \tag{7.14}$$

$$T_{mD} \to 0 \qquad \text{as} \qquad z_D \to \infty \tag{7.15}$$

Using Laplace transform, where Laplace space variable s corresponds to real space time variable t_D, the following Laplace domain solutions of injection period are obtained:

$$\dot{T}_D = \frac{1}{s} \exp(-s x_D) \exp(-\sqrt{\theta s}\, x_D) \tag{7.16}$$

$$\dot{T}_{mD} = \frac{\exp(-s x_D)}{s} \exp(-\sqrt{\theta s}\, x_D) \exp(-\sqrt{\theta s}\, z_D) \tag{7.17}$$

During the shut-in period, the time variable should be written as t_s and the heat transport equations become as follows:

$$\rho_f c_f \frac{\partial T}{\partial t_s} - \frac{k_m}{b} \frac{\partial T_m}{\partial z} \bigg]_{z=0} = 0 \qquad (7.18)$$

$$\rho_m c_m \frac{\partial T_m}{\partial t_s} - k_m \frac{\partial^2 T_m}{\partial z^2} = 0 \qquad (7.19)$$

Since we have initiated a new time domain during shut-in the related initial condition becomes as follows:

$$T = T(t_i, x) \quad \text{at} \quad t_s = 0 \qquad (7.20)$$

where t_i is the total injection time and hence

$$t_{Di} = \frac{k_m u t_i}{\rho_r c_r b^2} \qquad (7.21)$$

No boundary condition is required in the x direction for Equation (7.18). The boundary conditions for matrix are the same as Equation (7.4) and Equation (7.5).

Using earlier defined dimensionless variables and the following dimensionless shut-in time

$$t_{sD} = \frac{k_m u t_s}{\rho_r c_r b^2} \qquad (7.22)$$

The governing dimensionless equations becomes:

$$\frac{\partial T_D}{\partial t_{sD}} - \frac{\partial T_{mD}}{\partial z_D} \bigg]_{z_D=0} = 0 \qquad (7.23)$$

$$\theta \frac{\partial T_{mD}}{\partial t_{sD}} - \frac{\partial^2 T_{mD}}{\partial z_D^2} = 0 \qquad (7.24)$$

The dimensionless initial and boundary conditions:

$$T_D = T_D(t_{Di}, x_D) \qquad \text{at} \qquad t_{sD} = 0 \qquad (7.25)$$

$$T_{mD} = T_{mD}(t_{Di}, x_D, z_D) \qquad \text{at} \qquad t_{sD} = 0 \qquad (7.26)$$

$$T_{mD} = T_D \qquad \text{at} \qquad z_D = 0 \tag{7.27}$$

$$T_{mD} \to 0 \qquad \text{as} \qquad z_D \to \infty \tag{7.28}$$

Again using Laplace transform where t_{pD} corresponds to Laplace variable p, the solution during shut-in period in double Laplace space is given as:

$$\ddot{T}_D = \left(1 + \frac{\sqrt{\theta}}{\sqrt{p} + \sqrt{s}}\right) \frac{\dot{T}_D(s)}{p + \sqrt{\theta p}} \tag{7.29}$$

$$\ddot{T}_{mD} = \ddot{T}_D \exp\left(-z_D \sqrt{\theta p}\right) + \frac{\dot{T}_D(s)}{p-s} \left(\exp\left(-z_D \sqrt{\theta s}\right) - \exp\left(-z_D \sqrt{\theta p}\right)\right) \tag{7.30}$$

Finally for the backflow period, the time variable should be written as t_p. For the fracture zone equation, the advective term must change sign and we may assume an unequal injection to backflow rate, yielding:

$$\rho_f c_f \frac{\partial T}{\partial t_p} - \rho_w c_w \phi u_b \frac{\partial T}{\partial x} - \frac{k_m}{b} \frac{\partial T_m}{\partial z}\bigg]_{z=0} = 0 \tag{7.31}$$

The matrix equation remains unchanged.

The corresponding initial and boundary conditions become as follows:

$$T = T(t_i, t_s, x) \qquad \text{at} \qquad t_p = 0 \tag{7.32}$$

$$T = T_o \qquad \text{at} \qquad x = L = ut_i \tag{7.33}$$

$$T_m = T_m(t_i, t_s, x, z) \qquad \text{at} \qquad t_p = 0 \tag{7.34}$$

Where t_i is the total injection time and t_s is the total shut-in time and the ratio of the injection rate to backflow rate and dimensionless backflow time are defined respectively as:

$$\lambda = \frac{u}{u_b} \tag{7.35}$$

and

$$t_{pD} = \frac{k_m t_p}{\rho_r c_r b^2} \tag{7.36}$$

Using t_{pD} as the dimensionless time variable for the backflow period, dimensionless governing equations for the backflow period are:

$$\frac{\partial T_D}{\partial t_{pD}} - \frac{1}{\lambda}\frac{\partial T_D}{\partial r_D} - \frac{\partial T_{mD}}{\partial z_D}\bigg]_{z_D=0} = 0 \tag{7.37}$$

$$\theta \frac{\partial T_{mD}}{\partial t_{pD}} - \frac{\partial^2 T_{mD}}{\partial z_D^2} = 0 \tag{7.38}$$

The initial and boundary conditions for the backflow period are specified in Equations (7.39), (7.41) and (7.42):

$$T_D = T_D(t_{Di}, t_{sD}, x_D) \qquad \text{at} \qquad t_{pD} = 0 \tag{7.39}$$

Where t_i is the total injection time and, hence,

$$t_{Di} = \frac{k_m t_i}{\rho_r c_r b^2} \tag{7.40}$$

$$T_{mD} = T_{mD}(t_{Di}, x_D) \qquad \text{at} \qquad t_{pD} = 0 \tag{7.41}$$

$$T_D = 0 \qquad \text{at} \qquad x_D = x_{DL} = \frac{k_m t_i}{\rho_w c_w \phi b^2} \tag{7.42}$$

The boundary conditions for the bounding layer remain unchanged, and hence, Equations (7.27) and (7.28) apply.

Applying a triple Laplace transform with respect to injection shut-in and pumping times (where t_{Di} relates to s, t_{sD} relates to p and t_{pD} relates to q in Laplace space) we reach in the triple Laplace space domain:

$$\dddot{T}_D = \frac{\lambda}{s}\frac{e^{-sx_D}e^{-\sqrt{\theta s}x_D}}{s + \sqrt{\theta s} + \lambda q + \lambda\sqrt{\theta q}}[F] \tag{7.43}$$

with

$$F = \left(1 + \frac{\sqrt{\theta}}{\sqrt{p} + \sqrt{S}}\right)\frac{1}{p + \sqrt{\theta p}}\left(1 + \frac{\sqrt{\theta}}{\sqrt{q} + \sqrt{p}}\right) - \frac{1}{p-s}\left(\frac{\sqrt{\theta}}{\sqrt{q} + \sqrt{p}} + \frac{\sqrt{\theta}}{\sqrt{q} + \sqrt{s}}\right) \tag{7.44}$$

Note that $\overset{\cdots}{T}_D$ composes of six summands, where each is inverted separately to real space applying the method of iterated Laplace transform (Sneddon, 1972). A more detailed derivation is found in Appendix A. The final real space solution reads:

$$T_D = \left(T_{D1\_1} + T_{D1\_2}\right) + \left(T_{D2\_1} + T_{D2\_2}\right) - T_{D3} + T_{D4} \tag{7.45}$$

with the summands given in Table 7.1.

Table 7.1: *Summands of the real space solution obtained from the iterative Laplace transformation.*

$$T_{D1\_1} = \lambda e^{\theta t_{sD}} erfc\sqrt{\theta t_{sD}} \int_0^{\min\left(t_D - \chi_D, \frac{t_{pD}}{\lambda}\right)} erfc\frac{\sqrt{\theta}(x_D + \tau)}{2\sqrt{t_D - x_D - \tau}} \frac{\lambda\sqrt{\theta}\tau}{2\sqrt{\pi(t_{pD} - \lambda\tau)^3}} e^{-\frac{\lambda^2\theta\tau^2}{4(t_{pD} - \lambda\tau)}} d\tau$$

$$T_{D1\_2} = \lambda e^{\theta t_{sD}} \int_0^\infty \int_0^{\min\left(t_D - x_D, \frac{t_{pD}}{\lambda}\right)} erfc\frac{\sqrt{\theta}(x_D - \tau) + \frac{\omega}{\sqrt{\theta}}}{2\sqrt{t_D - x_D - \tau}} \frac{\lambda\sqrt{\theta}\tau}{2\sqrt{\pi(t_{pD} - \lambda\tau)^3}} e^{-\frac{\lambda^2\theta\tau^2}{4(t_{pD} - \lambda\tau)}} d\tau$$
$$e^\omega erfc\frac{\omega + 2\theta t_{sD}}{2\sqrt{\theta t_{sD}}} d\omega$$

$$T_{D2\_1} = \lambda e^{\theta t_{sD}} \int_0^\infty \int_0^{\min(t_D - x_D, t_{pD} - \lambda\tau)} erfc\frac{\sqrt{\theta}(x_D + \tau)}{2\sqrt{t_D - x_D - \tau}} \frac{\lambda\sqrt{\theta}\tau + \frac{\varepsilon}{\sqrt{\theta}}}{2\sqrt{\pi(t_{pD} - \lambda\tau)^3}} e^{-\frac{\left(\lambda\sqrt{\theta}\tau + \frac{\varepsilon}{\sqrt{\theta}}\right)^2}{4(t_{pD} - \lambda\tau)}}$$
$$e^\varepsilon erfc\frac{\varepsilon + 2\theta t_{sD}}{2\sqrt{\theta t_{sD}}} d\tau\, d\varepsilon$$

$$T_{D2\_2} = \lambda e^{\theta t_{sD}} \int_0^\infty \int_0^\infty \int_0^{\min\left(t_D - x_D, \frac{t_{pD}}{\lambda}\right)} erfc\frac{\sqrt{\theta}(x_D + \tau) + \frac{\omega}{\sqrt{\vartheta}}}{2\sqrt{t_D - x_D - \tau}} \frac{\lambda\sqrt{\theta}\tau + \frac{\varepsilon}{\sqrt{\theta}}}{2\sqrt{\pi(t_{pD} - \lambda\tau)^3}} e^{-\frac{\left(\lambda\sqrt{\theta}\tau + \frac{\varepsilon}{\sqrt{\theta}}\right)^2}{4(t_{pD} - \lambda\tau)}}$$
$$e^{\varepsilon + \omega} erfc\frac{\varepsilon + \omega + 2\theta t_{sD}}{2\sqrt{\theta t_{sD}}} d\tau\, d\varepsilon\, d\omega$$

$$T_{D3} = \lambda \int_0^\infty \int_0^{t_{sD}} \int_0^{\min\left(t_D + \tau_s - x_D, \frac{t_{pD}}{\lambda}\right)} erfc\frac{\sqrt{\theta}(x_D + \tau)}{2\sqrt{t_D + \tau_s - x_D - \tau}} \frac{\lambda\sqrt{\theta}\tau + \frac{\varepsilon}{\sqrt{\theta}}}{2\sqrt{\pi(t_{pD} - \lambda\tau)^3}} e^{-\frac{\left(\lambda\sqrt{\theta}\tau + \frac{\varepsilon}{\sqrt{\theta}}\right)^2}{4(t_{pD} - \lambda\tau)}}$$
$$\frac{\varepsilon}{2\sqrt{\pi\theta(t_{sD} - \tau_s)^3}} e^{-\frac{\varepsilon^2}{4\theta(t_{sD} - \tau_s)}} d\tau\, d\tau_s\, d\varepsilon$$

$$T_{D4} = \lambda \int_0^\infty \int_0^{\min\left(t_D + t_{sD} - x_D, \frac{t_{pD}}{\lambda}\right)} erfc\frac{\sqrt{\theta}(x_D + \tau) + \frac{\eta}{\sqrt{\theta}}}{2\sqrt{t_D + t_{sD} - x_D - \tau}} \frac{\lambda\sqrt{\theta}\tau + \frac{\eta}{\sqrt{\theta}}}{2\sqrt{\pi(t_{pD} - \lambda\tau)^3}} e^{-\frac{\left(\lambda\sqrt{\theta}\tau + \frac{\eta}{\sqrt{\theta}}\right)^2}{4(t_{pD} - \lambda\tau)}} d\tau\, d\eta$$

Mathematically Equation (7.45) converges with $t_{sD} \rightarrow 0$ against the simpler solution for an injection withdrawal test only (Maier and Kocabas, 2013).

7.4 Computational efficiency

The closed form analytical solution is implemented in a nonlinear regression tool implemented in Matlab$^{®}$. That allows a convenient evaluation of Equation (7.45). The two and three dimensional integrals (Table 7.1) were evaluated numerically using build-in Matlab® functions. Note that the problem can entirely described by three dimensionless numbers:

- λ ratio of flow velocities,

- $\alpha = \theta t_{Di}$ parameter product which accounts for the ratio of heat storage capacity in the fracture and matrix, as well as the heat transfer which is a function of the fracture width.

- x_D the dimensionless distance which allows interpretation of a nearby observation well and also influences of the flow velocity.

For the evaluation of Equation (7.45) the most computational power is needed for the summands T_{D2} and T_{D3} as they contain triple integrals (Figure 7.2). One evaluation round of for a set of 25 data points on a state of the art desktop computer has a solution time in the order of one to few minutes, depending on the actual dimensionless parameters. This is a superior computational feature compared to that is presented by Jung and Pruess (2012).
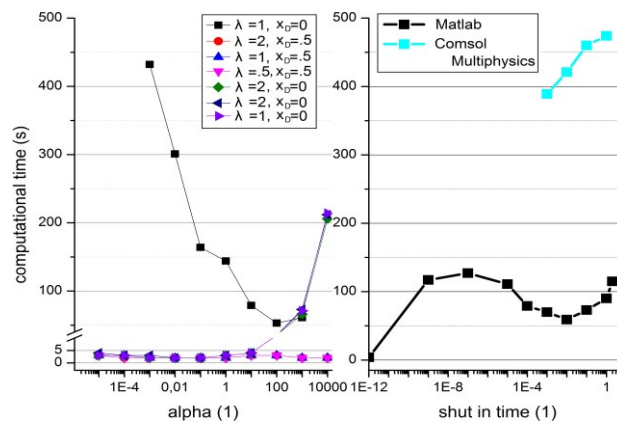

Figure 7.2: *Left: Evaluation time of Equation (7.45). All evaluations used $T_{sD} \approx 0$. Except the black curve where $T_{sD} = 0.4$. For longer shut-in times and for higher α values the computational demand increase.*

     Right: Comparison of the computational time for the numerical simulator and Equation (45) for $\alpha = 10$, $\lambda = 1$ and $x_D = 0$

7.5 Solution verification

For a vanishing shut-in time the problem reduces to a simpler thermal injection pumping test. Hence Equation (7.45) must converge against that simpler injection backflow solution. The evaluation of $t_{sD} \to 0$ can be compared to the analytical solution presented by Maier and Kocabas (2013). Note that all three above mentioned dimensionless parameters were varied. The deviations were all in the order of the computational accuracy (Figure 7.3). To validate the solution including a considerable shut-in phase the evaluations were compared to the results from a numerical simulator. The injection shut-in pumping test was modeled with Comsol Multiphysics[®] (Maier et al., 2012). Comsol Multiphysics[®] is proprietary software employing the Finite Element method. The results show a very good fit in the considered range for $\alpha = 10$ and shut-in times ranging between 1% and 100% of the injection time (Figure 7.4).
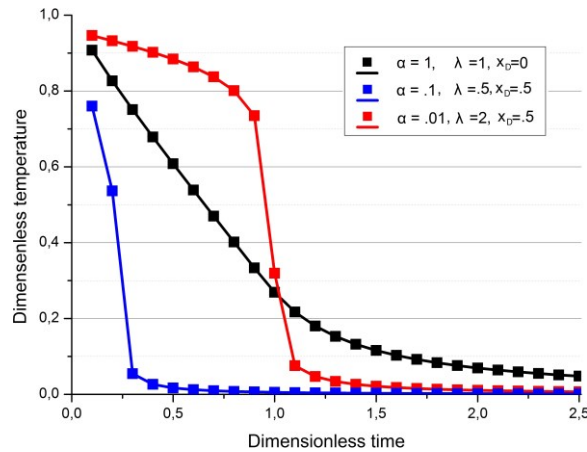
Figure 7.3: Comparison of the results from Equation (7.45) with $t_{sD} = 0$ (solid line) with the results from the simpler injection-pumping solution (squares) (Maier and Kocabas, 2013)
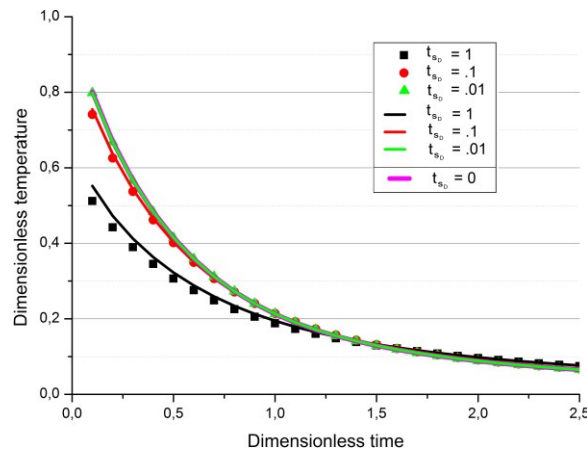
Figure 7.4: Comparison of Comsol model (symbols) with Matlab evaluation (solid lines) of Equation (7.45) for different shut-in times and $\alpha = 10$. In pink is the simpler injection backflow solution (Maier and Kocabas, 2013)

One can clearly see that the solution converges for short shut-in times against the simpler injection-pumping test solution. Significant differences arise when the shut-in phase is longer than 1% of the injection phase. For longer shut-in phases the results of the numerical simulator are affected by numerical dispersion (Maier et al., 2012) but show still a good agreement (Figure 7.5). For very low or very high α values the temperature return profile becomes more insensitive to measure fracture aperture, especially when noise is considered. The introduction of a shut-in phase could widen the sensitivity of thermal injection shut-in backflow test in terms of a measure for heat transfer since for different shut-in times the higher/lower heat transfer has a significant different impact (Figure 7.6) on the temperature return profile.
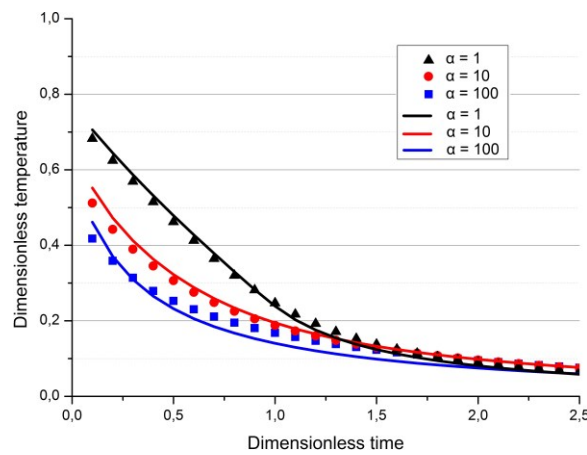
Figure 7.5: Comparison of the results from the Comsol model model (symbols) with evaluations of Equation (7.45) (solid lines) for $t_{sD} = 1$

Figure 7.6:   *Impact of the shut-in time on the temperature return profil with $\lambda = 1$ and $x_D = 0$.*

7.6 Conclusion

With the applied methods of triple Laplace transformation and iterative Laplace transformation a novel solution for thermal injection shut-in backflow test has been developed. It is an important extension over earlier solutions since it extends the insights on the collective role of parameters dominating the heat transfer in a single geothermal fracture zone or sensible energy storage aquifer.

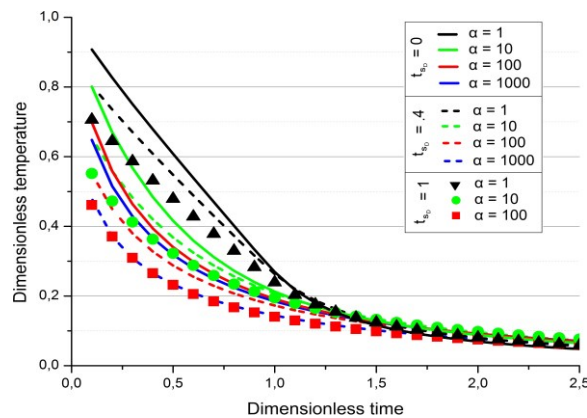The triple Laplace transformation is applied on governing equations to obtain the Laplace space solution. The very same in turn is inverted to real space employing the method of iterated Laplace transformation. The combination of these two methods results in mathematically efficient closed form solutions.

The presented closed form analytical solution for a thermal injection shut-in backflow test allows the implementation in nonlinear regression tools. It meets the prerequisite to be solvable in reasonable time. For a good initial guess the number of iteration is in the order of 10, which results in a regression time of roughly 10 min.

The introduction of an additional decision variable, namely shut-in time provides a small increase in sensitivity. Considering the shut-in time will probably not increase the sensitivity dramatically so that the applicability in fractured reservoirs is still questioned. Due to very long injection times, which is needed to have a representable feed-zone and fracture apertures in geothermal reservoirs, which were normally very small one has to deal with high α values. Hence injection shut-in backflow tests are probably most useful for sensible energy storage in aquifers where the permeable layer is of considerable thickness.

Beside the heat transport rate the obtained solution resolves temporal influences arising from applying different pumping/injection rates. By the introduction of a third dimensionless number questions on spatial behaviour of the injected temperature front can be answered.

Finally one important finding is that the new developed solution must be applied when shut-in time is longer than 1% of injection time. The new solution also allows best design of the single well tests. It shows that if the shut in time is short then it gives no additional information on the system. That is the results are almost identical to simple injection backflow tests.

Acknowledgements

7.7 References

De Smedt, F., Wierenga, P.J., 1981. A generalized solution for solute flow in soils with mobile and immobile water. Water Resources Research, 15(5), 1137-1141.

De Smedt, F., Brevis, W., Debels, P., 2005. Analytical solution for solute transport resulting from instantaneous injection in streams with transient storage. Journal of Hydrology, 315(1), 25-39.

Dogru, A. H., Dixon, T. N., Edgar, T.F., 1977. Confidence Limits on the Parameters and Predictions of Slightly Compressible Single-Phase Reservoirs. Society of Petroleum Engineers Journal, 17(01), 42-56.

Falade, G.K., Antunez, E., Brigham, W.E., 1987. Mathematical analysis of single-well tracer tests. Tecnical Report Supri Tr-57, Stanford University Petroleum Research Institute, Stanford, CA.

Falade, G.K., Brigham W.E., 1989. Analysis of radial transport of reactive tracer in porous media. SPE reservoir engineering, 4(01), 85-90.

Haggerty, R., Schroth, M.H., Istok, J.D., 1998. Simplified Method of "Push‐Pull" Test Data Analysis for Determining In Situ Reaction Rate Coefficients. Groundwater, 36(2), 314-324.

IPCC, 2011. IPCC Special Report on Renewable Energy Sources and Climate Change Mitigation. Prepared by Working Group III of the Intergovernmental Panel on Climate Change [O. Edenhofer, R. Pichs-Madruga, Y. Sokona, K. Seyboth, P. Matschoss, S. Kadner, T. Zwickel, P. Eickemeier, G. Hansen, S. Schlömer, C. von Stechow (eds)]. Cambridge University Press, Cambridge, United Kingdom and New York, NY, USA, 1075 pp.

Jung, Y., Pruess K., 2012. A closed-form analytical solution for thermal single-well injection-withdrawal tests. Water Resources Research, 48(3).

Jung, Y., Pruess K., 2013. Reply to comment by Maier and Kocabas on "A closed-form analytical solution for thermal single-well injection-withdrawal tests. Water Resources Research, 49(1). 644-646

Kocabas, I., Horne, R.N., 1987. Analysis of injection-backflow tracer tests in fractured geothermal reservoirs. In: Proceedings of the 12th Workshop on Geothermal Engineering, Stanford Univ., Stanford, CA, January 20-22, 1987, SGP-TR-109.

Kocabas, I., Horne, R.N., 1990. A new method of forecasting thermal breakthrough time during the reinjection in geothermal reservoirs. In: Proceedings of the 15th Workshop on Geothermal Engineering, Stanford Univ., Stanford, CA, January 23-25, 1990, SGP-TR-130.

Kocabas, I., 2005. Geothermal reservoir characterization via thermal injection backflow and interwell tracer testing. Geothermics, 34, 27–46.

Kocabas, I., 2010. Designing Thermal and Tracer Injection Backflow Tests. Proceedings World Geothermal Congress 2010 Bali, Indonesia, 25−29 April 2010.

Kocabas, I., 2011. Application of iterated Laplace transformation to tracer transients in heterogeneous porous media. J. Franklin Institute, 348(7) Sept. 2011, 1339-1362.

Maier, F., Oberdorfer, P., Kocabas, I., Ghergut, I., Sauter, M., 2012. Using Temperature Signals to Estimate Geometry Parameters in Fractured Geothermal Reservoirs. Proceedings of the 2012 Comsol Conference Milan

Maier, F., Kocabas, I., 2013. Comment on "A closed‐form analytical solution for thermal single‐well injection‐withdrawal tests" by Jung and Pruess. Water Resources Research, 49(1), 640-643.

Palmer, C.D., Blowes, D.W., Frind, E.O., Molson, J.W., 1992. Thermal energy storage in an aquifer 1. Field Injection experiment. Water resources Research, 28(10), 2845-2856.

Pruess, K., Doughty C., 2010. Thermal single-well injection-withdrawal tracer tests for determining fracture-matrix heat transfer area. In: Proceedings of the 35th Workshop on Geothermal Reservoir Engineering Stanford University, Stanford, California, February 1-3, 2010, SGP-TR-188

Sauty, J.P, Gringarten, A., Landel, P.A., 1978. The effect of thermal dispersion on injection of hot water in aquifers. Proc. The Second Invitational Well Testing Symposium, Div. Of Geothermal Energy, U.S. Dept. of Energy. Berkeley CA., 122-131.

Sauty, J.P., Gringarten, A., Menjoz, A., Landel, P.A., 1982. Sensible energy storage in aquifers: 1. Theoretical study. Water Resources Research, 18(2), 245-252.

Sneddon, I.A., 1972. The use of integral Transforms. MCGRaw Hill, NY.

8 General conclusions and perspectives

Because applied tracers are transported with the working fluid, tracer tests provide valuable insights regarding the probed reservoirs. Recorded tracer signals contain an integral footprint of the in-situ interaction between the tracer and the reservoir. In order to extract information from such tests, a sound understanding of the occurring processes is required. This work provides a contribution to the necessary step of tracer examination prior to field experiments. With approaches that are based on experimental laboratory work and theoretical considerations, it narrows the gap, in particular for hydrolysis tracers and heat injection, between tracer preparation and field application. The developments help to mitigate evaluation uncertainties of tracer response in field experiments, enabling a reliable quantitative analysis instead of a more common qualitative interpretation. The examined tracers can provide reservoir management applications with such significant metrics as: thermal state, cooling fraction, liquid/liquid interface area, fracture width and heat transport rate. An effective application of thermo-sensitive tracers is performed for the first time in a dynamic system, finding sensitivity to both thermal-state and cooling fraction specifications. With the proven selective and boundary condition specific reaction, the utilization of hydrolysis is successfully extended to further evaluate the liquid/liquid interface area. The joint application with heat injection is also advanced. A set of analytical solutions are derived to analyze the SWIW temperature signals, measured during (hydrolysis) tracer tests. The new solutions provide fresh insights in the collective role of the various parameters controlling heat transport.

Eventually, the joint application of thermo-sensitive tracers and heat has the potential to provide a powerful test routine. When the application of thermo-sensitive tracers is accompanied with a conservative reference tracer, the recorded data from the combined experiment can be analyzed for the following complementing reservoir properties:

- Transport-relevant Properties e.g., residence time (distribution), hydraulic connection, dispersion, etc. from the conservative tracer
- Thermal-state, e.g., cooling fraction and in-situ temperatures from the thermo-sensitive tracers
- Heat Transfer Rates and Fracture-width (or equivalent heat exchange surface density) from the heat injection experiments.

For some reservoirs, this set of metrics may be sufficient for the evaluation of thermal state and future evolution; however, further research is needed to reduce ambiguity and uncertainty arising from reservoir heterogeneities, geometry variations and/or non-representative reservoir volumes. Further evaluation is also needed for the specific design of a combined tracer test. While a significant temperature contrast between the tracer fluid and reservoir conditions is essential for a heat injection experiment, such a difference should be minimized for thermo-sensitive tracers. In cases where a pronounced temperature-disparity is present due to heat injection, the faster transport of solute tracers could be advantageous, since the short residence time in the disturbed entry zone would serve to minimize the bias on the thermo-sensitive signal. Further experiments and modeling approaches could help to solve these questions.

8.1 Examination of hydrolysis tracers

This work identifies hydrolysis tracers as a powerful tool to enhance the potential metrics of tracer tests for optimal reservoir management. Since control over the experimental conditions in field experiments is often impossible, systematic laboratory conditions are needed to better understand the properties and dynamic interactions of hydrolysis tracers before their introduction in field experiments.

8.1.1 Thermo-sensitive tracers in dynamic systems

Thermo-sensitive tracers are believed to have significant potential as a tool for reservoir management procedures, particularly for the estimation of two important reservoir metrics: thermal state and thermal evolution. This thesis contributes an effective application of this tool, which, to date, has never before been demonstrated. The capability of thermo-sensitive tracers is reliably demonstrated through the employment of a unique experimental design, which implements columns in a controlled lab-setting, the results of which contribute to the important step of tracer evaluation prior to application in a field experiment. Due to the establishment of known boundary conditions (e.g. temperature, water chemistry, pumping rate, geometry and material properties) the quantification of the contributing processes is possible.

The results from Flow-through, Push-pull and Moving-front Experiments validate the underlying theory while yielding precise and accurate evaluations of the targeted metrics. The results are found to be independent of changes in residence time and/or measured concentrations, while the degree of uncertainty is quickly minimized with

multiple experiments. While expressing the results in absolute temperatures is very intuitive, the transformations from the obtained reaction rates could yield an additional (unnecessary) error source. Furthermore, compared with thermo-sensitive tracers, where the analysis is based on attenuation, the hydrolysis thermo-sensitive tracers used in this study have several advantages. First of all, both the reaction products and the reaction mechanism are well understood. Hence, the influence of pH, or more precisely OH-, concentration can be considered. Furthermore, due to its fluorescing property and the signal increase with longer residence time, the reaction product can be measured more easily. Moreover, it is essential to accompany the hydrolysis thermo-sensitive tracer with a conservative tracer. Also an intensive evaluation of the occurring temperatures, pH of the reservoir, and expected residence time should be performed, in order to choose the most suitable thermo-sensitive tracer compound.

The presented results can serve as a benchmark problem for more complex scenarios. The model should be expanded to evaluate other flow scenarios, in order to accommodate a residence time distribution that is based on multiple pathways. Methods are needed to estimate in-situ temperature distribution from the obtained break-through curves. For a reliable use as a reservoir management tool a revival of field scale experiments is proposed. Also, the results enable a better implementation, supporting the necessary planning steps. Being that the phenol acetate used in this work is suitable for low-temperature domains, it might be implemented in low-temperature reservoirs, or for SWIW experiments in the cooled vicinity of the injection well. These experiments should be accompanied with an investigation of the chemical compatibility of the various materials that are intended to be used: e.g. chemicals, storage containers, piping, in situ reservoir water and rock, etc. It would be very useful to revise the experimental setup to extend its application to high-pressure and high-temperature conditions. Compounds which feature a relatively higher stability, such as amides and carbamates, should also be tested prior to application in field experiments.

For a successful transfer of the laboratory results, a comprehensive understanding of the base catalyzed hydrolysis is necessary. The application of numerical simulations which consider the dependence of water-chemistry on temperature is vital for a comprehensive understanding of the catalyzed hydrolysis reaction. Furthermore, since such an insight would enable the successful transfer of laboratory results into high-temperature settings, as well as those that feature stark temperature disparities and distinct chemical

equilibrium conditions, such models are essential for accurate interpretations of experimental results.

8.1.2 Development of Interface-sensitive Tracers

A concept and methodology is proposed for the design and application of tracers for the estimation of the interfacial area between scCO2 and water. Such a tracer (referred to as the KIS-tracer) must satisfy several requirements. The tracer itself should feature a high solubility in the non-aqueous phase with a negligible amount of partitioning, while one of the tracer products must feature a high solubility in the aqueous phase with negligible partitioning. Phenyl naphthalene-2-sulfonate, which is synthesized via esterification of the naphthalenesulfonate base structure, fulfills these requirements for a KIS-tracer. While the ester is non-polar (log K_{OW} = 4.29) the polar, anionic reaction product features a high solubility (log $D_{OW \ (pH \ > \ 5)}$ = −2.87) in water with a behavior that is expected to be conservative. The transfer-rate over the interface can then be expressed by a pseudo zero-order reaction, which is driven by the size of the interface. In order to test this methodology, an analogue approach is presented first; then, numerically evaluated. A linear increase of the reaction product (2-naphthalenesulfonic acid) over time is obtained through the use of n-octane and water as the two phases with a fixed interface area and volume. This verifies the expected zero-order reaction kinetics at the interface, which means that a constant mass flux across the interface can be determined. A derived macroscopic numerical model is calibrated, in order to test the experimental results and various reference scenarios.

On this basis, the next step in research should be the implementation of KIS-tracer in two-phase porous media models, in order investigate the spreading of the plume in reservoirs. Such models can also help predict required reaction-speeds for application in laboratory and field experiments. The target design can then be employed in other base structures that meet the time and space requirements. Based on these results, the extension of the static batch experiment to dynamic systems (analogue to the approach described for thermo-sensitive tracers) would be of interest. Furthermore the tracer examination must be extended to quantify the influence of pH and temperature on KIS-tracers. To understand/interpret the results a comprehensive physicochemical model is necessary. Eventually, all of these results lead to target-designed KIS-tracers for case studies in field application.

8.2 Derivation of analytical solutions for thermal single well injection (shut-in) withdrawal experiments

Analytical solutions provide a powerful tool for the evaluation of temperature data obtained from thermal single-well injection (shut-in) withdrawal experiments. Compared with numerical simulations, such solutions are not skewed by space and time discretization errors. The presented exact solutions support a full-understanding of the occurring transport phenomena inside idealized fractured media with insights regarding the impact of rock-matrix interaction and fracture aperture under consideration of convective heat transfer within both the fracture and the adjacent rock matrix. The revised solutions for a thermal SWIW experiment illustrate how the inversion method impacts the complexity of the obtained solutions. The most efficient solutions are obtained with an inversion based on the iterated Laplace transform. This method leads to, what are in mathematical terms, relatively simple and computationally efficient solutions. The existing problem regarding the inversion of the solution in the Laplace domain, under consideration of the shut-in period in the derivation process is also overcome. With the introduction of a shut-in duration as an additional independent decision variable, more flexibility is possible. Finally, the exact solutions are extended to consider observations from a distant well.

The formulation of the problem in dimensionless form allows the description of heat transport in a fractured system with the following three characterizing numbers: λ ratio of flow velocities; $\alpha = \theta t_{Di}$ parameter product which accounts for the ratio of heat storage capacity in the fracture and matrix, as well as the heat transfer which is a function of the fracture width; and x_D the dimensionless distance which allows interpretation of a nearby observation well and considers the influence of flow velocity.

Analytical solutions help to improve a quantitative analysis; therefore, they can be implemented as kernels in non-linear optimization algorithms. The possibilities and limitations for determining the thermal characteristics of fracture-matrix interactions with thermal SWIW tests can also be explored through the use of such algorithms. A sensitivity analysis along with the quantification of the sensitivity increase, due to such chosen decision variables as the applied 'shut-in time' should be performed as well. Furthermore, for wider fracture-widths, the influence of longitudinal and transversal dispersion would be of interest. Finally, a generalization of the solutions towards more realistic systems, featuring multiple (parallel) fractures, would be valuable. Further

experiments are needed to investigate practical and useful applications in georeservoirs, as well as the required representative volumes. Finally, the analytical solution should be applied to experimental data, in order to test the applicability and sensitivity of thermal SWIW tests.

Appendix

Appendix A
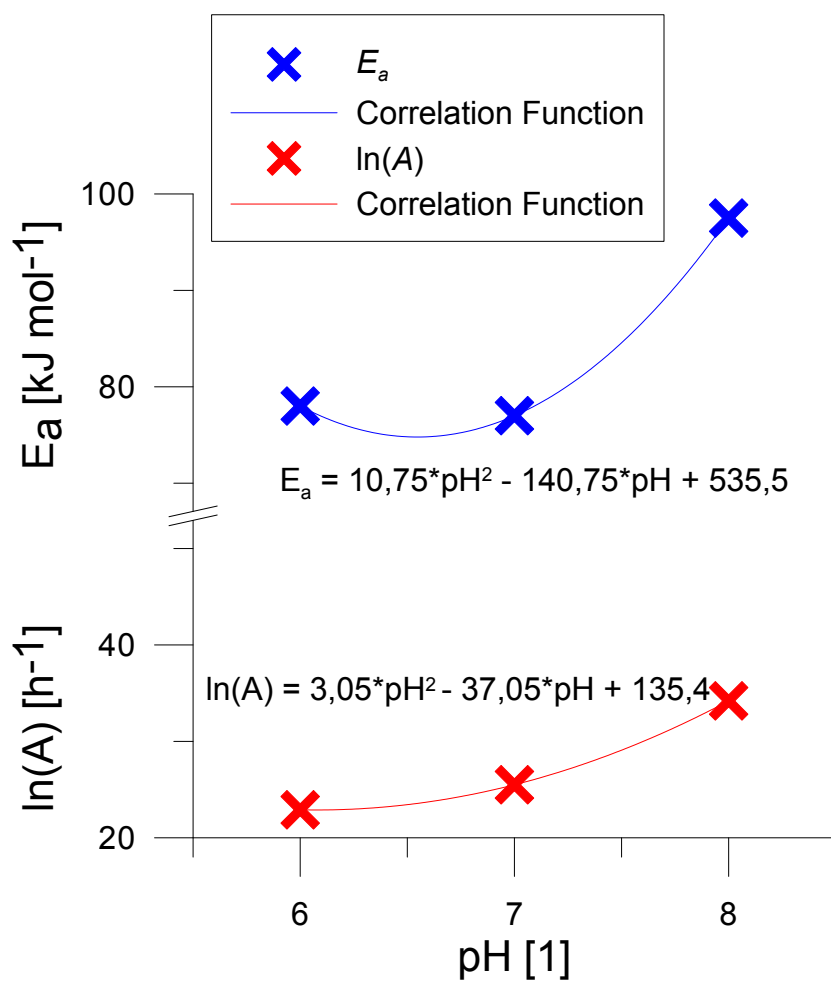
Figure A1: pH dependence of the kinetic parameters and hence the reaction rate of phenol acetate. The quadratic fitting functions applied to the data published by Nottebohm et al. (2012) were used as correlation functions in Eq. (7) to correct the influence of pH on the reaction speed.
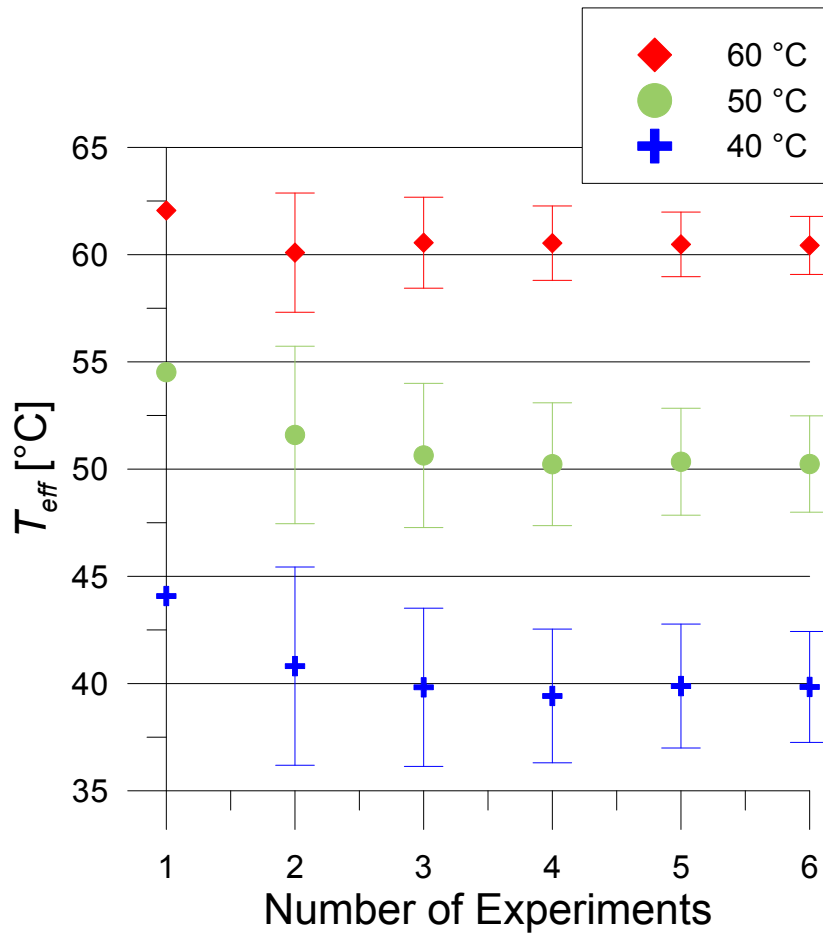
Figure A2: Temperature estimates and standard deviations for an increasing number of analyzed independent experiments. Herby the considered experiments are arranged by their deviation from the expected temperature in descending order. While a fast convergence of the statistical mean is already obtained within three independent measurements, the standard deviation converges for this worst case scenario after four to five independent experiments.

Appendix B

Starting from the solution in the triple Laplace space

$$\ddot{T}_D = \frac{\lambda}{s} \frac{e^{-sx_D} * e^{-\sqrt{\theta s}x_D}}{s + \sqrt{\theta s} + \lambda q + \lambda\sqrt{\theta q}} \left[F\right]$$

(B1)

with

$$F = \left(1 + \frac{\sqrt{\theta}}{\sqrt{p} + \sqrt{s}}\right) \frac{1}{p + \sqrt{\theta p}} \left(1 + \frac{\sqrt{\theta}}{\sqrt{q} + \sqrt{p}}\right)$$
$$- \frac{1}{p - s}\left(\frac{\sqrt{\theta}}{\sqrt{q} + \sqrt{p}} + \frac{\sqrt{\theta}}{\sqrt{q} + \sqrt{s}}\right)$$

(B2)

Note that $\ddot{T}_D$ is composed of six summands. The following transformations are shown for the first summand, but they apply also for the others similarly.

Let us rewrite the first summand of F as:

$$F_1 = \left(1 + \frac{\sqrt{\theta}}{\sqrt{p} + \sqrt{s}}\right) \frac{1}{p + \sqrt{\theta p}} =$$
$$\frac{1}{p + \sqrt{\theta p}}\left(1 + \int_0^\infty e^{-\left(\sqrt{\frac{p}{\theta}} + \sqrt{\frac{s}{\theta}}\right)\omega} d\omega\right)$$

(B3)

Similarly let's rewrite the full solution as:

$$\ddot{T}_D = \frac{\lambda}{s} e^{-sx_D} e^{-\sqrt{\theta s}x_D}$$
$$\int_0^\infty e^{-\left(s + \sqrt{\theta s} + \lambda q + \lambda\sqrt{\theta q}\right)\tau} d\tau\left(F_1 + F_2 - F_3 - F_4\right)$$

(B4)

where

$$\ddot{T}_D = \ddot{T}_{D1} + \ddot{T}_{D2} - \ddot{T}_{D3} - \ddot{T}_{D4}.$$

(B5)

Where

$$\dddot{T}_{D1\_1} = \lambda \int_0^\infty \frac{e^{-sx_D}}{s} e^{-\sqrt{\theta s}x_D} e^{-\left(s+\sqrt{\theta s}+\lambda q+\lambda\sqrt{\theta q}\right)\tau} d\tau * \frac{1}{p+\sqrt{\theta p}}$$

<div align="right">(B6)</div>

$$\ddot{T}_{D1\_1} = \lambda \int_0^\infty H(t_D - x_D - \tau)$$
$$erfc\frac{\sqrt{\theta}(x_D+\tau)}{2\sqrt{t_D - x_D - \tau}} e^{-\left(\lambda q+\lambda\sqrt{\theta q}\right)\tau} d\tau \frac{1}{p+\sqrt{\theta p}}$$

<div align="right">(B7)</div>

and so on.

Writing $\dddot{T}_{D1} = \dddot{T}_{D1\_1} + \dddot{T}_{D1\_2}$, where $\dddot{T}_{D1\_1}$ reads:

$$\dddot{T}_{D1\_1} = \lambda \int_0^\infty \frac{e^{-sx_D}}{s} e^{-\sqrt{\theta s}x_D} e^{-\left(s+\sqrt{\theta s}+\lambda q+\lambda\sqrt{\theta q}\right)\tau} d\tau * \frac{1}{p+\sqrt{\theta p}}$$

<div align="right">(B8)</div>

Let us invert $\dddot{T}_{D1\_1}$ with respect to s and obtain:

$$\ddot{T}_{D1\_1} = \lambda \int_0^\infty H(t_D - x_D - \tau)$$
$$erfc\frac{\sqrt{\theta}(x_D+\tau)}{2\sqrt{t_D - x_D - \tau}} e^{-\left(\lambda q+\lambda\sqrt{\theta q}\right)\tau} d\tau \frac{1}{p+\sqrt{\theta p}}$$

<div align="right">(B9)</div>

Then, inverting $\ddot{T}_{D1\_1}$ with respect to q and after implementing the Heaviside step function we reach:

$$\dot{T}_{D1\_1} = \lambda \int_0^{\min\left(t_P - \chi_D, \frac{t_{pD}}{\lambda}\right)} erfc\frac{\sqrt{\theta}(x_D+\tau)}{2\sqrt{t_D - x_D - \tau}}$$
$$\frac{\lambda\sqrt{\theta}\tau}{2\sqrt{\pi\left(t_{pD} - \pi\tau\right)^3}} e^{-\frac{\lambda^2\theta\tau^2}{4\left(t_{pD} - \lambda\tau\right)}} d\tau \frac{1}{p+\sqrt{\theta p}}$$

<div align="right">(B10)</div>

The final inversion with respect to p gives us the desired real space solution for this part:

$$T_{D1\_1} = \lambda \int_0^{\min\left(t_P - \chi_D, \frac{t_{pD}}{\lambda}\right)} erfc\frac{\sqrt{\theta}(x_D+\tau)}{2\sqrt{t_D - x_D - \tau}}$$
$$* \frac{\lambda\sqrt{\theta}\tau}{2\sqrt{\pi\left(t_{pD} - \lambda\tau\right)^3}} * e^{-\frac{\lambda^2\theta\tau^2}{4\left(t_{pD} - \lambda^2\right)}} d\tau$$
$$* e^{\theta t_{sD}} erfc\sqrt{\theta t_{sD}}$$

<div align="right">(B11)</div>

Appendix C

List of publication authored or co-authored by me, and related to the present work:

Journal Paper

Maier, F., Schaffer, M., Licha, T., Determination of Temperatures and Cooling Fractions in a Permeable Media with Internal Temperature Distribution Using Thermo-Sensitive Tracers. Geothermics (under review)

Maier, F., Schaffer, M., Licha, T., 2015. Temperature determination using thermo-sensitive tracers: Experimental validation in an isothermal column heat exchanger. Geothermics, 53, 533-539.

Idzik, K. R, Nödler, K, **Maier, F**, Licha, T., 2014. Efficient synthesis and reaction kinetics of readily water soluble esters containing sulfonic groups. Molecules. 19(12), 21022-21033.

Maier, F., Kocabas, I., 2013. Comment on "A closed-form analytical solution for thermal single-well injection-withdrawal tests" by Jung and Pruess. Water Resources Research, 49(1), 640-643.

Schaffer, M., **Maier, F.**, Licha, T., Sauter, M., 2013. A new generation of tracers for the characterization of interfacial areas during supercritical carbon dioxide injections into deep saline aquifers: Kinetic interface-sensitive tracers (KIS tracer). International Journal of Greenhouse Gas Control, 14, 200-208.

Peer reviewed conference paper

Maier, F., Schaffer, M., Nur, Silvia.N., Licha, T., 2014. Ability of Thermo-Sensitive Tracers for Precisely Estimating System Temperatures in Column Experiments with Thermal Gradient. In: Proceedings of the 39th Workshop on Geothermal Reservoir Engineering, Stanford University, Stanford, California, February 11-13, 2013, SGP-TR-202

Maier, F., Olloni, A., Licha, T., 2013. Controlled column experiments to determine the theory and sensitivity of thermo-sensitive tracers. In: Proceedings of the 38th Workshop on Geothermal Reservoir Engineering, Stanford University, Stanford, California, February 11-13, 2013, SGP-TR-198

Maier, F., Kocabas, I., 2013. Efficient analytical solution for parameter estimation of push shut-in pull experiments in an idealized single fracture system. In: Proceedings of the 38th Workshop on Geothermal Reservoir Engineering, Stanford University, Stanford, California, February 11-13, 2013, SGP-TR-198

Kocabas, I., **Maier, F.,** 2013. Analytical and Numerical Modeling of Tracer Flow in Oil Reservoirs Containing High Permeability Streaks. In: SPE Middle East Oil and Gas Show and Conference. Society of Petroleum Engineers. March 10-13, 2013, Bahrain

Ghergut, I., Behrens, H., Licha, T., **Maier**, **F.,** Nottebohm, M., Schaffer, M., Ptak, T., Sauter M., 2012. Single-well and inter-well dual-tracer test design for quantifying phase volumes and interface areas. In: Proceedings of the 37th Workshop on Geothermal Reservoir Engineering, Stanford University, Stanford, California, January 30 February 1, 2012, SGP-TR-194

Ghergut I., Behrens H., **Maier F.**, Karmakar S., Sauter M., 2011. A note about 'heat exchange areas' as a target parameter for SWIW tracer tests. In: Proceedings of the 36th Workshop on Geothermal Reservoir Engineering, Stanford University, Stanford, California, 2011, SGP-TR-191: 303-312

Miscellaneous (Conference paper, Conference abstract, Book Chapter, Report)

Maier, F., Licha, T., 2014. Möglichkeit zur Bestimmung von in-situ Temperaturen geothermischer Reservoire durch den Einsatz von thermo-sensitiven Tracern. In: 74. Jahrestagung der Deutschen Geophysikalischen Gesellschaft in Karlsruhe. Karslruhe, Germany, March 2014

Tatomir, A., Jyot, A., **Maier, F.,** Sauter M., 2014. Modeling of Kinetic Interface Sensitive Tracers for Two Phase Immiscible Flow in Porous Media with COMSOL Multiphysics. In: Proceedings of the 2014 COMSOL Conference Cambridge.

Tatomir, A., Schaffer, M., Kissinger, A., Hommel, J., **Maier, F.,** Licha, T., Nuske, P., Sauter, M., Helmig, R., 2014. Optimizing supercritical CO2 injection into deep saline aquifers using kinetic interface sensitive tracers: A numerical sensitivity study, in: Models, Analysis, and Simulation of Flow and Reactive Transport in Porous Media. Presented at the Computational Methods in Water Resources, Stuttgart, Germany.

Tatomir, A., **Maier, F.**, Schaffer, M., Licha, T., Sauter, M., 2013. Modelling of Kinetic Interface Sensitive Tracers for Two-Phase Systems, in: Hou, M.Z., Xie, H., Were, P. (Eds.), Clean Energy Systems in the Subsurface: Production, Storage and Conversion, Springer Series in Geomechanics and Geoengineering. Springer Berlin Heidelberg, pp. 65–74.

Maier, F., Oberdorfer, P., Tatomir, A., Holzbecher, E., Ghergut, I., Sauter, M., 2012. Numerische Simulation tiefer geothermischer Reservoire unter Ausnutzung von Dimensionsreduktion am Beispiel der geothermischen Anlage Bruchsal, Der Geothermiekongress 2012 (Karlsruhe), CD-ROM-Publikation

Maier, F., Oberdorfer, P., Kocabas, I., Ghergut, I., Sauter, M., 2012. Using Temperature Signals to Estimate Geometry Parameters in Fractured Geothermal Reservoirs. In: Proceedings of the 2012 Comsol Conference Milan.

Maier, F., Olloni, A., Idzik, K., Licha, T., 2012. Validierung der Theorie für thermosensitive Tracer mittels eines Säulenexperimentes mit angelegtem bekanntem Temperaturfeld, Der Geothermiekongress 2012 (Karlsruhe), CD-ROM-Publikation

Maier, F., Oberdorfer, P., Tatomir, A., Holzbecher, E., Ghergut, I., Sauter, M., 2012. Numerische Simulation tiefer geothermischer Reservoire unter Ausnutzung von Dimensionsreduktion am Beispiel der geothermischen Anlage Bruchsal, Der Geothermiekongress 2012 (Karlsruhe), CD-ROM-Publikation

Rettenmaier, D., Wolfgramm, M., Sauter, M., Zorn, R., Kölbel, T., Meixner, J., Gaucher, E., **Maier F.,** Kohl, T., 2012. LOGRO - Langzeitbetrieb und Optimierung eines Geothermiekraftwerks – Reservoirmanagement Bruchsal, Der Geothermiekongress 2012 (Karlsruhe), CD-ROM-Publikation

Holzbecher, E., **Maier, F.,** 2012. Single-Well Injection-Withdrawal Experiments for Ground Flow Estimation. In EGU General Assembly Conference Abstracts (Vol. 14, p. 13827).

Ghergut, I., Meixner, J., Rettenmaier, D., **Maier, F.,** Nottebohm, M., Ptak, T., Sauter, M., 2012. Expected fluid residence times, thermal breakthrough, and tracer test design for characterizing a hydrothermal system in the Upper Rhine Rift Valley. In EGU General Assembly Conference Abstracts (Vol. 14, p. 13687). 2

Schaffer, M., **Maier, F.**, Licha, T., Sauter, M., 2012. Development of Kinetic Interface Sensitive Tracers (KIS-Tracer) for Supercritical Carbon Dioxide Injections into Deep Saline Aquifers. In EGU General Assembly Conference Abstracts (Vol. 14, p. 2048).

Maier, F., Oberdorfer, P., Ghergut, I., Zorn R., Sauter M., 2011. Mathematische Kopplung eindimensionaler Bohrlöcher in dreidimensionalen Umfeldern zur Simulation des geothermischen Wärmetransportes. In: Geothermische Vereinigung – Bundesverband Geothermie (Hrsg.), Der Geothermiekongress 2011 (Bochum), CD-ROM-Publikation

Maier, F., Hebig, K., Jin, Y., Holzbecher, E., 2011. Ability of Single-Well Injection-Withdrawal Experiments to Estimate Ground Water Velocity. In Proceedings of the 2011 COMSOL Conference Stuttgart.

Holzbecher, E., Oberdorfer, P., **Maier, F.**, Jin, Y., Sauter, M., 2011. Simulation of Deep Geothermal Heat Production. In Proceedings of the 2011 COMSOL Conference Stuttgart.

Oberdorfer, P., **Maier, F.,** Holzbecher, E., 2011. Comparison of Borehole Heat Exchangers (BHEs): State of the Art vs. Novel Design Approaches. In Proceedings of the 2011 COMSOL Conference Stuttgart.

Ghergut, J., Bensabat, J., Behrens, H., Licha, T., **Maier, F.**, Schaffer, M., Sauter, M., 2011. Single-well and inter-well tracer test design for characterizing the Heletz site (Israel) with a view at CCS., EGU General Assembly Conference Abstracts,14,13549,2011

Licha T., Schaffer M., Sauter M., **Maier F.**, Nottebohm M., Fagerlund F., 2011 Report on batch experiment results for interfacial processes, Deliverable D041 of EU Project MUSTANG, 48p.

Maier, F., Holzbecher, E., Ghergut, I., Sauter, M., 2010. Numerische Simulationen zur Bestimmung von Wärmetauschflächen aus Wärme-Push-Pull-Tests. Geothermische Vereinigung – Bundesverband Geothermie (Hrsg.), Der Geothermiekongress 2010 (Karlsruhe), CD-ROM-Publikation

Ghergut, I., Behrens, H., Meixner, J., Rettenmaier, D., Hoetzl, H., **Maier, F.,** Sauter, M., 2010. Sorge und Freude bei Dimensionierung und Auswertung von Tracertests im Oberrheingraben. Geothermische Vereinigung – Bundesverband Geothermie (Hrsg.), Der Geothermiekongress 2010 (Karlsruhe), CD-ROM-Publikation

Curriculum vitae

Friedrich Maier

PERSONAL DATA

Date of birth   05.06.1980

Place of birth   Böblingen

Nationality   German

EDUCATION

06/2010 – Current	Georg-August-Universität Göttingen Geoscience Centre Department Applied Geology PhD. Student
10/2003 – 11/2009	Georg-August-Universität Göttingen Faculty of Physics (degree: Dipl.-Geophys.)

WORK EXPERIENCE

Since 06/2010	Georg-August-Universität Göttingen, Research associate
12/2009 – 02/2010	ETH Zürich, Research associate
08/2007 – 09/2007	UFZ Leipzig, Scientific assistant
06/2006 – 08/2009	Georg-August-Universität Göttingen, Scientific assistant